NUREG/CR-1845

FRAPCON-2: A Computer Code for the Calculation of Steady State Thermal-Mechanical Behavior of Oxide Fuel Rods

Prepared by G. A. Berna, M. P. Bohn, W. N. Rausch, R. E. Williford, D. D. Lanning

EG&G Idaho, Inc.

Pacific Northwest Laboratory

Prepared for
U.S. Nuclear Regulatory Commission

Available from

GPO Sales Program
Division of Technical Information and Document Control
U. S. Nuclear Regulatory Commission
Washington, D. C. 20555

Printed copy price: $7.00

and

National Technical Information Service
Springfield, Virginia 22161

NUREG/CR-1845
R3

FRAPCON-2: A Computer Code for the Calculation of Steady State Thermal-Mechanical Behavior of Oxide Fuel Rods

Manuscript Completed: December 1980
Date Published: January 1981

Prepared by
G. A. Berna, EG&G Idaho, Inc.
M. P. Bohn, formerly with EG&G Idaho, Inc., currently with Lawrence Livermore Laboratory
W. N. Rausch, Pacific Northwest Laboratory
R. E. Williford, Pacific Northwest Laboratory
D. D. Lanning, Pacific Northwest Laboratory

EG&G Idaho, Inc.
Idaho Falls, ID 83401

Pacific Northwest Laboratory
Richland, WA 99352

Prepared for
Division of Reactor Safety Research
Office of Nuclear Regulatory Research
U.S. Nuclear Regulatory Commission
Washington, D.C. 20555
NRC FIN A6050, B2043

CONTENTS

NOTE: Appendix D to this report is presented on microfiche attached to the inside back cover.

FIGURES

TABLES

ABSTRACT

FRAPCON-2 is a FORTRAN IV computer code that calculates the steady state response of light water reactor fuel rods during long-term burnup. The code calculates the temperature, pressure, deformation, and failure histories of a fuel rod as functions of time-dependent fuel rod power and coolant boundary conditions. The phenomena modeled by the code include (a) heat conduction through the fuel and cladding, (b) cladding elastic and plastic deformation, (c) fuel-cladding mechanical interaction, (d) fission gas release, (e) fuel rod internal gas pressure, (f) heat transfer between fuel and cladding, (g) cladding oxidation, and (h) heat transfer from cladding to coolant. The code contains necessary material properties, water properties, and heat transfer correlations. FRAPCON-2 is programmed for use on the CDC Cyber 175 and 176 computers.

The FRAPCON-2 code is designed to generate initial conditions for transient fuel rod analysis by either the FRAP-T6 computer code or the thermal-hydraulic code, RELAP4/MOD7 Version 2.

ACKNOWLEDGMENTS

The authors acknowledge Dr. G. P. Marino of the U.S. Nuclear Regulatory Commission for his technical guidance on the models and the modeling processes presented herein. Also we acknowledge Tim Howe, Mitch Cunningham and Frank Panisko for their careful technical review; Nancy Wildung, Wendy Bennett, and Sue Watson for their general technical assistance; and Mary Ann Hansen for her efforts in typing this document. Finally, the authors acknowledge Tom Laats for his help in isolating problems in the FRAPCON-2 code which were subsequently corrected.

FRAPCON-2: A COMPUTER CODE FOR THE CALCULATION OF STEADY STATE THERMAL-MECHANICAL BEHAVIOR OF OXIDE FUEL RODS

1. INTRODUCTION

1.1 Objectives of the FRAPCON Series

The ability to accurately calculate the performance of light water reactor (LWR) fuel rods under long-term burnup conditions is a major objective of the Reactor Safety Research Program being conducted by the U.S. Nuclear Regulatory Commission (NRC). To achieve this objective, the NRC has sponsored an extensive program of analytical computer code development, as well as both in-pile and out-of-pile experiments to benchmark and assess the analytical code capabilities. The computer code being developed for the calculation of the long-term burnup response of a single fuel rod is FRAPCON. This report describes FRAPCON-2, the second released code of the FRAPCON series.

FRAPCON-2 is an analytical tool that calculates LWR fuel rod behavior when power and boundary condition changes are sufficiently slow for the term "steady state" to apply. This includes situations such as long periods at constant power and slow power ramps which are typical of normal power reactor operations. The code calculates the variation with time of all significant fuel rod variables, including fuel and cladding temperatures, cladding hoop strain, cladding oxidation, fuel irradiation swelling, fuel densification, fission gas release, and rod internal gas pressure. In addition, the code is designed to generate initial conditions for transient

fuel rod analysis by either FRAP-T6,[1] the companion transient fuel rod analysis code, or RELAP4/MOD7,[2] a thermal-hydraulic code for transient analysis of LWR systems.

FRAPCON-2 is linked with the MATPRO[3] materials properties package. Thus, the user is not required to provide any material property input. The MATPRO subcode is composed of modular subroutines that define materials properties for temperatures ranging from room temperatures to temperatures above melting. Each subroutine defines only a single material property. For example, MATPRO contains subroutines defining fuel thermal conductivity as a function of fuel temperature and fuel density; fuel thermal expansion as a function of fuel temperature; and the cladding stress-strain relation as a function of cladding temperature, strain rate, cold work, and fast neutron fluence.

The development of the FRAPCON series is a joint effort of Idaho National Engineering Laboratory (INEL) and Pacific Northwest Laboratory (PNL)[a] which began with the development of FRAPCON-1. The basis of the FRAPCON-1 code is the FRAP-S3[4] code developed at INEL with two major changes. First, the code was modified for dynamic dimensioning to increase the number of computer facilities on which the code could be installed. Second, the FRAP-S3 temperature subcode was replaced by a more versatile subcode developed at PNL. The major improvements in FRAPCON-2 with respect to FRAPCON-1[b] include three advanced mechanics options, FRACAS-II and AXISYM developed at INEL and PELET from GAPCON-THERMAL-3[5]

---

a. INEL and PNL are operated for the Department of Energy by EG&G Idaho Inc., and Battelle Memorial Institute, respectively.

b. FRAPCON-1, MATPRO-10A, Idaho National Engineering Laboratory, EG&G Idaho, Inc., Code Configuration Control Number H00730IB.

developed at PNL, four additional fission gas release options, and an uncertainty analysis option.[6]

1.2 Limitations of FRAPCON-2

The code has inherent limitations. The major limitations are:

1. The thermal models of the code are based on steady state data and equations. Therefore, calculated temperatures will become progressively inaccurate due to this assumption alone as input power histories result in power ramp rates greater than about 0.02% per second. Similiarly, the gas release models are based on steady state data and do not reflect release rates expected for rapid power changes.

2. Only small cladding deformations are meaningful. All of the thermal and mechanics modeling options assume an axisymmetric fuel rod. Large deformations (>5% strain), which tend to become asymmetric, will not be traced well by the FRAPCON-2 code. In addition, rapid deformation (greater than about 0.002% per second) will not be accurately calculated since a transient temperature calculation would be required to properly include the thermal-mechanical feedback.

3. Large power changes are not acceptable to the PELET mechanics model. If the PELET option is chosen, power step changes greater than 5 kW/m (1.5 kW/ft) per time step should not be used. The PELET solution routine is

incremental and path dependent, and power steps larger than the limit stated above result in an unacceptably large stress-strain increment.

1.3 Report Outline and Relation to Other Reports

Sections 2. and 3. of this report deal with the modeling concepts and the code description, respectively. Input instructions, a sample case, materials properties, and subroutine interrelation are discussed in the appendixes. The reader is cautioned that, although the thermal and mechanical models are described separately, they actually are highly interrelated. Section 2.2 is included prior to the detailed modeling descriptions to outline these interrelationships.

This report does not present an assessment of the code performance with respect to in-reactor data. Critical comparisons with experimental data from well-characterized, instrumented test rods will be presented in a separate report describing the developmental assessment of the code. General comparison with a much larger body of data will be presented in a report describing the independent assessment of the FRAPCON-2 code conducted at INEL.

2. GENERAL MODELING DESCRIPTIONS

2.1 FRAPCON-2 Solution Scheme

The FRAPCON-2 code iteratively calculates the interrelated effects of fuel and cladding temperature, rod internal gas pressure,

fuel and cladding deformation, release of fission product gases, fuel swelling and densification, cladding thermal expansion and irradiation-induced growth, cladding corrosion, and crud deposition as functions of time and fuel rod specific power.

The calculational procedure is illustrated in Figure 1, a simplified flowchart of FRAPCON-2. (A detailed flowchart is provided in Section 3). The calculation begins with processing of input data. Next, the initial fuel rod state is determined through a self-initialization calculation. Time is advanced according to the input-specified time step size, a steady state solution is performed, and the new fuel rod state is determined. The new fuel rod state provides the initial state conditions for the next time step. The calculations are cycled in this manner for the user-specified number of time steps.

The solution for each time step consists of (a) a calculation of the temperature of the fuel and the cladding, (b) a calculation of fuel and cladding deformation, and (c) a calculation of the fission product generation and, void volume, and fuel rod internal gas pressure. When the FRACAS-I mechanics model is chosen, the fuel rod failure probability is also calculated. Each of these calculations is made in a separate subcode. As is shown in Figure 1, the fuel rod response for each time step is determined by repeated cycling through two nested loops of calculations until the fuel rod temperature, deformation, and internal gas pressure converge.

For the FRACAS mechanics models, the fuel temperature and deformation are alternately calculated in the inner loop. On the first cycle through this loop for each time step, the gap conduc-

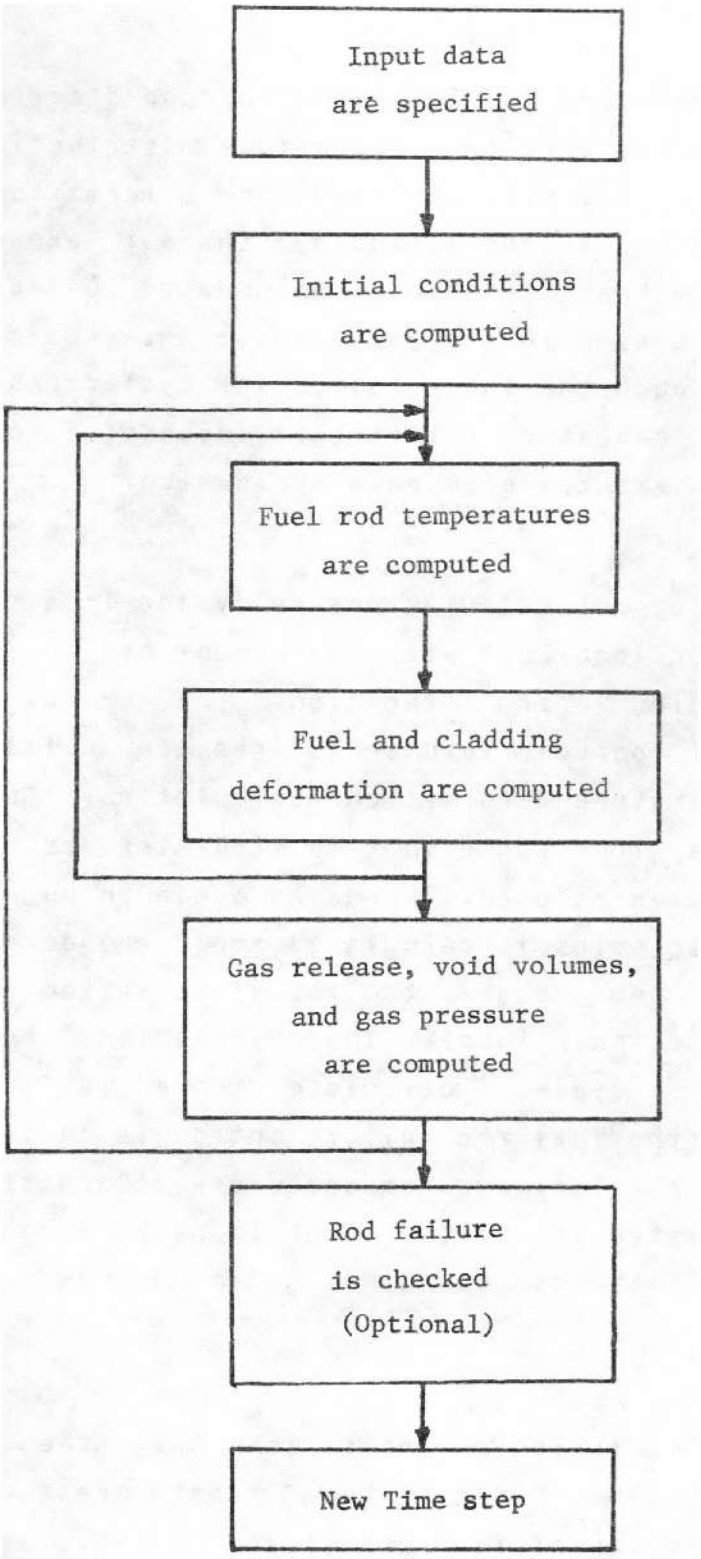

Figure 1. Simplified FRAPCON-2 flow chart.

tance is computed using the fuel-cladding gap size from the previous time step. Then the fuel rod temperature distribution is computed. This temperature distribution feeds the deformation calculation by influencing the fuel and cladding thermal expansions and the cladding stress-strain relation. An updated fuel-cladding gap size is calculated and used in the gap conductance calculation on the next cycle through the inner loop. The cyclic process through the inner loop is repeated until two successive cycles calculate essentially the same temperature distribution.

The outer loop of calculations is cycled in a manner similar to that of the inner loop, but with the amount of internal gas being determined during each iteration. The calculation alternates between the fuel rod void volume-gas pressure calculation and the fuel rod temperature-deformation calculation. On the first cycle through the outer loop for each time step, the gas pressure from the previous time step is used. For each cycle through the outer loop, the number of gas moles is calculated and the updated gas pressure computed and fed back to the deformation and temperature calculations (the inner loop). The calculations are cycled until two successive cycles calculate essentially the same gas pressure. When the fuel rod failure option is chosen (see Section 2.6), and after the fuel rod temperatures, deformation and number of gas moles calculated in the two inner loops have converged, fuel rod failure probability is computed. Then a new power time step is begun.

A different solution scheme is used when the PELET mechanics option is chosen. During the first pressure iteration, a simultaneous solution of fuel stress and fuel-cladding gap size is performed for each axial region prior to the fuel temperature calculation. These calculations are updated during subsequent gas

pressure calculation iterations. After convergence on fuel rod internal gas pressure, an incremental elastic-plastic deformation calculation is performed for the entire fuel rod. These incremental results are used to update the stress and strain arrays.

2.2 Coupling of Thermal and Mechanical Models

The coupling of thermal and mechanical models is such that the packages cannot be used interchangeably. Each thermal-mechanical package and its unifying principles are discussed below starting with the two FRACAS packages and then the PELET/RADIAL package.

2.2.1 The FRACAS Models. The close coupling of the thermal modeling and mechanical modeling is the result of the existence of the fuel-cladding gap, and therefore, the space for fuel cracking and relocation. As the fuel temperature increases, the extreme stresses resulting from the large temperature gradients in the fuel cause fuel cracking and relocation to occur. Void space which is originally in the fuel-cladding gap is relocated into the fuel as fragments of fuel move outwardly into the fuel-cladding gap. The fuel cracking causes a change in the effective fuel thermal conductivity from the as-fabricated state value.

As the fuel becomes hotter, the fuel expands filling some of the voids within the fuel. However asperities do not align exactly, thereby causing the fuel diameter to appear larger and the fuel to interact with the cladding at a lower power than that expected due to normal expansion mechanisms (thermal expansion, swelling, and densification).

The modeling of the cracked and relocated fuel, both thermally and mechanically, requires accounting for the changed fuel conductivity, changed fuel-cladding gap size (and hence gap conductance), and the changed fuel pellet diameter as the fuel interacts with the cladding. Two models are used to account for these phenomena: effective fuel thermal conductivity and fuel surface relocation. The effective fuel conductivity model is a correlation which provides a multiplier on the MATPRO fuel conductivity. The fuel surface relocation provides a new fuel-cladding gap size for use in gap conductance calculations and mechanical interaction calculations. Also considered is the shift of voids from the fuel-cladding gap into the fuel pellet (and the resultant pressure change) and the feedback into the mechanics and thermal calculations.

FRACAS-I[7] uses the effective fuel conductivity and the relocated fuel-cladding gap size for the thermal calculations but does not make use of the fuel surface relocation in the mechanics calculation.

FRACAS-II uses the effective fuel conductivity and the relocated fuel-cladding gap size for the thermal calculations but, unlike FRACAS-I, the relocated fuel surface is used in the mechanics calculations. A model is used to account for time dependent "hot-pressing" of misaligned fuel fragments.

2.2.2 PELET/RADIAL. The thermal and mechanical responses of a fuel rod to power changes are known to be interdependent. In the conventional view of a solid pellet stack located concentrically within the cladding, this mutual dependence can be summarized as follows:

1. The symmetric fuel-cladding gap closes with increasing power due to differential thermal expansion. After fuel-cladding contact occurs, further power increase results in increasing fuel-cladding interfacial pressure and an axial and radial load on the cladding.

2. On the other hand, the fuel-cladding gap closure and interfacial pressure changes due the increase in rod power result in an increasing thermal conductance at the fuel-cladding interface. This feedback tends to counteract the decrease in fuel intrinsic thermal conductivity with increasing fuel temperature.

In the above view, the "free area" within a given cross-section of the rod resides totally in the fuel-cladding gap. The model is unified by accounting for how various submodels (thermal expansion, fuel relocation, fuel densification, etc.) change the fuel-cladding gap size.

A different view is now proposed which has a more complete set of unifying principles. This new view is based on the fuel pellets being randomly cracked, as is shown in Figure 2. These cracks are commonly observed in fuel pellets even after very little irradiation. They are caused by the thermal hoop stresses resulting from the steep radial temperature gradients in the fuel. The new modeling of this phenomenon includes a function that relates the crack geometry (width) to the fuel stresses. The fuel stresses in turn are related to the fuel temperatures by the differential thermal expansions of fuel and cladding. Thus the crack geometry is related to the fuel rod thermal and mechanical responses and to power changes. The concept is briefly discussed below.

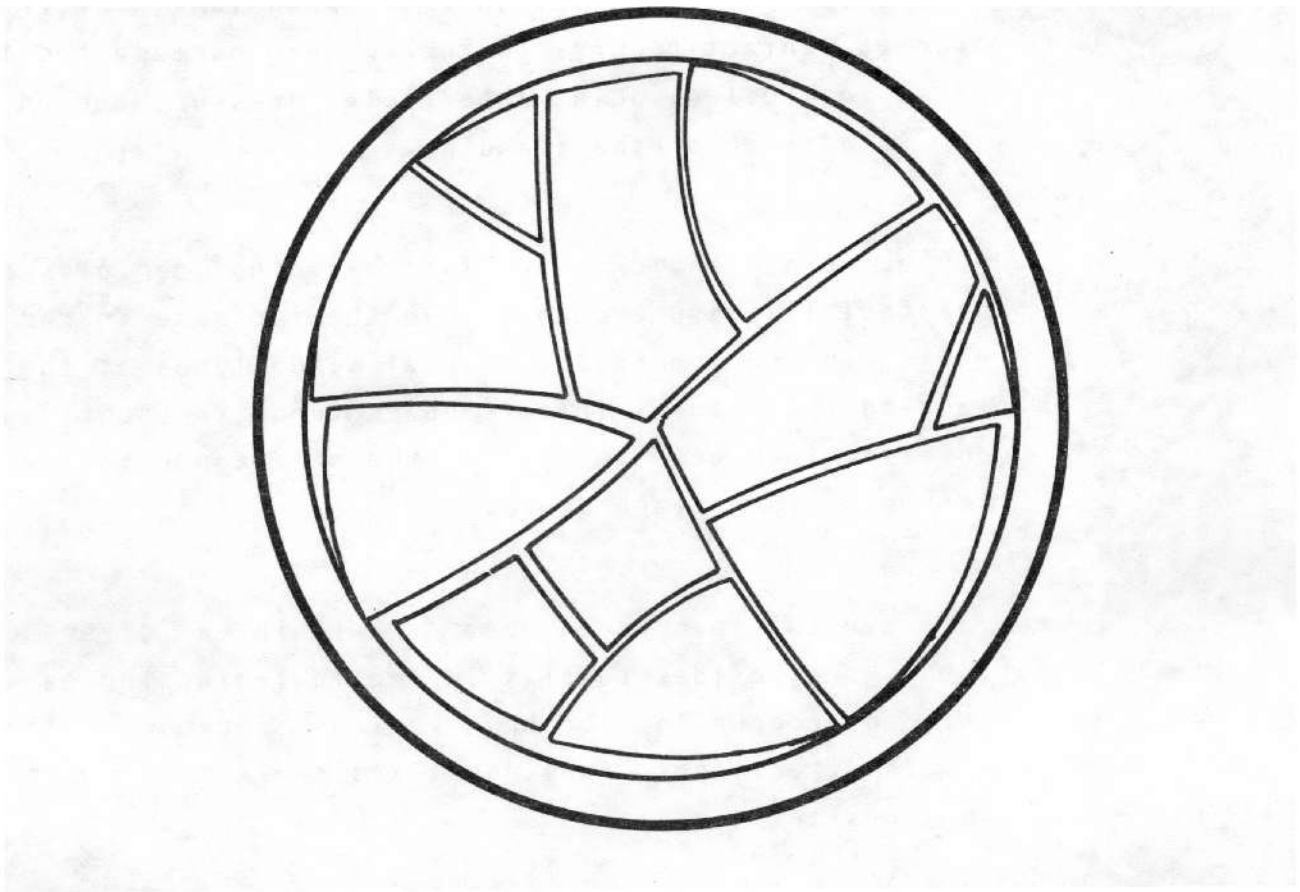

Figure 2. Unifying principles of cracked fuel.

The "free area" is actually distributed between the fuel cracks and the fuel-cladding gap. The amount of free area that is occupied by the cracks is determined by the lengths and the widths of the cracks. The lengths of the cracks can be defined by choosing an appropriate crack pattern from postirradiation examination data. The width of a crack is determined by the interfragment loads (fuel stresses) that cause the cracks to close during an increase in power. A relationship between crack width and applied stress was

given by Mikic[8]

$$1/2 \text{ erfc}\left(\frac{d}{R\sqrt{2}}\right) = \frac{\sigma}{\sigma+H} \qquad (1)$$

where

erfc = complimentary error function

= 1 − erf

d = separation between mean surface planes of crack interfaces (crack width)

R = surface roughness of crack face (1 standard deviation of asperity heights)

σ = normal stress applied to crack

H = Meyer hardness of uranium dioxide.

In this application, the surface roughness is actually the roughness which is composed of a combination of the microroughness and the surface waviness. If all cracks are assumed to have the same effective roughness and if the fuel is assumed to be in a hydrostatic stress state in the (r, θ) plane, then all cracks will have the same width for a specified stress (power) level. Crack width multiplied by total crack length equals total crack area, and the free area occupied by the cracks is thus determined.

Because the cracks consume some of the free area, they cause the fuel perimeter to increase in length. This is known as relocation. However, the fragments become misaligned during this relocation so that the fuel-cladding gap also has an effective roughness. By virtue of the Mikic surface interaction model, there is always some finite amount of contact between fragments and between fragments and cladding. This occurs because of the error function formulation of the model and provides equilibrium for all the fragments at all times. At low powers the contact may be very small, but still finite. At higher powers the contact is usually increased substantially. This radial equilibrium condition allows for simultaneous solution of the crack and gap widths via the Mikic model by equating the fuel hydrostatic stress to the radial stress at the fuel-cladding gap.

There is also axial force equilibrium between the fuel and cladding. Because of the fuel-cladding friction that is induced by constant contact, the fuel and cladding are assumed to be unable to slip axially with respect to each other.

In general, the fuel-cladding gap sizes (fuel-cladding surface separations) calculated by this model are substantially less than those calculated by the solid cylinder model. About half of the free area is usually consumed by cracks in the fuel. The degradation of the fuel thermal conductivity is dependent on the voids (cracks) that exist within the fuel. Thus, the primary feedback mechanism between fuel temperatures and fuel-cladding thermal expansion is crack closure and its effect on fuel thermal conductivity, rather than fuel-cladding gap closure and its effect on gap conductance.

The axiomatic foundations of the approach are now summarized.

1. The fuel is cracked and the free area is distributed between fuel cracks and the fuel-cladding gap.

2. The amount of free area occupied by the cracks is determined by crack geometry (length and width) and the stress level. Crack width is related to the fuel stress by the Mikic surface interaction model.

3. The fuel stress state in the (r, θ) plane is assumed to be hydrostatic, and all cracks within the fuel have equal roughness. Thus, all crack widths are assumed equal. (A separate roughness is assigned to the fuel-cladding gap).

4. The fuel fragments and cladding are always in radial and axial equilibrium. Thus, there is always fuel-cladding contact and never axial slippage between fuel and cladding.

5. The primary thermal-mechanical feedback is due to crack width effects on the effective fuel thermal conductivity, rather than by the fuel-cladding gap closure effects on gap conductance.

The above principles have been used to reinterpret in-reactor power, fuel temperature and cladding elongation data.[9] From this reinterpretation came numerical estimates (empirical correlations) for the fuel conductivity and effective fuel elastic moduli as a function of the estimated free area partition and hydrostatic stress

state of the fuel. The procedure used for this reinterpretation will now be reviewed to explain both how the correlations were derived and how they are used in PELET/RADIAL.

The data used came primarily from Halden Reactor Tests IFA-432[10] and IFA-513.[11] For those tests the following information for a large range of fuel-cladding gap sizes and fill gas composition was available:

1. Accurate steady state power versus temperature data

2. Transient temperature versus time data (yielding an estimate of total thermal resistance apportioned to fuel and gap thermal resistance)[a]

3. Cladding elongation as a function of time and power.

Gap and crack roughness (assumed proportional) were found by trial as a function of the as-fabricated fuel-cladding gap size so that the calculated conductances matched those deduced from transient data. These then became fixed values in the data analysis, as they are now in the code. A fixed value of total crack length (3.5 pellet diameters) was also chosen, based on inspection of many photographs of irradiated pellets. With these parameters fixed, the Mikic model could be used to arrive simultaneously at

---

a. Total thermal resistance is defined as the difference between fuel centerline and coolant temperatures divided by the local linear heat rate. Reference 12 provides an expanded discussion of thermal resistance and the use of transient temperature data.

fuel-cladding gap size, crack size, and hydrostatic stress in the fuel, given fuel centerline temperature and fuel power. The incremental changes in deduced fuel strain and stress from one power level to the next were used to estimate an effective radial fuel elastic modulus. Similarly, incremental changes in cladding elongation were used to estimate an effective elastic modulus. The moduli were correlated to the estimated free area while the deduced change (degradation) in the fuel thermal conductivity was correlated to the fuel hydrostatic stress.

Within PELET/RADIAL, the same principles apply in the sense that the thermal-mechanical state in the current time step is estimated from the previous time step plus the incremental change in power and temperature. The thermal and mechanical models are coupled in the following manner:

1. Given the current power and the previous cladding radius, the amount and partition of free area within the fuel rod is found for each axial node, together with the corresponding hydrostatic stress.

2. From item 1, fuel-cladding gap size and interfacial pressure are immediately available. Both of these variables go into the gap conductance calculation, and the fuel-cladding interfacial pressure feeds the calculation of radial and axial cladding stress and strain via the finite element formulation in PELET.

3. The thermal conductivity degradation is estimated from an empirical correlation involving hydrostatic stress and

fill gas composition. This feeds to the fuel temperature, and hence, to the fission gas release calculations.

4. The radial and axial fuel elastic moduli are estimated from empirical correlations with the free area. These feed directly to the calculation of cladding stress and strain at the end of the time step.

Within the PELET/RADIAL package, fuel-cladding gap size and interfacial pressure are not varied during the iterations that determine the temperature drop across the fuel-cladding gap, and the computer time normally spent performing these calculations has been transferred to determining the hydrostatic stress state for the cracked fuel. This stress state determination lies within the gas iteration loop and is updated due to temperature changes resulting from gas release. The mechanical calculation of incremental cladding deformation lies outside both iteration loops and is done at the end of the time step.

In summary, the thermal and mechanical models are intimately interrelated. But by handling that interrelationship on an incremental basis, computer running time needed is minimized.

2.3 Fuel Rod Thermal Response

The temperature distribution throughout the fuel and the cladding is calculated at each axial node. A simplified flowchart of the temperature distribution solution is shown in Figure 3. A schematic drawing of the temperature distribution at an arbitrary axial node is shown in Figure 4.

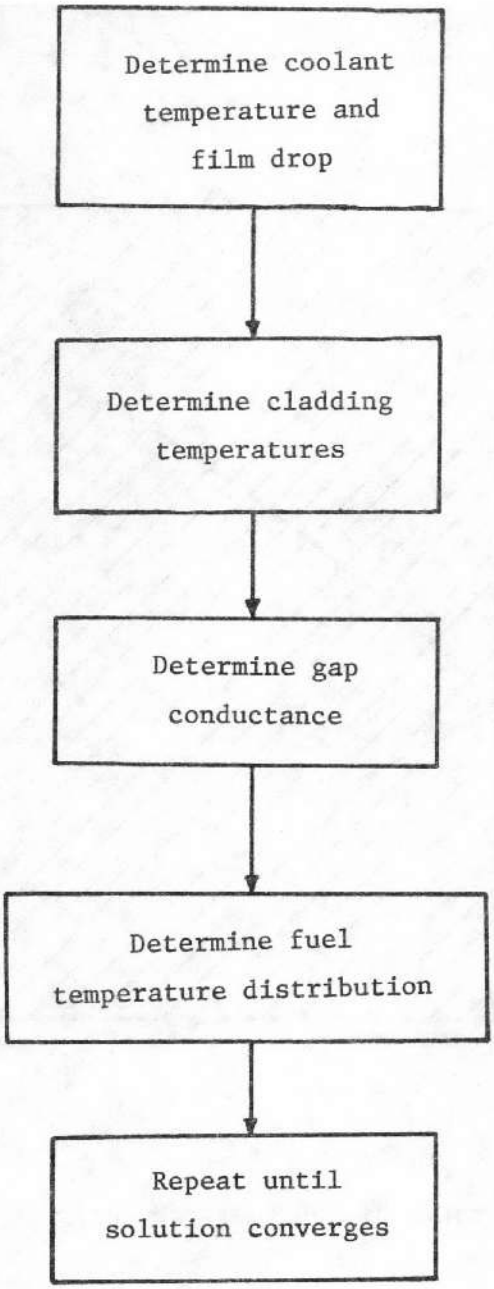

Figure 3. Flow chart of the fuel and cladding temperature calculation.

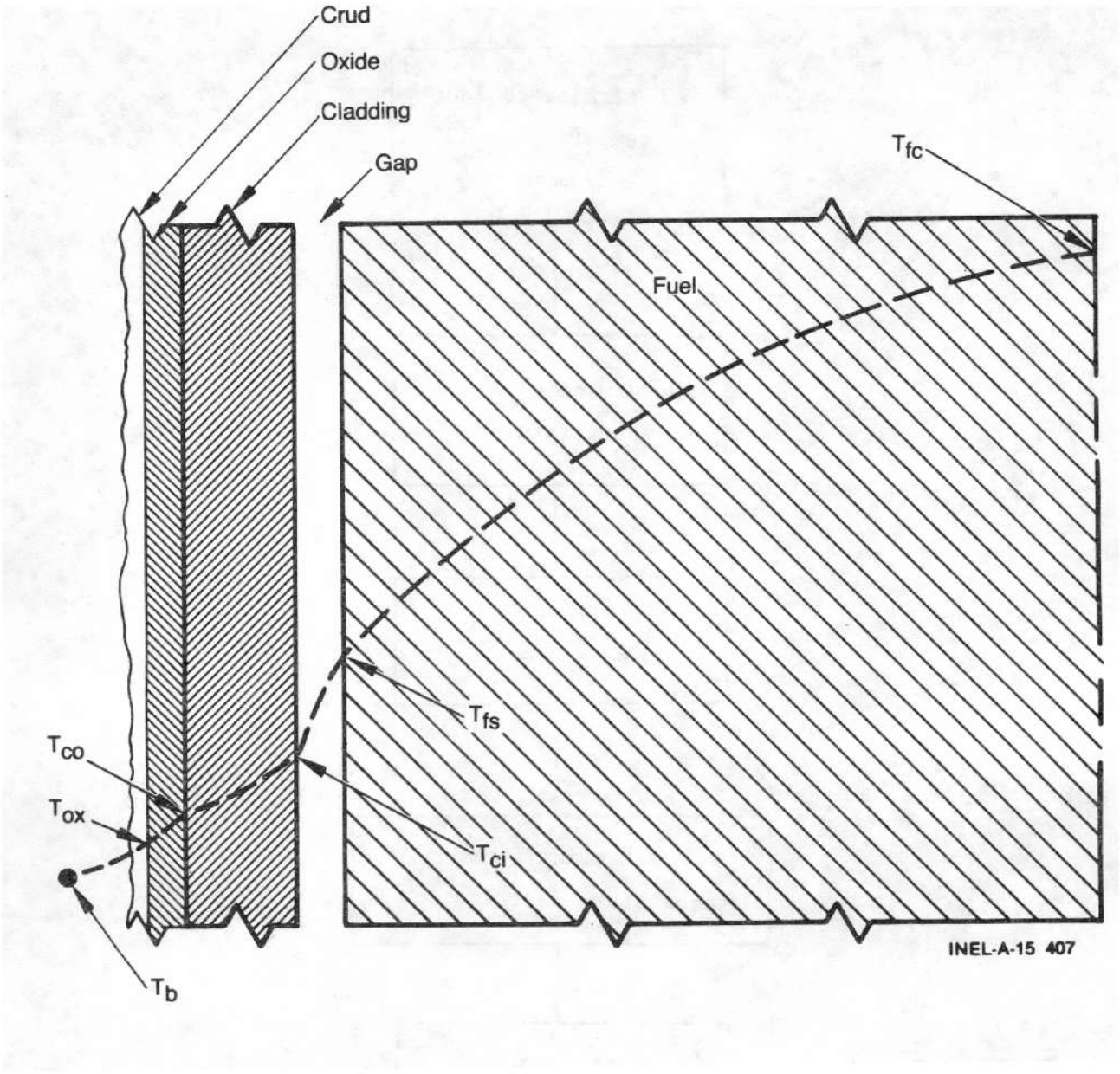

Figure 4. Schematic of the fuel rod temperature distribution.

The models used in the fuel rod temperature calculations assume a cylindrical fuel rod surrounded by coolant. User supplied boundary conditions (coolant inlet temperature, coolant channel equivalent heated diameter, and the coolant mass flux) and the user supplied axial linear heat generation rate are used to calculate the

coolant bulk temperature, T_b, using a single channel coolant enthalpy rise model. A film temperature rise, T_f, is then calculated from the coolant to the surface of the fuel rod through any crud layer which may exist. The cladding inside surface temperature, T_{ci}, is found by calculating the temperature rise across the zirconium oxide and the cladding using Fourier's Law. The temperature rise to the fuel surface is determined from an annular gap conductance model, thereby establishing the fuel surface temperature, T_{fs}. Finally, the temperature distribution in the fuel is calculated, accounting for fuel cracking effects using the fuel surface temperature and assumed symmetry at the centerline as boundary conditions.

The models used in the temperature calculations involve a number of assumptions and limitations. The most important are:

1. No heat conduction in the axial direction

2. No heat conduction in the azimuthal direction

3. Constant boundary conditions during each time step

4. Steady state

5. The fuel rod is a right circular cylinder surrounded by water coolant.

2.3.1 Coolant Conditions. FRAPCON-2 calculates bulk coolant temperatures assuming a single, closed coolant channel according to

$$T_b(z) = T_{in} + \int_o^z \left[\frac{4\dot{q}''(z)}{C_p\, GD_e}\right] dz \qquad (2)$$

where

$T_b(z)$ = bulk coolant temperature at elevation z on the rod axis (K)

T_{in} = inlet coolant temperature (K)

$\dot{q}''(z)$ = rod surface heat flux at elevation z on the rod axis (W/m)

C_p = heat capacity of the coolant (J/kg.K)

G = coolant mass flux ($kg/s.m^2$)

D_e = coolant channel heated diameter (m).

2.3.2 Fuel Rod Surface Temperature. The cladding surface temperature at axial elevation z is taken as the minimum value of

$$T_w(z) = T_b(z) + \Delta T_f(z) + \Delta T_c(z) \qquad (3)$$

$$T_w(z) = T_{sat} + \Delta T_{JL} \qquad (4)$$

where

$T_w(z)$ = rod surface temperature at elevation z on the rod axis (K)

$\Delta T_f(z)$ = forced convection film temperature drop at elevation z on the rod axis (K)

$\Delta T_c(z)$ = crud temperature drop at elevation z on the rod axis (K)

T_{sat} = coolant saturation temperature (K)

ΔT_{JL} = nucleate boiling temperature drop at elevation z on the rod axis (K).

The choice of the minimum value is a simple means of deciding whether heat is transferred from the cladding surface to the coolant by forced convection or nucleate boiling. It also provides a smooth numerical transition from forced convection to nucleate boiling thereby avoiding convergence problems. For forced convection heat transfer, the temperature drop across the coolant film layer at the rod surface is based on

$$\Delta T_f(z) = \dot{q}''(z)/h_f \qquad (5)$$

where h_f is the Dittus-Boelter[13] film conductance given by

$$h_f = (0.023k/D_e)\ R_e^{0.8} P_r^{0.4} \quad (6)$$

where

h_f = conductance ($W/m^2.K$)

k = conductivity of the water (W/m.K)

D_e = coolant channel heated diameter (m)

R_e = Reynolds Number

P_r = Prandtl Number.

The temperature drop across the crud is given by

$$\Delta T_c(z) = \dot{q}''(z)\ \frac{\delta_c}{k_{cr}} \quad (7)$$

where

δ_c = crud thickness (m)

k_{cr} = crud thermal conductivity

= 0.8648 (W/m.K).

For nucleate boiling heat transfer, the temperature drop across the coolant film layer at the rod surface is based on the Jens-Lottes[14] formulation

$$\Delta T_{JL}(z) = 60 \left[\dot{q}''(z)/10^6\right]^{0.25} / e^{(P/6.2 \times 10^6)} \qquad (8)$$

where

P = system bulk coolant pressure (Pa).

No additional temperature drop from the cladding surface to the coolant is assumed to occur due to crud deposition when nucleate boiling exists. The coolant is assumed to boil through the crud blanket.

The temperature drop across the zirconium oxide layer at elevation z on the rod axis is determined by

$$\Delta T_o(z) = \frac{\dot{q}''(z)\ \delta_o(z)}{k_o} \qquad (9)$$

where

$\Delta T_o(z)$ = oxide temperature drop at elevation z on the rod axis (K)

$\delta_o(z)$ = oxide thickness at elevation z on the rod axis (m)

k_o = oxide thermal conductivity (W/m.K).

2.3.3 Cladding Temperature Drop. The cladding temperature drop for each axial location is calculated according to the following expression for steady state heat transfer through a cylinder with uniform thermal conductivity:

$$\Delta T_{clad} = \dot{q}''(z) r_o \ln(r_o/r_i)/k_{clad} \quad (10)$$

where

ΔT_{clad} = cladding temperature drop (K)

r_o = cladding outside radius (m)

r_i = cladding inside radius (m)

k_{clad} = temperature and material dependent thermal conductivity of the cladding (W/m.K).

2.3.4 Fuel-Cladding Gap Temperature Drop. The fuel-cladding gap conductance is the sum of three components: the conductance due to radiation, the conduction through the gas, and the conduction through regions of solid-solid contact. The equations and models for each of these components are discussed below.

Radiation Heat Transfer--The net radiant heat transfer of heat from the fuel to the cladding is the infinite-cylinder, gray body form as derived by Kreith[15] and others:

$$\text{Net surface heat flux (S.H.F)} = \sigma F \left[T_{fs}^4 - T_{ci}^4\right] \qquad (11)$$

where

$F = 1/\left[\, 1/e_f + (r_{fs}/r_{ci})\,(1-1/e_c)\,\right]$

σ = Stefan-Boltzman constant

= 5.6697×10^{-8} $(W/m^2.K^4)$

e_f = fuel emissivity

e_c = cladding emissivity

T_{ci} = fuel surface temperature (K)

T_{fs} = cladding inner surface temperature (K)

r_{fs} = fuel outer surface radius (m)

r_{ci} = cladding inner surface radius (m).

The conductance due to radiation, h_r $(W/m^2.K)$, is defined by

$$h_r (T_{fs} - T_{ci}) = S.H.F. \quad (12)$$

Combining Equations (11) and (12) and dividing by $(T_{fs} - T_{ci})$ gives

$$h_r = \sigma F [T_{fs}^2 + T_{ci}^2] [T_{fs} + T_{ci}] \quad (13)$$

Conduction Through The Interfacial Gas--The form of the conductance due to conductive heat tranfer through the gas in the fuel-cladding gap gas , h_{gas} $(W/m^2.K)$, is that universally applied to small annular gaps:

$$h_{gas} = \frac{k_{gas}}{d + (g_1 + g_2)} = \frac{k_{gas}}{\Delta x} \quad (14)$$

where

d = effective physical gap width (m)

k_{gas} = gas thermal conductivity (W/m.K)

(g_1+g_2) = temperature jump distances at fuel and cladding surfaces, respectively (m)

ΔX = total effective gap width (m).

The various mechanical modeling options separately contribute values of Δx. If either of the FRACAS mechanics options are chosen, Δx is given by[16]

$$\Delta x = 1.8\,[d_{eff} + g_1 + g_2] - b + d \qquad (15)$$

where

d = value from FRACAS for open fuel-cladding gap size (m)

d_{eff} = $2\exp(-0.00125P)\,(R_1 + R_2)$ for closed fuel-cladding gaps (m)

= $2\,(R_1 + R_2)$ for open fuel-cladding gaps (m)

P = fuel-cladding interfacial pressure (kg/cm^2)

R_1+R_2 = cladding plus fuel surface roughness (m)

b = 1.397×10^{-6} (m).

If the PELET option is chosen, fuel-cladding contact is always assumed, and

$$\Delta x = d_{eff} + 1.8\,(g_1 + g_2) \qquad (16)$$

where d is defined in the PELET/RADIAL model.

In either case, the quantity $(g_1 + g_2)$ is calculated from the GAPCON-2[16] model which is

$$(g_1 + g_2) = A\left[\frac{k_{gas}\sqrt{T_{gas}}}{P_{gas}}\right]\left[\frac{1}{\sum a_i f_i/\sqrt{M_i}}\right] \quad (17)$$

where

A = 0.7816

k_{gas} = gas conductivity (W/m.K)

P_{gas} = gas pressure (Pa)

T_{gas} = average gas temperature (K)

a_i = accommodation coefficient of i-th gas component

M_i = gram-molecular weight of i-th gas component (Kg. moles)

f_i = mole fraction of i-th gas component.

Conductance Through Points of Contact--The FRACAS and PELET mechanics models utilize expressions for h_{solid} which are similar in form but differ in magnitude. If the FRACAS models are selected, h_{solid} is dependent on both the fuel-cladding interfacial pressure

and the microscopic roughnesses, R, as follows

$$
\begin{aligned}
h_{solid} &= A\ km\ P_{rel}/RE, && P_{rel} > 0.01 \\
&= A\ km\ (0.01)/RE, && 0.01 > P_{rel} > 0.0001 \\
&= A\ km\ P_{rel}^{0.5}/RE, && P_{rel} < 0.0001
\end{aligned}
\tag{18}
$$

where

P_{rel} = ratio of interfacial pressure to cladding Meyer hardness

Km = mean conductivity (W/m.K)

$= 2K_f K_c / (K_f + K_c)$

$R = \sqrt{R_1^2 + R_2^2}$ (m)

K_c = cladding thermal conductivity (W/m.K)

K_f = fuel thermal conductivity (W/m.K)

E = $\exp[-3.51 - 0.528 \ln(R_1)]$.

The above comes from a fit to Ross and Stoute[17] data plus that by Rapier[18] using the Mikic-Todreas model.[19]

If the PELET option is chosen, h_{solid} is dependent only upon fuel-cladding interfacial pressure, according to the relation

$$h_{solid} = 0.038 + 0.017\ P_{int}\ (w/cm^2.k) \qquad (19)$$

where

P_{int} = fuel-cladding interfacial pressure (MPa).

This equation is an estimatec fit to recent out-of-pile cata by J. A. Garnier.[20]

2.3.5 Pellet Heat Conduction. The pellet temperature distribution is calculated using the Method of Weighted Residuals proposed by Finlayson.[21] The method is described below.

2.3.5.1. General Procedures--The model used to solve the steady state radial heat transfer in the fuel is based on the assumption that the fuel is a homogeneous, continuous right circular cylinder with a constraint surface temperature about its perimeter. The method used has been extended to handle a restructured zone. Heat conduction in the radial direction in the fuel is described by

$$\frac{d^2T(r)}{dr^2} + \frac{1}{r}\frac{dT}{dr} + \frac{1}{K(T)}\left(\frac{dK}{dT}\right)\left(\frac{dT}{dr}\right)^2 + \frac{Q(r)}{K} = 0 \qquad (20)$$

where

$T(r)$ = the fuel temperature (K)

$Q(r)$ = the volumetric heat generation rate (W/m^3)

K = the conductivity of the fuel (W/m.K).

The equation is nonlinear because of the temperature dependence of the fuel conductivity. The boundary conditions are

$$T\Big|_{r = r_{FS}} = T_{FS} \tag{21}$$

and

$$\frac{dT}{dr}\Big|_{r = r_I} = 0 \tag{22}$$

where

r_I = fuel inner radius (m)

r_{FS} = fuel outer radius (m)

T_{FS} = fuel surface temperature (K).

There are several methods which can be used to solve Equation (20). The method used in FRAPCON-2 is a collocation technique using the method of weighted residuals, and has the following advantages: (a) the solution time on a computer is minimal, and (b) coefficients are produced which permit calculation of correct temperatures at any radial position in the fuel without resolving the entire problem. The specific steps used are a slight variation of the method proposed by B. A. Finlayson, and proceed as follows:

1. A trial solution of the form $T = \sum_{j=1}^{N+2} d_j r^{j-1}$ is assumed, where the d_j are unknown coefficients.

2. To find estimates of the d_j, Equation (20) is forced to be satisfied at N collocation points within the fuel or annular subregion. This requirement plus the boundary conditions result in N+2 simultaneous equations for the N+2 d_j coefficients. Fourth-order (4 point) collocation has been found to yield temperatures accurate to within 1 K compared with exact solutions. Thus, six coefficients are generated.

3. In order to solve the six simultaneous equations, the terms involving conductivity are considered known by evaluating the conductivity using temperatures from the previous iteration. The temperatures for the very first iteration are calculated using a constant typical value for the conductivity.

4. The procedure is repeated until convergence of the

temperatures occurs.

2.3.5.2 Formulation of Equations for c_j--To avoid reformulating the equations for each gap conductance iteration, it is convenient to perform the calculations in the normalized coordinate, $y = r/r_{FS}$. With this variable change, Equation (20) becomes

$$\frac{d^2T(y)}{dy^2} + \frac{1}{y}\frac{dT}{dy} + \frac{1}{K(T)}\frac{dK}{dT}\left(\frac{dT}{dy}\right)^2 + \frac{Q(y)r_{FS}^2}{K} = 0 \qquad (23)$$

with boundary conditions

$$\left.\frac{dT}{dy}\right|_{y = y_I} = 0 \qquad (24)$$

$$\left.T\right|_{y = 1} = T_{FS}. \qquad (25)$$

Using the collocation technique, six simultaneous equations are formulated as

$$\left.\frac{dT_n}{dy}\right|_{y = y_I} = 0 \qquad i = 1 \qquad (26)$$

$$\left.\frac{d^2T_n}{dy^2}\right|_{y=y_i} + \frac{1}{y_i}\left.\frac{dT_n}{dy}\right|_{y=y_i} = \frac{1}{K_{n-1}}\left[r_{RS}^2 Q_i + \left(\frac{dK_{n-1}}{dT_i}\right)\left(\left.\frac{dT_{n-1}}{dy}\right|_{y=y_i}^2\right)\right] \quad i=2,3,4 \text{ and } 5 \qquad (27)$$

$$T_n \Big|_{y=1} = T_{FS} \qquad i = 6 \tag{28}$$

where subscripts n and n-1 refer to the current and previous iteration, respectively, and

$$Q_i = Q(y_i), \tag{29}$$

$$K_{n-1} = K(T_{n-1}) \tag{30}$$

$$\frac{dK_{n-1}}{dT_i} = \frac{dK}{dT}\Big|_{T=T_{n-1}(y_i)} . \tag{31}$$

The equations for i = 2 through 5 need to be modified by eliminating the term

$$\left(\frac{dT_{n-1}}{dy}\Big|_{y=y_i}\right)^2 \tag{32}$$

The most accurate way to do this is to use the relationship

$$-K\frac{dT}{dr}\Big|_{r=r_i} = \text{surface heat flux at } r_i = 2\pi\int_{r_I}^{r_i} Q(r)\, r dr / \pi 2r . \tag{33}$$

Q(r) is expressed as $Q(r) = N(Z + YYr^2 + Wr^4)$ where N is a normalization constant which transforms Q(r) into physical units. Thus, Equation (33) becomes

$$-K\frac{dT}{dr} = \frac{N}{r}\left[\frac{Z}{2}(r^2 - r_I^2) + \frac{YY}{4}(r^4 - r_I^4) + \frac{W}{6}(r^6 - r_I^6)\right] . \tag{34}$$

Transforming to normalized coordinates and solving for $\left.\frac{dT}{dy}\right|_{y=y_i}$ Equation (34) becomes

$$\left.\frac{dT}{dy}\right|_{y=y_i} = -\left(\frac{Nr_{FS}^2}{y_i K}\right)\left[\frac{Z}{2}(y_i^2 - y_I^2) + \frac{YY}{4}(y_i^4 - y_I^4) + \frac{W}{6}(y_i^6 - y_I^6)\right] \tag{35}$$

$$= \left[\frac{N\, r_{FS}^2}{y_i K}\right] C_i \equiv I_i . \tag{36}$$

Thus, the collocation equations i = 2 through 5 can be written as

$$T_n(y_i) = \sum_{j=1}^{6} d_j\, y_i^{j-1} \tag{37}$$

with I defined in Equation (36). Substituting the following expression into Equation (37),

$$\left.\frac{d^2T}{dy^2}\right|_{y=y_i} + \frac{1}{y_i}\left.\frac{dT}{dy}\right|_{y=y_i} = \frac{-1}{K_{n-1}}\left[r_{FS}^2 Q_i + \left(\frac{dK_{n-1}}{dT_i}\right) I_i^2\right] \tag{38}$$

the following six equations are obtained:

$$\sum_{j=1}^{6} d_j \left[(j-1)y_i^{\,j-2}\right] = 0 \qquad i = 1 \tag{39}$$

$$\sum_{j=1}^{6} d_j \left[(j^2-2j+1)y_i^{\,j-3}\right] = \frac{-1}{K_{n-1}} \left[r_{FS}^{\,2} Q_i + \left(\frac{dK_{n-1}}{dT_i}\right) I_i^{\,2}\right] \quad i = 2,3,4, \text{ and } 5 \tag{40}$$

$$\sum_{j=1}^{6} d_j = T_{FS} \qquad i = 6 \tag{41}$$

In matrix form, the above set can be written as

$$[A]\begin{pmatrix} d_1 \\ d_2 \\ d_3 \\ d_4 \\ d_5 \\ d_6 \end{pmatrix} = \begin{pmatrix} 0.0 \\ B_2 \\ B_3 \\ B_4 \\ B_5 \\ T_{FS} \end{pmatrix} \tag{42}$$

where

$$\left.\begin{aligned} A_{ij} &= (j-1)y_I^{(j-2)}, && i = 1 \\ &= (j^2 - 2j + 1)y_i^{j-3}, && i = 2,3,4,5 \\ &= 1.0 && i = 6 \end{aligned}\right\} \; j = 1,2,3,4,5,6 \qquad (43)$$

and

$$B_i = \frac{-1}{K_{n-1}} \left[r_{FS}^{\,2} Q_i + \left(\frac{dK_{n-1}}{dT_i} \right) I_i^{\,2} \right], \; i = 2,3,4,5. \qquad (44)$$

Notice that in succeeding iterations, the matrix A need not be recalculated, but only the B_i.

This procedure can be applied to annular subregions of the fuel, which are then coupled by the condition of temperature and heat flow continuity between regions. The motive for doing so comes from the possibility for deviation in the fuel thermal conductivity function above and below a transition temperature (see Section 2.3.7).

2.3.6 Plenum Gas Temperature. The plenum gas temperature is calculated based on energy transfer between the top of the pellet stack and the plenum gas, between the coolant channel and the plenum gas, and between the spring and the plenum gas. A discussion of these contributions follows.

Natural convection from the top of the fuel stack is calculated based on heat transfer coefficients from McAdams[22] for laminar or turbulent natural convection from flat plates.

The heat transfer coefficient is calculated from

$$h_p = \frac{k\ Nu}{D} \qquad (45)$$

where

h_p = the heat transfer coefficient from the top of the pellet stack to the plenum gas ($w/m^2.K$)

Nu = Nusselt Number

D = inside diameter of the cladding of the top node (m)

K = conductivity of the plenum gas (w/m.K).

The Nusselt Number is calculated using

$$Nu = C(GrPr)^m \qquad (46)$$

where

Gr = the Grashof Number

Pr = the Prandtl Number

and for

$GrPr \leq 2.0 \times 10^7$, C = 0.54 and m = 0.25,

or

$GrPr > 2.0 \times 10^7$ C = 0.14 and m = 0.33.

The overall effective conductivity from the coolant to the plenum is defined as the inverse of the sum of the individual heat flow resistances. The three resistances are (a) the resistance across the inside surface film, (b) the resistance across the cladding, and (c) the resistance across the outside surface film. The overall conductivity is therefore found as

$$U_c = \frac{1.0}{\frac{2.0}{D\,h_f} + \frac{\ln\left(\frac{D_o}{D_i}\right)}{k_{clad}} + \frac{2.0}{D_o\,(1.0 + \alpha\Delta T)\,h_{DB}}} \qquad (47)$$

where

U_c = overall effective conductivity from the coolant to the plenum gas (w/m.K)

D = hot-state inside cladding diameter (m)

h_f = cladding inside surface film coefficient ($w/m^2.K$)

D_o = cold-state outsice cladding diameter (m)

D_i = cold-state inside cladding diameter (m)

k_{clad} = temperature anc material dependent thermal conductivity of the cladding (w/m.k)

α = coefficient of thermal expansion of the cladding (1/K)

ΔT = temperature difference between cladding average temperature and datum temperature (K)

h_{DB} = heat transfer coefficient between the coolant and the cladding ($W/m^2.K$).

Gamma heating in the hold down spring is calculated assuming a volumetric heating rate of 3.76 w/m^3 for every W/m^2 of rod average heat flux. The expression is

$$Q_{sp} = 3.76\ \dot{q}''\ V_s \qquad (48)$$

where

Q_{sp} = energy generated in the spring due to gamma heating (W)

$\dot{q}''$ = average heat flux of the rod (W/m^2)

V_s = volume of the spring (m^3).

The plenum temperature is approximated from

$$T_{plen} = \frac{Q_{sp} + U_c \frac{V_p}{D^2} T_{BLK} + T_{pa} h_p \pi D^2/4}{U_c \frac{V_p}{D^2} + \frac{h_p \pi D^2}{4}} \quad (49)$$

where

T_{plen} = plenum temperature (K)

V_p = volume of the plenum (m^3)

T_{BLK} = bulk coolant temperature at the top axial node (K)

T_{pa} = temperature associated with the insulator or top pellet (K).

2.3.7 Effective Fuel Conductivity. The thermal conductivity of cracked fuel is not the same as that of uncracked fuel. In order to compute the effective thermal conductivity of cracked fuel, a conductivity factor, R, is applied to the uncracked fuel conductivity. The conductivity factor is

$$k_{eff} = R\, k_{lab} \quad (50)$$

where

k_{eff} = effective fuel thermal conductivity (w/m.K)

k_{lab} = uncracked fuel thermal conductivity as a function of temperature (w/m.K).

2.3.7.1 The Cracked Conductivity Factor Used with FRACAS--The cracked conductivity factor used with FRACAS is an empirical correlation which accounts for the presence of cracks in the fuel. This correlation was developed from fuel centerline and off-center thermocouple data taken as part of the gap conductance tests series[23] performed in the Power Burst Facility at the Idaho National Engineering Laboratory. The equation for R is

$$R = 1.0 - C\, C_{rel} \left[1.0 - \frac{k_g}{k_{lab}} \right] \tag{51}$$

where

C = 0.30 (1/m) for FRACAS-I

= 0.48 (1/m) for FRACAS-II

C_{rel} = $\dfrac{3\delta\ (\delta_s - \delta_T)}{r_p V\ (0.8 \times 10^{-4})}$ (m) for FRACAS-I

= $\dfrac{V}{4\ r_p\ (0.8 \times 10^{-4})}$ (m) for FRACAS-II

k_g = conductivity of gas in gap (W/m.K)

δ = as-fabricated fuel-cladding gap size (m)

δ_s = fuel-cladding gap size assuming no fuel surface relocation (m)

δ_T = fuel-cladding gap size assuming fuel surface relocation (m)

r_p = as-fabricated pellet radius (m)

and k_{lab} is as used in Equation (5C).

The term $(1-k_g/k_{lab})$ accounts for the fact that the gas in the cracks in the fuel has a lower conductivity than the fuel, and thus degrades the effective conductivity of the fuel.

C_{rel} is a measure of the instantaneous volume available for cracking. This term decreases as the fuel-cladding gap size decreases. Recognizing that cracked fuel can never fully reconsolidate, this term is never allowed to be less than 0.25. C was chosen to best fit the experimental data base for rods containing He, Xe, and Ar.

Crack healing is assumed when the local fuel temperature reaches or exceeds some transition temperature. The transition temperature has been chosen to be nine-tenths of the user-specified fuel sintering temperature. Crack healing is enforced as

$$R = 1.0 \text{ when } T_r \geq T_{trans} \quad (52)$$

where

T_r = local fuel temperature (K)

T_{trans} = fuel transition temperature (K).

Assumptions made are that (a) cracks instantaneously heal when fuel regions are above the transition temperature, (b) once a region has healed no recracking of that region occurs and (c) the relative gas and fuel conductivities are laboratory values.

2.3.7.2 The Effective Fuel Conductivity Used with PELET/RADIAL--The effective value of the fuel thermal conductivity is degraded by fuel cracking. This follows directly from the observation that the cracks in fuel pellets observed in postirradiation examinations have nonradial components. As noted in Section 2.2.2, certain assigned values for crack length and fuel and gap roughness are given to various rods from which in-reactor power/temperature measurements are available. The assignment of these values permits the calculation of fuel-cladding gap size, gap conductance, and hydrostatic fuel stress. From the gap conductance, fuel surface temperature can be estimated. The estimated surface temperature, T_s, and measured fuel centerline temperature, T_c, can be used to calculate the effective fuel conductivity as

$$CFAC \int_{T_s}^{T_c} K_M dT = \frac{Pf}{4\pi} \qquad (53)$$

where

P = linear heat generation rate (W/m)

f = flux depression factor (dimensionless function of enrichment)

CFAC = effective fuel conductivity factor

K_M = intrinsic or "laboratory" function for fuel conductivity (W/m.K).

Generally, CFAC is found to be less than 1.0. A plot of CFAC values versus the corresponding fuel hydrostatic stress is shown for various Halden rods in Figure 5.

Note in Figure 5 that the CFAC values for all of the helium filled rods tend to overlap (except at exceedingly low stress) and tend to be linear. Similarly the data from the mixed-gas rod also tend to be linear. This is the basis for the correlation that is applied in FRAPCON-2 when the PELET/RADIAL option is used. The dependence of the conductivity for a given rod is nearly linear, but the slope and intercept of the lines are functions of the gas

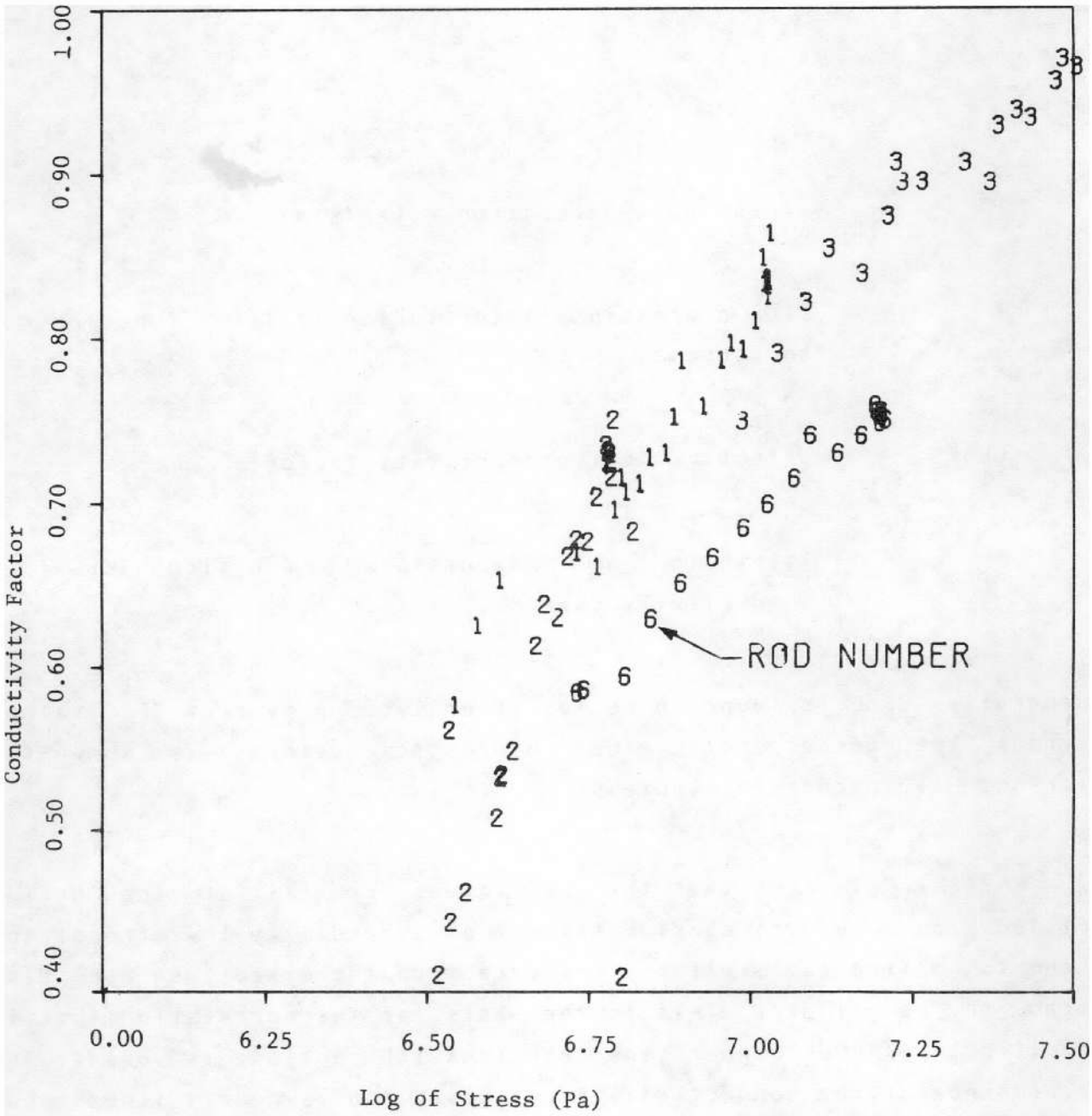

Figure 5. Thermal conductivity factor versus hydrostatic stress (data points identified by rod number).

conductivity relative to that for pure helium.

Figure 6 shows the correlation for CFAC as it is applied in RADIAL. Note that the low-cutoff for the conductivity multiplier (CFAC) has been arbitrarily chosen as 0.3. Note also that even at zero power, converged values for the hydrostatic stress are in excess of 1.4×10 Pa (200 psia) which is why the correlation is based on the intercept at log(stress) = 6 plus the slope estimated from data. The correlations for intercept and slope of CFAC versus log(stress) as a function of gas conductivity ratio (the gas conductivity ratio is defined as the ratio of current gas conductivity to pure helium gas conductivity) are shown in Figures 7 and 8, respectively. Note that combinations of slope, intercept and log(stress) resulting in CFAC values less than 0.3 are discounted since 0.3 is the low-value cutoff for CFAC.

2.3.8 Stored Energy. The stored energy in the fuel rod is calculated by summing the energy of each pellet ring calculated at the ring temperature. The expression for stored energy is

$$E_s = \frac{\sum_{i=1}^{I} m_i \int_{298\ K}^{T_i} C_p(t)dT}{m} \qquad (54)$$

where

E_s = stored energy (J/kg)

m_i = mass of ring segment i (kg)

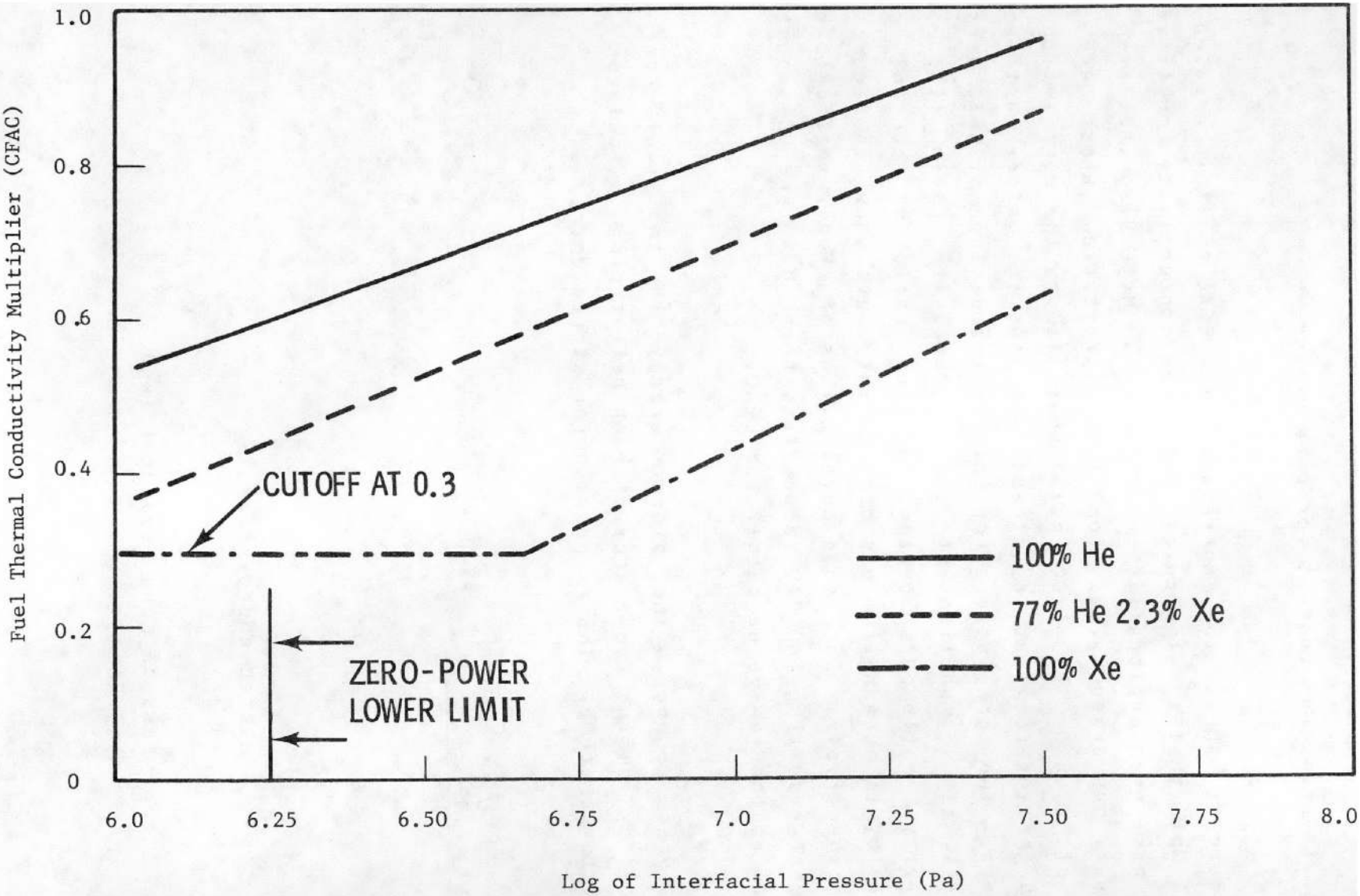

Figure 6. Fuel conductivity multiplier (CFAC) as a function of interfacial pressure and gas composition.

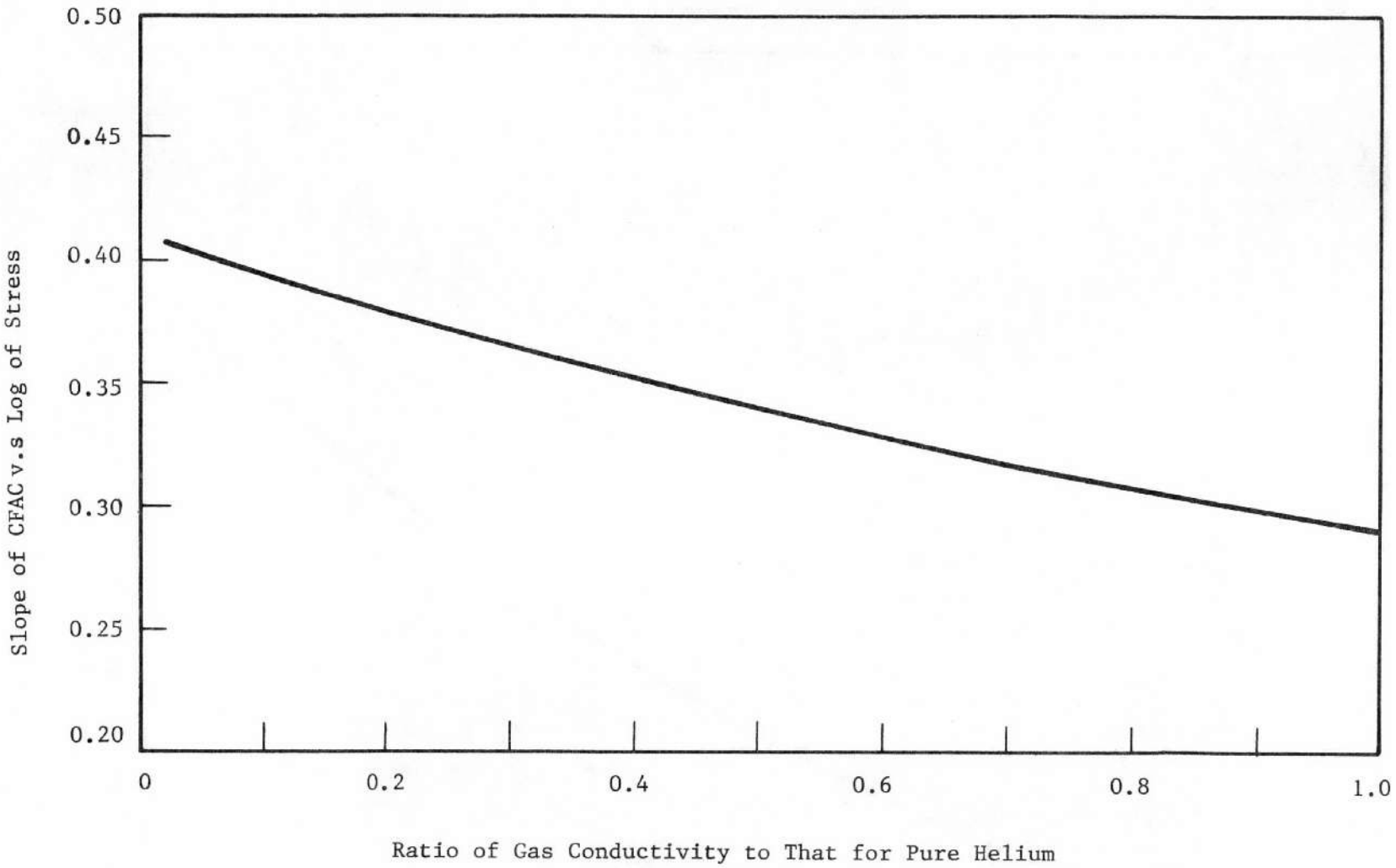

Figure 7. Slope of CFAC versus log (pressure) curve as a function of fill gas conductivity.

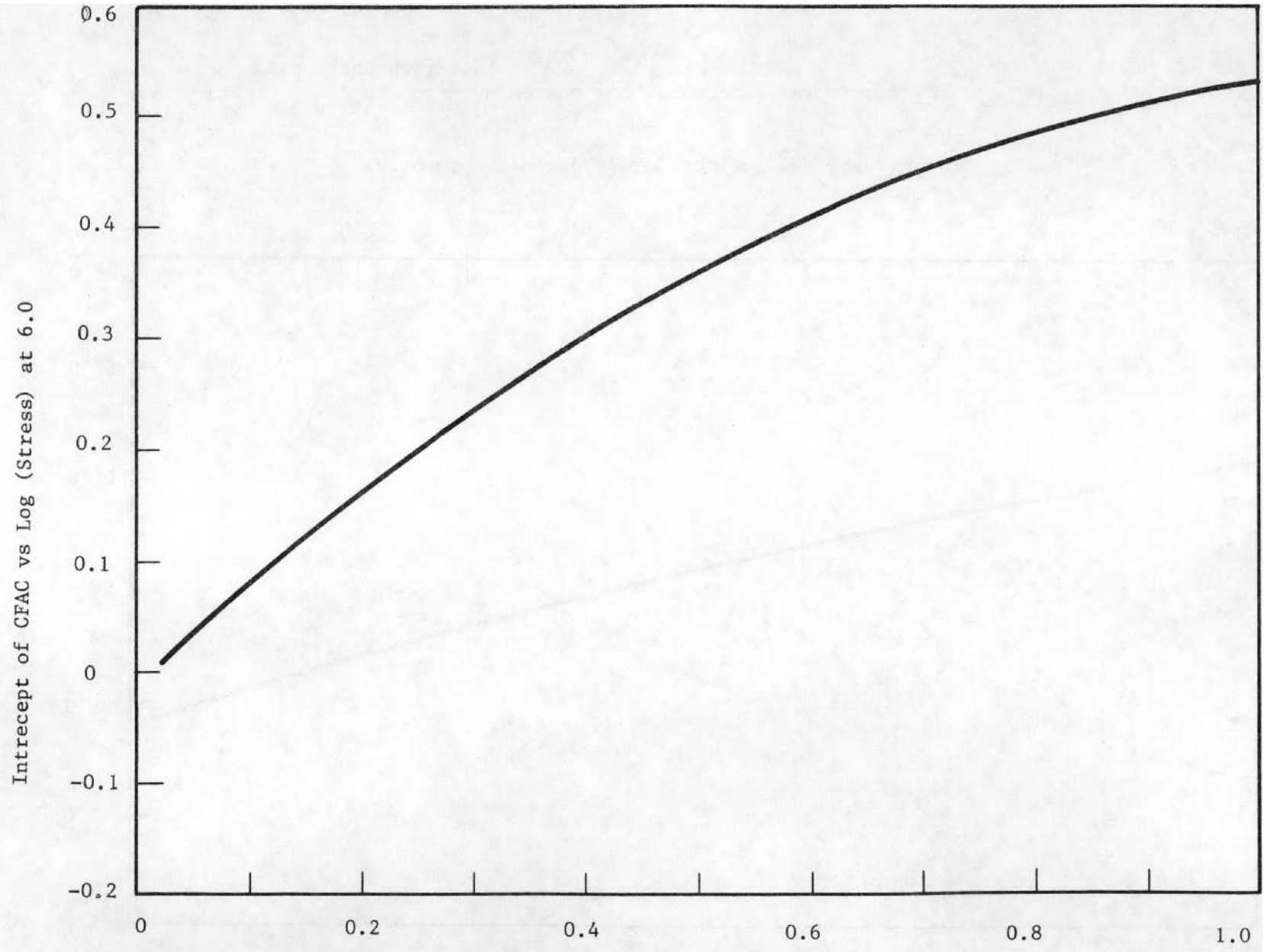

Figure 8. Intercept of CFAC versus log (pressure) curve (at 6.0) as a function of fill gas conductivity.

T_i = temperatue of ring segment i (K)

$C_p(T)$ = specific heat evaluated at temperature T (J/kg.K)

m = total mass of the axial node (kg)

I = number of annular rings.

The stored energy is calculated for each axial node.

2.4 Fuel Rod Mechanical Response

An accurate calculation of fuel and cladding deformation is necessary in any fuel rod response analysis because the heat transfer coefficient across the fuel-cladding gap is a function of both the effective fuel-cladding gap size and the fuel-cladding interfacial pressure. In addition, an accurate calculation of stresses in the cladding is needed so that an accurate calculation of the onset of cladding failure (and subsequent release of fission products) can be made.

FRAPCON-2 has four deformation modeling options: FRACAS-I, FRACAS-II, PELET/RADIAL and AXISYM. The models are described in the following sections.

2.4.1 The FRACAS Models. Two FRACAS models are available for the calculation of the small displacement deformation of the fuel and cladding. The more simplified model, FRACAS-I, neglects the stress-induced deformation of the fuel, and is called the rigid pellet

model. The second option, FRACAS-II, includes stress-induced fuel deformation, and is called the deformable pellet model.

In analyzing the deformation of fuel rods, two physical situations are envisioned. The first situation occurs when the fuel and cladding are not in contact. Here the problem of a cylindrical shell (the cladding) with specified internal and external pressures and a specified cladding temperature distribution must be solved. This situation is called the "open gap" regime.

The second situation envisioned is when the fuel (considerably hotter than the cladding) has expanded so as to be in contact with the cladding. Further heating of the fuel results in "driving" the cladding outwardly. This situation is called the "closed gap" regime. Alternatively, this closed gap regime can occur due to the creep of the cladding onto the fuel due to elevated cladding temperatures and a high coolant pressure.

The preceding two regimes of fuel rod deformation are characterized by small cladding strains and by the cladding retaining its essentially cylindrical shape.

The deformation analysis in FRAPCON-2 consists of a small-deformation analysis and when using FRACAS-I, a cladding failure analysis. A small deformation analysis of the stresses, strains and displacements in the fuel and cladding is performed first for the entire fuel rod. This analysis is based on the assumption that the cladding retains its cylindrical shape during deformation, and includes the effects of:

1. Fuel thermal expansion, creep, swelling, densification and

relocation

2. Cladding thermal expansion, creep and plasticity

3. Fission gas and external coolant pressures.

As part of the small displacement analysis, the applicable local deformation regime (open gap, or closed gap) is determined. Finally, an analysis is performed to determine if cladding failure has occurred.

In Section 2.4.1.1, the general theory of plastic analysis is outlined and the method of solution used in the FRACAS models is presented. This method of solution is used in both the rigid pellet and deformable pellet models. In Sections 2.4.1.2, and 2.4.1.3, the equations for the rigid pellet model and deformable pellet model, respectively, are described.

2.4.1.1 General Theory and Method of Solution--The general theory of plastic analysis and the method of solution are used in both the rigid pellet and deformable pellet models.

General Consicerations in Elastic-Plastic Analysis--Problems involving elastic-plastic deformation and multiaxial stress states involve a number of aspects that do not require consideration in a uniaxial problem. In the following discussion, an attempt is made to briefly outline the structure of incremental plasticity, and to outline the Method of Successive Substitutions[22] (also called the Method of Successive Elastic Solutions), which has been used successfully in treating multiaxial elastic-plastic problems. The

method can be used for any problem for which a solution based on elasticity can be obtained. This method is used in both the rigid pellet and deformable pellet models.

In a problem involving only uniaxial stress, σ_1, the strain, ε_1, is related to the stress by an experimentally determined stress-strain curve as shown in Figure 9, and Hooke's law is taken as

$$\varepsilon_1 = \frac{\sigma_1}{E} + \varepsilon_1^P + \int \alpha \, dT \tag{55}$$

where ε_1^P is the plastic strain and E is the modulus of elasticity. The onset of yielding occurs at the yield stress, which can be determined directly from Figure 9. Given a load (stress) history, the resulting deformation can be determined in a simple manner. The increase of yield stress with work-hardening is easily computed directly from Figure 9.

In a problem involving multiaxial states of stress, however, the situation is not as clear. In such a problem, a method of relating the onset of plastic deformation to the results of a uniaxial test is required, and further, when plastic deformation occurs, some means is needed for determining how much plastic deformation has occurred and how that deformation is distributed among the individual components of strain. These two complications are taken into account by use of the so-called "yield function" and "flow rule", respectively.

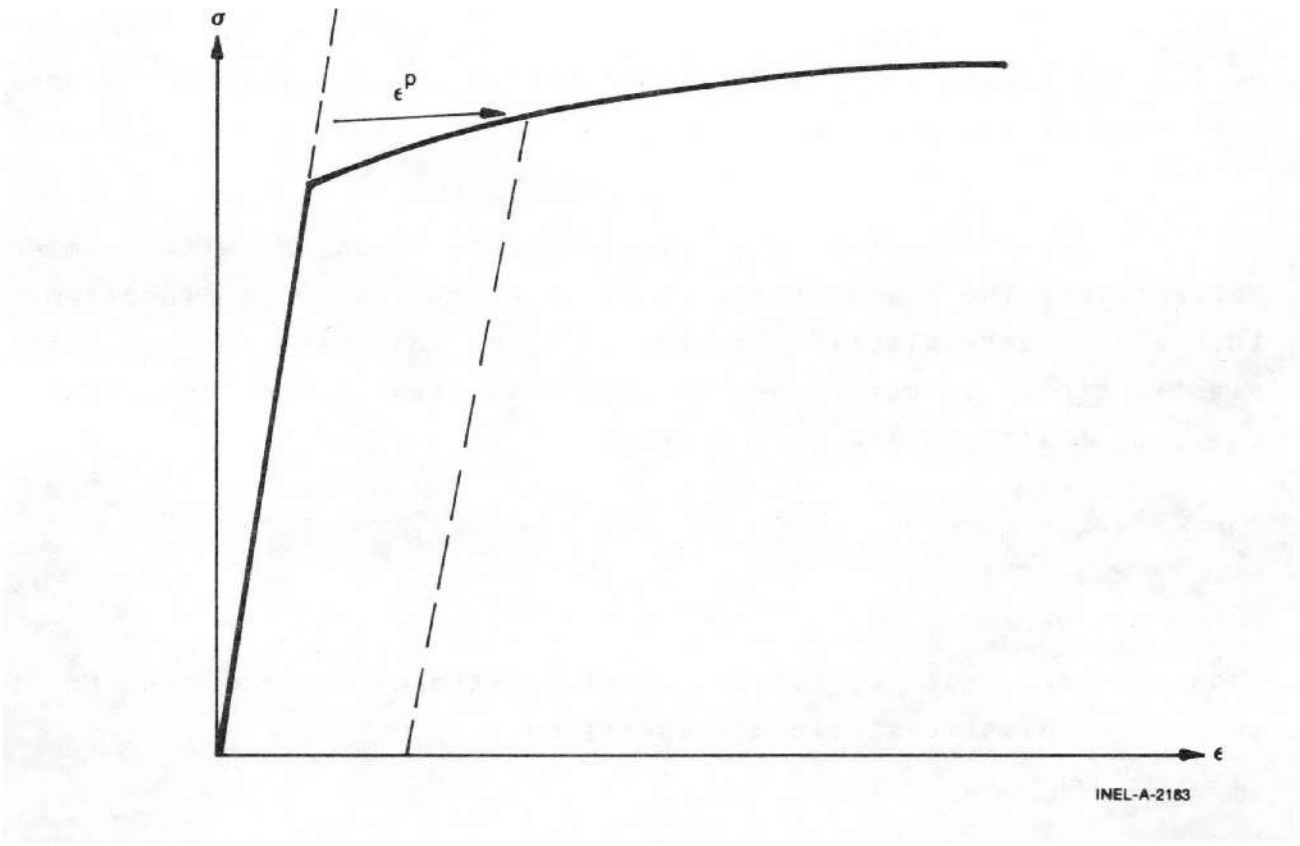

Figure 9. Typical isothermal stress-strain curve.

A considerable wealth of experimental evidence exists on the onset of yielding in a mulitaxial stress state. The bulk of this evidence supports the Von Mises yield criterion, which asserts that yielding occurs when the stress state is such that

$$0.5\ [(\sigma_1 - \sigma_2)^2 + (\sigma_2 - \sigma_3)^2 + (\sigma_3 - \sigma_1)^2] = \sigma_y^2 \qquad (56)$$

where the σ_1 values are the principle stresses, and σ_y is the yield stress as determined in a uniaxial stress-strain test. The square root of the left side of this equation is referred to as the

"effective stress", σ_e, and this effective stress is one commonly used type of yield function.

To determine how the yield stress changes with permanent deformation, the yield stress is hypothesized to be a function of the equivalent plastic strain, ε^P. An increment of equivalent plastic strain is determined at each load step, and ε^P is defined as the sum of all increments incurred:

$$\varepsilon^P \triangleq \sum d\varepsilon^P \tag{57}$$

Each increment of effective plastic strain is related to the individual plastic strain components by

$$d\varepsilon^P = \frac{\sqrt{2}}{3}\left[(d\varepsilon_1^P - d\varepsilon_2^P)^2 + (d\varepsilon_2^P - d\varepsilon_3^P)^2 + (d\varepsilon_3^P - d\varepsilon_1^P)^2\right]^{1/2} \tag{58}$$

where the $d\varepsilon_1^P$ are the plastic strain components in principle coordinates. Experimental results indicate that at pressures on the order of the yield stress, plastic deformation occurs with no change in volume, which implies that

$$d\varepsilon_1^P + d\varepsilon_2^P + d\varepsilon_3^P = 0 \tag{59}$$

Therefore, in a uniaxial test with $\sigma_1 = \sigma$, $\sigma_2 = \sigma_3 = 0$, the plastic strain increments are

$$d\varepsilon_2^P = d\varepsilon_3^P = -1/2\ d\varepsilon_1^P \tag{60}$$

Therefore in a uniaxial test, Equations (56) and (58) reduce to

$$\sigma_e = \sigma \tag{61}$$

$$d\varepsilon^P = d\varepsilon_1^P \tag{62}$$

Thus, when the assumption is made that the yield stress is a function of the total effective plastic strain (called the Strain Hardening Hypothesis), the functional relationship between yield stress and plastic strain can be taken directly from a uniaxial stress-strain curve by virtue of Equations (61) and (62).

The relationship between the magnitudes of the plastic strain increments and the effective plastic strain increment is provided by the Prandtl-Reuss Flow Rule:

$$d\varepsilon_i^P = \frac{3\, d\varepsilon^P}{2\sigma_e} S_i \qquad i = 1,2,3 \tag{63}$$

where the S_i values are the deviatoric stress components (in principal coordinates) defined by

$$S_i = \sigma_i - \frac{1}{3}(\sigma_1 + \sigma_2 + \sigma_3) \qquad i = 1,2,3 \tag{64}$$

Equation (63) embodies the fundamental observation of plastic deformation; that is, plastic strain increments are proportional to the deviatoric stresses. The constant of proportionality is determined by the choice of the yield function.[24] Direct substitution shows that Equations (56), (58), (63), and (64) are

consistent with one another.

Once the plastic strain increments have been determined for a given load step, the total strains are determined from a generalized form of Hooke's law given by

$$\varepsilon_1 = \frac{1}{E}\{\sigma_1 - \nu(\sigma_2 + \sigma_3)\} + \varepsilon_1^P + d\varepsilon_1^P + \int \alpha_1 dT$$

$$\varepsilon_2 = \frac{1}{E}\{\sigma_2 - \nu(\sigma_1 + \sigma_3)\} + \varepsilon_2^P + d\varepsilon_2^P + \int \alpha_2 dT$$

$$\varepsilon_3 = \frac{1}{E}\{\sigma_3 - \nu(\sigma_2 + \sigma_1)\} + \varepsilon_3^P + d\varepsilon_3^P + \int \alpha_3 dT \qquad (65)$$

in which ε_1^P, ε_2^P, and ε_3^P are the total plastic strain components at the end of the previous load increment.

The remaining continuum field equations of equilibrium, strain displacement, and strain compatibility are unchanged. The complete set of governing equations is presented in Table 1, written in terms of rectangular Cartesian coordinates and employing the usual indicial notation in which a repeated Latin index implies summation. This set of equations is augmented by an experimentally determined uniaxial stress-strain relation.

The Method of Solution--When the problem under consideration is statically determinate so that stresses can be found from equilibrium conditions alone, the resulting plastic deformation can be determined directly. However, when the problem is statically indeterminate and the stresses and deformation must be found simulataneously, the full set of plasticity equations proves to be quite formidable, even in the case of simple loadings and

TABLE 1. SUMMARY OF GOVERNING EQUATIONS

Equilibrium

$$\sigma_{ji,j} + \rho f_i = 0$$

where σ = stress tensor

ρ = mass density

f_i = components of body force per unit mass

Stress Strain

$$\varepsilon_{ij} = \frac{1+\nu}{E}\sigma_{ij} - \delta_{ij}\left(\frac{\nu}{E}\sigma_{kk} - \int \alpha dT\right) + \varepsilon^P_{ij} + d\varepsilon^P_{ih}$$

Compatibility

$$\varepsilon_{ij,k\ell} + \varepsilon_{k\ell,ij} - \varepsilon_{ik,j\ell} - \varepsilon_{j\ell,ik} = 0$$

Definitions Used in Plasticity

$$\sigma_e \triangleq \sqrt{\frac{3}{2} S_{ij} S_{ij}}$$

$$S_{ij} \triangleq \sigma_{ij} - \frac{1}{3}\sigma_{kk}$$

$$d\varepsilon^P \triangleq \sqrt{\frac{2}{3} d\varepsilon^P_{ij} \; d\varepsilon^P_{ij}}$$

Prandtl-Reuss Flow Rule

$$d\varepsilon^P_{ij} = \frac{3}{2}\frac{d\varepsilon^P}{\sigma_e} S_{ij}$$

geometries.

One numerical procedure which has been used with considerable success is the Method of Successive Substitutions. This method can be applied to any problem for which an elastic solution can be obtained, either in closed form or numerically. A full discussion of this technique, including a number of technologically useful examples, is contained in Reference 24.

Briefly, the method involves breaking the loading path up into a number of small increments. For example, in the present application, the loads are external pressure, temperature, and either internal pressure or a prescribed displacement of the inside surface of the cladding. These loads all vary during the operating history of the fuel rod. For each new increment of the loading, the solution to all the plasticity equations listed in Table 1 is obtained as follows.

First, an initial estimate of the plastic strain increments, $d\varepsilon_{ij}^{P}$, is made. On the basis of these values, the equations of equilibrium, Hooke's Law, and strain-displacement and compatibility [Equations (119), (121), (125) and (126)] are solved as for any elastic problem. From the stresses so obtained, the deviatoric stresses, S_{ij}, may be computed. This "pseudo-elastic" solution represents one path in the computational scheme.

Independently, through use of the assumed $d\varepsilon_{ij}^{P}$ values, the increment of effective plastic strain, $d\varepsilon^{P}$, may be computed. From this result and the stress-strain curve, a value of the effective stress, σ_e, is obtained.

Finally, a new estimate of the plastic strain increments is obtained from the Prandtl-Reuss flow rule

$$d\varepsilon_{ij}^{P} = \frac{3}{2}\frac{d\varepsilon^{P}}{\sigma_e} S_{ij} \tag{66}$$

and the entire process is continued until the $d\varepsilon_{ij}^{P}$ converge. A schematic of the iteration scheme is shown in Figure 10.

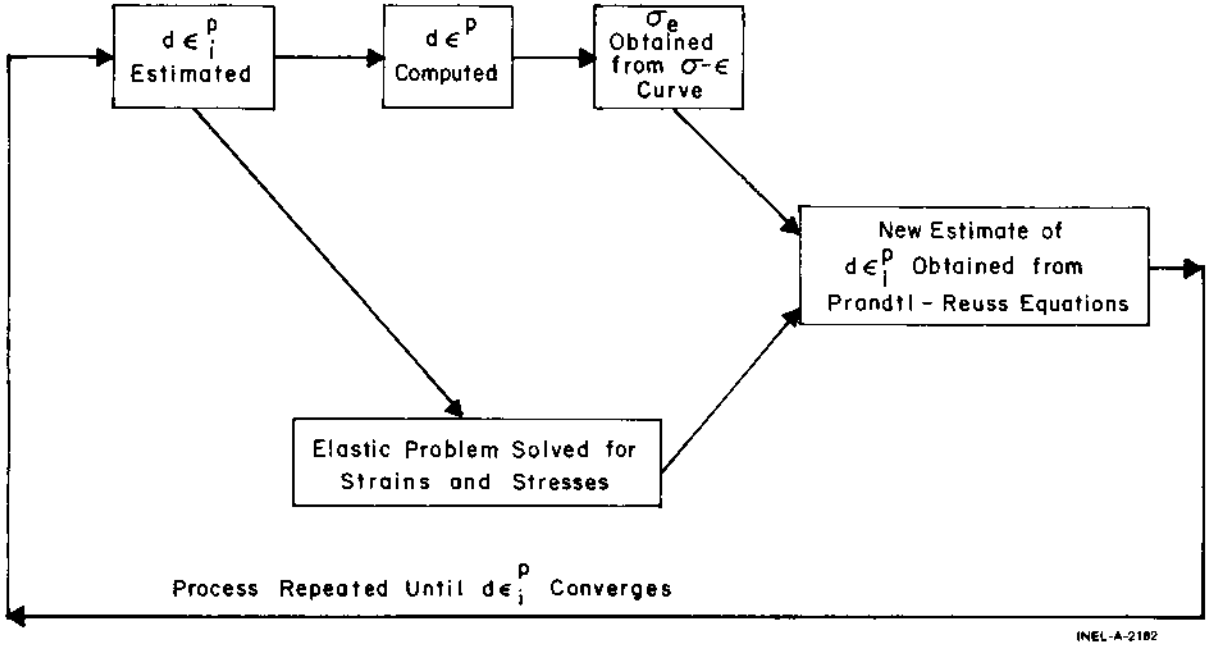

Figure 10. Schematic of the method of successive elastic solutions.

The mechanism by which improved estimates of $d\varepsilon^P_{ij}$ are obtained results from the fact that the effective stress obtained from $d\varepsilon^P$ and the stress-strain curve will not be equal to the effective stress that would be obtained with the stresses from the elastic solution. The effective stresses will only agree when convergence is obtained.

The question of convergence is one that cannot, in general, be answered a priori. However, convergence can be shown[24] to be obtained for sufficiently small load increments. Experience has shown that this technique is suitable for both steady state and transient fuel rod analyses.

Extension to Creep and Hot-Pressing--The method of solution described for the time-independent plasticity calculations can also be used for time-dependent creep and hot-pressing calculations. In this context, the term creep refers to any time-dependent constant volume permanent deformation, whereas the term hot-pressing refers to any time-dependent process which results in a permanent change in volume. Both creep and hot-pressing are stress-driven processes and are usually highly dependent on temperature.

The only change required to extend the Method of Successive Elastic Solutions to allow consideration of creep and hot-pressing is to rewrite the Prandtl-Reuss flow rule [Equation (63)] as

$$d\varepsilon_1^c = 1.5 \frac{\dot{\varepsilon}^c \Delta t}{\sigma_e} S_1 + \frac{\dot{V}^c \Delta t}{9} \frac{(\sigma_1 + \sigma_2 + \sigma_3)}{\sigma_m}$$

$$d\varepsilon_2^c = 1.5 \frac{\dot{\varepsilon}^c \Delta t}{\sigma_e} S_2 + \frac{\dot{V}^c \Delta t}{9} \frac{(\sigma_1 + \sigma_2 + \sigma_3)}{\sigma_m}$$

$$d\varepsilon_3^c = 1.5 \frac{\dot{\varepsilon}^c \Delta t}{\sigma_e} S_3 + \frac{\dot{V}^c \Delta t}{9} \frac{(\sigma_1 + \sigma_2 + \sigma_3)}{\sigma_m} \quad (67)$$

The first term on the right hand side of each of these equations computes the constant volume creep strain, whereas the second term in each equation computes the permanent change in volume. To use this form of the flow rule, two additonal material property correlations must be available. The first is a correlation for constant volume creep strain, ε^c (taken in a uniaxial test), as a function of stress, time, temperature, and neutron flux; that is,

$$\varepsilon^c = f(\sigma, T, t, \dot{F}) \quad (68)$$

where

σ = uniaxial stress (MPa)

T = temperature (K)

t = time (s)

$\dot{F}$ = neutron flux (neutrons/m^2.s).

In the FRACAS models, the strain hardening hypothesis is assumed, which implies that the creep strain correlation can be differentiated and solved for creep strain rate in the form

$$\dot{\varepsilon}^c = h(\sigma, \varepsilon^c, T, \dot{F}) \tag{69}$$

which is no longer an explicit function of time. This equation is obtained from the MATPRO package during the creep calculations.

The second additional correlation required is a relationship between the rate of permanent volumetric strain and the applied loads; that is,

$$\dot{V}^c = g(\sigma_m, T, t, V_{avail}) \tag{70}$$

where

σ_m = $(\sigma_1 + \sigma_2 + \sigma_3)/3$, the mean stress (MPa)

T = temperature (K)

t = time (s)

V_{avail} = measure of maximum permanent volumetric change possible.

The permanent volumetric strain increment dV^c is related to the creep strain increments by the equation

$$dV^c = d\varepsilon_1^c + d\varepsilon_2^c + d\varepsilon_3^c \qquad (71)$$

In FRACAS-II, hot-pressing is considered only in the fuel. The source of the permanent volume change is assumed to be the healing of cracks in the relocated fuel. The maximum amount of volume available for permanent volume change is thus the amount of volume generated by fuel relocation. The equation for the permanent volume change was generated by comparing FRACAS-II calculated and measured length changes for experimental fuel rods irradiated in the Power Burst Facility and the Halden Test Reactor. The correlation which resulted in the best agreement with measured fuel rod length changes was found to be

$$\Delta V = -V[1 - \exp(-A\sigma^B \Delta t)] \qquad (72)$$

where

ΔV = rate of volume change (m^3/s)

A = 1.0×10^{-17}

σ = fuel-cladding interface pressure (MPa)

V = relocation volume remaining (m^3)

Δt = time step size (s)

β = 4.5.

The relocation displacement for the deformable pellet model (FRACAS-II) is computed by the equation

$$U_r = \alpha\delta - \beta \qquad (73)$$

where

δ = as-fabricated fuel-cladding gap size (m)

α = 0.79

β = 0.0334 (m)

This equation for relocation displacement is based on the assumption that the fuel has not been subjected to repeated power cycles, as does the equation for relocation displacement discussed under the heading "fuel surface relocation" in section 2.4.1.2. No positive permanent volume change is permitted, and as the volumetric strain V^c approaches the volume available from relocation, V_{reloc}, the permanent volumetric strain rate goes to zero.

As previously noted, two FRACAS models are available for analyzing the small deformation of the fuel and cladding. The first model considers the fuel pellets to be essentially rigid and to deform due to thermal expansion, swelling, and densification only. Thus, in the rigid pellet model, the displacement of the fuel is calculated independently of the deformation of the

cladding. This rigid pellet analysis is performed with the FRACAS-I subcode.

The second model available for the small deformation analysis is a more general analysis in which the fuel is assumed to deform due to stress, and in this case the deformation of the fuel and cladding must be determined simultaneously. This deformable pellet analysis is performed with the FRACAS-II subcode.

The code user has the option of choosing either the rigid pellet or deformable pellet model. In general, the rigid pellet model (FRACAS-I) is less time-consuming and has proven to be adequate for a wide variety of reactor analysis in which pellet-cladding interaction is not the dominant failure mechanism. When pellet-cladding mechanical interaction is anticipated, however, the deformable pellet model (FRACAS-II) provides a more accurate calculation.

2.4.1.2 Rigid Pellet Cladding Deformation Model--FRACAS-I consists of a cladding deformation model and a fuel deformation model. If the fuel-cladding gap is closed, the fuel deformation model will apply a driving force to the cladding deformation model. The cladding deformation model, however, never influences the fuel deformation model.

The cladding deformation model in FRACAS-I is based on the following assumptions:

1. Incremental theory of plasticity

2. Prandtl-Reuss flow rule

3. Isotropic work-hardening

4. No creep deformation of cladding

5. Thin wall cladding (stress, strain, and temperature uniform through cladding thickness)

6. If fuel and cladding are in contact, no axial slippage occurs at fuel cladding interface

7. Bending strains and stresses in cladding are negligible

8. Axisymmetric loading and deformation of cladding.

The fuel deformation model in FRACAS-I is based on the following assumptions:

1. Thermal expansion, swelling, and densification are the only sources for fuel deformation

2. No resistance to expansion of fuel

3. No creep deformation of fuel

4. Isotropic fuel properties.

The cladding and fuel deformation models in FRACAS-I are described below.

Cladding Deformation Model--The rigid pellet cladding deformation subcode (FRACAS-I) consists of four sets of models, each used independently of the others.

Deformation and stresses in the cladding in the open gap regime are computed using a model which considers a thin cylindrical shell with specified internal and external pressures and a prescribed uniform temperature.

Calculations for the closed gap regime are made using a model which considers a thin cylindrical shell with prescribed external pressure and a prescribed radial displacement of the cladding inside surface. The prescribed displacement is obtained from the fuel expansion models described later in this section. Further, since no slippage is assumed to take place when the fuel and cladding are in contact, the axial expansion of the fuel is transmitted directly to the cladding, and hence, the change in axial strain in the shell is also prescribed.

The decision whether the fuel-cladding gap is open or closed is made by considering the relative movement of the cladding inside surface and the fuel outside surface. At the completion of the FRACAS-I analysis, either a new fuel-cladding gap size or a new fuel-cladding interfacial pressure and the elastic-plastic cladding stresses and strains are obtained.

Two additional models are used to compute changes in yield stress with work-hardening, given a uniaxial stress-strain curve. This stress-strain curve is obtained from MATPRO. The first model computes the effective total strain and new effective plastic strain, given a value of effective stress and the effective plastic strain at the end of the last loading increment. The second model computes the effective stress, given an increment of plastic strain and the effective plastic strain at the end of the last loading increment. Depending on the work-hardened value of yield stress, loading can be either elastic or plastic, and unloading is constrained to occur elastically. (Isotropic work-hardening is assumed in these calculations). These four sets of models are described below.

The decision as to whether or not the fuel is in contact with the cladding is made by comparing the radial displacement of the fuel surface with the radial displacement that would occur in the cladding due to the prescribed external (coolant) pressure and the prescribed internal (fission and fill gas) pressure. The free radial displacement of the cladding is obtained using equation (65). The following expression is used to decide if fuel-cladding contact has occured:

$$u_r^{fuel} \geq u_r^{clad} + \delta \qquad (74)$$

where

δ = as-fabricated fuel-cladding gap size (m).

If equation (74) is satisfied, the fuel is in contact with the cladding. The loading history enters into this decision by virtue

of the permanent plastic cladding strains which are applied to the as-fabricated geometry. These plastic strains, (and total effective plastic strain, ε^P , are retained for use in subsequent calculations.

If the fuel and cladding displacements are such that Equation (74) is not satisfied, the fuel-cladding gap has not closed during the current step and the solution obtained by the open gap solution is appropriate. The current value of the fuel-cladding gap size is then computed and is used in the temperature calculations. The plastic strain values may be changed in the solution if additional plastic straining has occurred.

If Equation (74) is satisfied, however, fuel and cladding contact has occurred during the current loading increment. At the contact interface, radial continuity requires that

$$u_r^{clad} = u_r^{fuel} - \delta \qquad (75)$$

while in the axial direction the assumption is made that no slippage occurs between the fuel and the cladding. This state is referred to as "lockup".

Note that only the additional strain which occurs in the fuel after lock-up has occurred is transferred to the cladding. Thus, if $\varepsilon_{z,o}^{clad}$ is the axial strain in the cladding just prior to contact, and $\varepsilon_{z,o}^{fuel}$ is the corresponding axial strain in the fuel, then the no-slippage condition in the axial direction becomes

$$\varepsilon_z^{clad} - \varepsilon_{z,o}^{clad} = \varepsilon_z^{fuel} - \varepsilon_{z,0}^{fuel} \qquad (76)$$

The values of the "prestrains", $\varepsilon_{z,o}^{fuel}$ and $\varepsilon_{z,o}^{clad}$, are set equal to the values of the strains that existed in the fuel and cladding at the time of fuel-cladding gap closure and are stored and used in the cladding sequence of calculations. The values are updated at the end of any load increment during which the fuel-cladding gap is closed.

After u_r^{clad} and ε_z^{clad} have been computed, they are used in a calculation which considers a thin cylindrical shell with prescribed axial strain, external pressure and prescribed radial displacement of the inside surface. After the solution is obtained, a value of the fuel-cladding interfacial pressure is computed along with new plastic strains and stresses.

The open gap modeling considers a thin cylindrical shell loaded by both internal and external pressures. Axisymmetric loading and deformation are assumed. Loading is also restricted to being uniform in the axial direction, and no bending is considered. The geometry and coordinates are shown in Figure 11. The displacements of the midplane of the shell are u and w in the radial and axial directions, respectively.

For this case, the equilibrium equations are identically satisfied by

$$\sigma_\theta = \frac{r_i P_i - r_o P_o}{t} \tag{77}$$

$$\sigma_z = \frac{r_i^2 P_i - r_o^2 P_o}{r_o^2 - r_i^2} \tag{78}$$

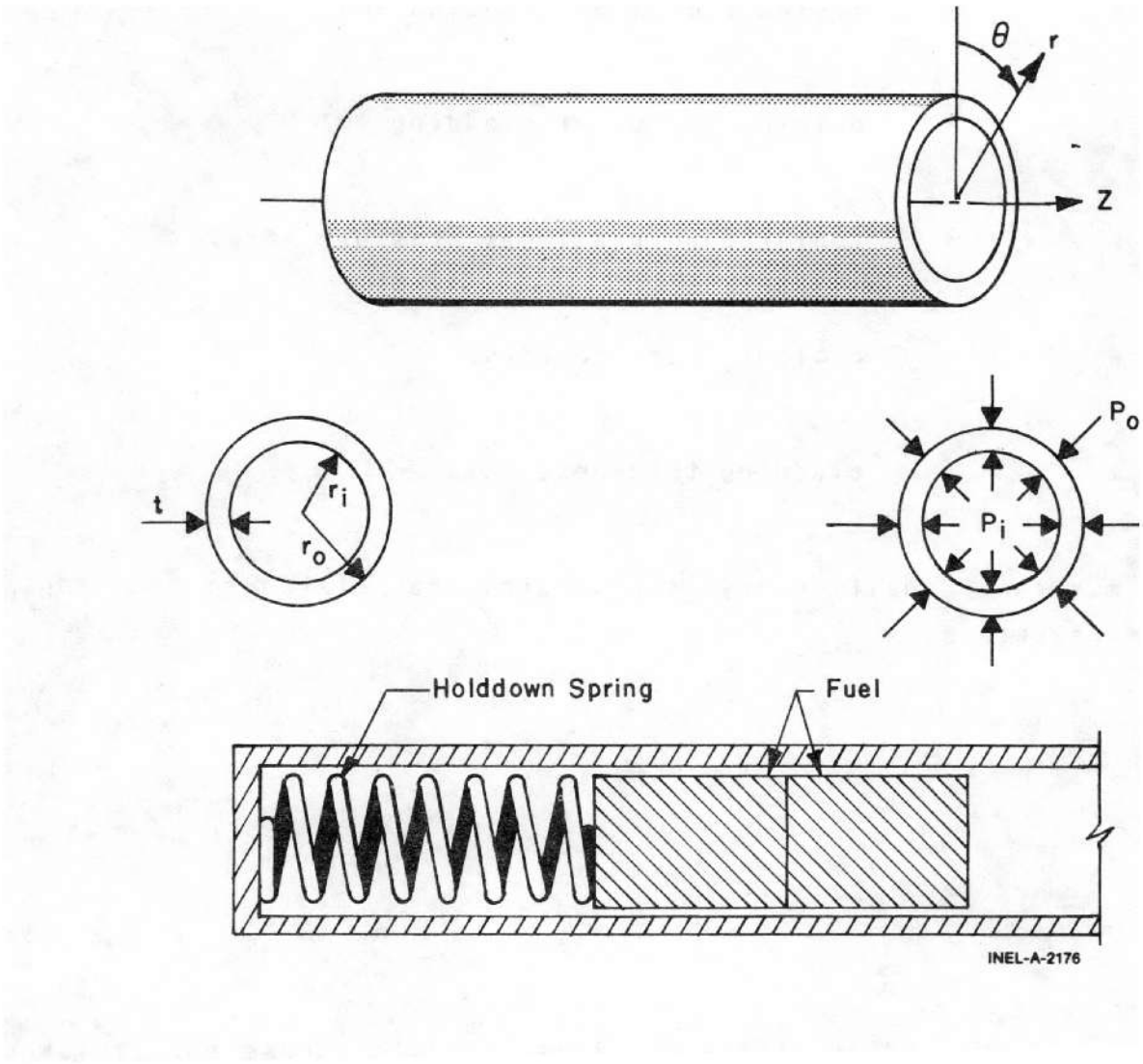

Figure 11. Fuel rod geometry and coordinates.

where

σ_θ = hoop stress (MPa)

σ_z = axial stress (MPa)

r_i = inside radius of cladding (m)

r_o = outside radius of cladding (m)

P_i = fuel rod internal gas pressure (MPa)

P_o = coolant pressure (MPa)

t = cladding thickness (m).

For membrane shell theory, the strains are related to the midplane displacements by

$$\varepsilon_z = \frac{\partial w}{\partial Z} \tag{79}$$

$$\varepsilon_\theta = \frac{u}{\bar{r}} \tag{80}$$

where $\bar{r}$ is the radius of the midplane. Strain across the thickness of the shell is allowed. In shell theory, since the radial stress can be neglected, and since the hoop stress, σ_θ, and axial stress, σ_z, are uniform across the thickness when bending is not considered, the radial strain is due only to the Poisson's effect and is uniform across the thickness. (Normally, radial strains are not considered in a shell theory, but plastic radial strains must be included when plastic deformations are considered).

The stress-strain relations are written in incremental form as

$$\varepsilon_\theta = \frac{1}{E}\{\sigma_\theta - \nu\,\sigma_z\} + \varepsilon_\theta^P + d\varepsilon_\theta^P + \int_{T_o}^{T} \alpha_\theta dT \qquad (81)$$

$$\varepsilon_z = \frac{1}{E}\{\sigma_z - \nu\,\sigma_\theta\} + \varepsilon_z^P + d\varepsilon_z^P + \int_{T_o}^{T} \alpha_z dT \qquad (82)$$

$$\varepsilon_r = -\frac{\nu}{E}\{\sigma_\theta + \sigma_z\} + \varepsilon_r^P + d\varepsilon_r^P + \int_{T_o}^{T} \alpha_r dT \qquad (83)$$

where

T_o = strain-free reference temperature (K)

α = coefficient of thermal expansion

T = current average cladding temperature (K)

E = modulus of elasticity

ν = Poisson's ratio.

The terms ε_θ^P, ε_z^P and ε_r^P are the plastic strains at the end of the last load increment, and $d\varepsilon_\theta^P$, $d\varepsilon_z^P$, and $d\varepsilon_r^P$ are the additional plastic strain increments which occur due to the new load increment.

The magnitude of the additional plastic strain increments is determined by the effective stress and the Prandtl-Reuss flow rule, expresses as

$$\sigma_e = \frac{1}{\sqrt{2}} \left[(\sigma_\theta - \sigma_z)^2 + (\sigma_z)^2 + (\sigma_\theta)^2 \right]^{1/2} \tag{84}$$

$$d\varepsilon_i^P = \frac{3}{2} \frac{d\varepsilon^P}{\sigma_e} S_i \quad \text{for } i = r,\theta,z \tag{85}$$

$$S_i = \sigma_i - \frac{1}{3} (\sigma_\theta + \sigma_z) \quad \text{for } i = r,\theta,z \tag{86}$$

The solution of the open gap case proceeds as follows. At the end of the last load increment the plastic strain components, ε_θ^P, ε_z^P, and ε_r^P are known. also the total effective plastic strain, ε^P, is known.

The loading is now incremented with the prescribed values of P_i, P_o, and T. The new stresses can be determined from Equations (77) and (78), and a new value of effective stress is obtained from Equation (84).

The increment of effective plastic strain, $d\varepsilon^P$, which results from the current increment of loading, can now be determined from the uniaxial stress-strain curve at the new value of σ_e, as shown in Figure 12. (The new elastic loading curve depends on the value of ε^P).

Once $d\varepsilon^P$ is determined, the individual plastic strain components are found from Equation (85), and the total strain

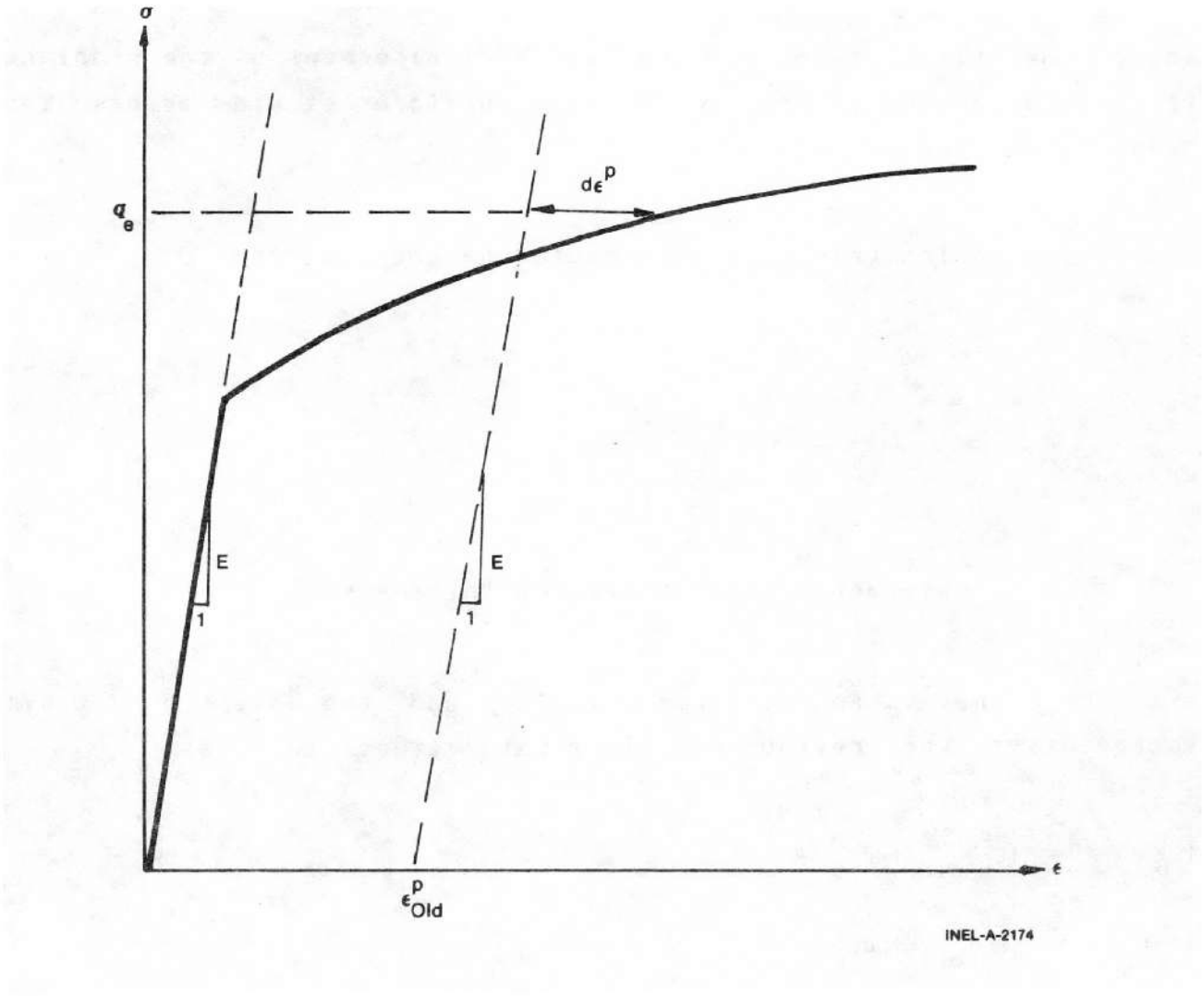

Figure 12. Calculation of effective stress σ_e from $d\varepsilon^p$.

components are obtained from Equations (81) thorugh (83).

The displacement of the inside surface of the shell must be determined so that a new fuel-cladding gap width can be computed. The radial displacement of the inside surface is given by

$$u(r_i) = \bar{r}\,\varepsilon_\theta - \frac{t}{2}\,\varepsilon_r \qquad (87)$$

where the first term is the radial displacement of the midplane [from Equation (80)] and ε_r is the uniform strain across the cladding thickness, t.

The cladding thickness is computed by the equation

$$t = (1 + \varepsilon_r)\, t_o \tag{88}$$

where

t_o = as-fabricated, unstressed thickness.

The final step performed is to add the plastic strain increments to the previous plastic strain values; that is,

$$\begin{aligned}
(\varepsilon_\theta^P)_{new} &= (\varepsilon_\theta^P)_{old} + d\varepsilon_\theta^P \\
(\varepsilon_z^P)_{new} &= (\varepsilon_z^P)_{old} + d\varepsilon_z^P \\
(\varepsilon_r^P)_{new} &= (\varepsilon_r^P)_{old} + d\varepsilon_r^P \\
(\varepsilon^P)_{new} &= (\varepsilon^P)_{old} + d\varepsilon^P
\end{aligned} \tag{89}$$

These values are used in or for the next load increment.

Thus all the stresses and strains can be computed directly, since in this case the stresses are determinate. In the case of the driven cladding displacement, the stresses depend on the displacement, and such a straightforward solution is not possible.

The closed gap modeling considers the problem of a cylindrical shell for which the radial displacement of the inside surface and axial strain are prescribed. Here the stresses cannot be computed directly since the pressure at the inside surface (the fuel-cladding interfacial pressure) must be determined as part of the solution.

As in the open gap modeling, the displacement at the inside surface is given by

$$u(r_i) = u - \frac{t}{2}\,\varepsilon_r \tag{90}$$

where u is the radial displacement of the midplane. From Equation (81), $u = r\varepsilon_\theta$ and

$$u(r_i) = \bar{r}\,\varepsilon_\theta - \frac{t}{2}\,\varepsilon_r \tag{91}$$

Thus, prescribing the displacement of the inside surface of the shell is equivalent to a constraining relation between ε_θ and ε_i. As before, Hooke's law is taken in the form

$$\varepsilon_\theta = \frac{1}{E}(\sigma_\theta - \nu\,\sigma_z) + \varepsilon_\theta^P + d\varepsilon_\theta^P + \int_{T_o}^{T} \alpha_\theta dT \tag{92}$$

$$\varepsilon_z = \frac{1}{E}(\sigma_z - \nu\,\sigma_\theta) + \varepsilon_z^P + d\varepsilon_z^P + \int_{T_o}^{T} \alpha_z dT \tag{93}$$

$$\varepsilon_r = -\frac{\nu}{E}(\sigma_\theta + \sigma_z) + \varepsilon_r^P + d\varepsilon_r^P + \int_{T_o}^{T} \alpha_r dT \tag{94}$$

Use of Equation (91) and (94) in Equation (92) results in a relation between the stresses σ_θ, σ_z, and the prescribed displacement $u(r_i)$:

$$\frac{u(r_i)}{\bar{r}} + \frac{1}{2}\left(\frac{t}{\bar{r}}\right)\left\{\varepsilon_r^P + d\varepsilon_r^P + \int_{T_o}^{T} \alpha dT\right\}$$

$$- \left\{\varepsilon_\theta^P + d\varepsilon_\theta^P + \int_{T_o}^{T} \alpha dT\right\} = \frac{1}{E}\left[\left(1 + \frac{\nu}{2}\,\frac{t}{\bar{r}}\right)\sigma_\theta\right.$$

$$\left. + \nu\left(\frac{1}{2}\,\frac{t}{\bar{r}} - 1\right)\sigma_z\right] \tag{95}$$

Equations (93) and (95) are now a pair of simultaneous algabraic equations for the stresses σ_θ and σ_z, which may be written as

$$\begin{bmatrix} A_{11} & A_{12} \\ A_{21} & A_{22} \end{bmatrix} \begin{bmatrix} \sigma_\theta \\ \sigma_z \end{bmatrix} = \begin{bmatrix} B_1 \\ B_2 \end{bmatrix} \tag{96}$$

where

$$A_{11} = 1 + \frac{\nu}{2}\,\frac{t}{\bar{r}}$$

$$A_{12} = \nu\left(\frac{1}{2}\,\frac{t}{\bar{r}} - 1\right)$$

$$A_{21} = -\nu$$

$$A_{22} = 1$$

$$B_1 = E\frac{u(r_i)}{\bar{r}} + \frac{E}{2}\left(\frac{t}{\bar{r}}\right)\left\{\varepsilon_r^P + d\varepsilon_r^P + \int_{T_o}^{T} \alpha dT\right\}$$

$$-E\left\{\varepsilon_\theta^P + d\varepsilon_\theta^P + \int_{T_o}^{T} \alpha dT\right\} .$$

$$B_2 = E\left[\varepsilon_z - E\,\varepsilon_z^P + d\varepsilon_z^P + \int_{T_o}^{T} \alpha dT\right]$$

Then the stresses can be written explicity as

$$\sigma_\theta = \frac{B_1 A_{22} - B_2 A_{12}}{A_{11} A_{22} - A_{12} A_{21}} \tag{97}$$

$$\sigma_z = \frac{B_2 A_{11} - B_1 A_{21}}{A_{11} A_{22} - A_{12} A_{21}} \tag{98}$$

These equations relate the stresses to $u(r_i)$ and ε_z, which are prescribed, and to $d\varepsilon_\theta^P$, $d\varepsilon_z^P$, and $d\varepsilon_r^P$ which are to be determined. The remaining equations which must be satisfied are

$$\sigma e = \frac{1}{\sqrt{2}}\left[(\sigma_\theta - \sigma_z)^2 + (\sigma_\theta)^2 + (\sigma_z)^2\right]^{1/2} \tag{99}$$

$$d\varepsilon^P = \frac{2}{3}\left[(d\varepsilon_r^P - d\varepsilon_\theta^P)^2 + (d\varepsilon_\theta^P - d\varepsilon_z^P)^2 + (d\varepsilon_z^P - d\varepsilon_r^P)^2\right]^{1/2} \tag{100}$$

and the Prandtl-Reuss flow equations [defined in Equation (85)]

$$d\varepsilon^P = \frac{3}{2} \frac{d\varepsilon^P}{\sigma_e} [\sigma_\theta - \frac{1}{3} (\sigma_\theta + \sigma_z)] \quad (101)$$

$$d\varepsilon_z^P = \frac{3}{2} \frac{d\varepsilon^P}{\sigma_e} [\sigma_z - \frac{1}{3} (\sigma_\theta + \sigma_z)] \quad (102)$$

$$d\varepsilon_r^P = - d\varepsilon_\theta^P - d\varepsilon_z^P \quad (103)$$

The effective stress, σ_θ, and the plastic strain increment, $d\varepsilon^P$, must of course, be related by the uniaxial stress-strain law. Equations (97) through (103) must be simultaneously satisfied for each loading increment.

As discussed in Section 2.4.1.1, a straightforward numerical solution to these equations can be obtained by means of the Method of Successive Elastic Solutions. By this method, arbitrary values are initially assumed for the increments of plastic strain, and Equations (97) through (103) are used to obtain improved estimates of the plastic strain components. The steps performed are as follows for each increment of load:

1. Values of $d\varepsilon_\theta^P$, $d\varepsilon_z^P$, and $d\varepsilon_r^P$ are assumed. Then, $d\varepsilon^P$ is computed from Equation (100) and the effective stress is obtained from the stress-strain curve at the value of .

2. From Hooke's law, still using the assumed plastic strain increments and the prescribed values of $u(r_i)$ and ε_z, values for the stresses can be obtained from Equations (97) and (98).

3. New values for $d\varepsilon_\theta^P$, $d\varepsilon_z^P$, and $d\varepsilon_r^P$ are now computed from the Prandtl-Reuss relations,

$$d\varepsilon_i^P = \frac{3}{2} \frac{d\varepsilon^P}{\sigma_e} [\sigma_i - \frac{1}{3} (\sigma_\theta + \sigma_z)] \quad i = r,\theta,z \tag{104}$$

using σ_e as computed in Step 1, and σ_i as computed in Step 2.

4. The old and new values of $d\varepsilon_\theta^P$, $d\varepsilon_z^P$, and $d\varepsilon_r^P$ are compared and the process continued until convergence is obtained.

5. Once convergence has been obtained, the fuel-cladding interfacial pressure is computed from the following equation.

$$P_{int} = \frac{t\,\sigma_\theta + r_o\,P_o}{r_i} \tag{105}$$

When Steps 1 through 5 have been accomplished, the solution is complete, provided that the fuel-cladding interface pressure is not less than the local gas pressure.

However, due to unequal amounts of plastic straining in the hoop and axial directions upon unloading, the fuel-cladding interfacial pressure as obtained in Step 5 is often less than the gas pressure even though the fuel-cladding gap has not opened. When this situation occurs, the frictional "locking" (which is assumed to constrain the cladding axial deformation to equal the fuel axial deformation) no longer exists. The axial strain and stress adjust themselves so that the fuel-cladding interfacial pressure equals the

gas pressure, at which point the axial strain is again "locked". Thus, upon further unloading, the axial strain and the hoop and axial stresses continually readjust themselves to maintain the fuel-cladding interfacial pressure equal to the gas pressure until the fuel-cladding gap opens. Since the unloading occurs elastically, a solution for this portion of the fuel-cladding interaction problem can be obtained directly as discussed below.

Since the external pressure and the fuel-caldding interfacial pressure are known, the hoop stress is obtained from Equation (135) as

$$\sigma_\theta = \frac{r_i P_{int} - r_o P_o}{t} \tag{106}$$

From Equation (91), the following expression can be written

$$\varepsilon_\theta = \frac{u_r^{fuel} - \delta + t/2\ \varepsilon_r}{\bar{r}} \tag{107}$$

Substitution of ε_θ and ε_r, as given by Equations (92) and (94), into Equation (107) results in an explicit equation for σ_z:

$$\nu r_i \sigma_z = (\bar{r} + \nu\, t/2)\, \sigma_\theta + \bar{r} E \left(\int \alpha dT + d\varepsilon_\theta^P \right) - \frac{t}{2} E \left(\int \alpha dT + d\varepsilon_r^P \right) - E\, u(r_i) \tag{108}$$

in which σ_θ is known from Equation (106). With σ_z and σ_θ known, the strains may be computed from Hooke's law, Equations (92) through (94). This set of equations is automatically invoked whenever P_{int}

is computed to be less than the local gas pressure.

As in the open gap modeling, the last step performed is to set the plastic strain components and total effective strain equal to their new values by adding in the computed increments $d\varepsilon_i^P$ and $d\varepsilon^P$.

The stress-strain modeling is used to relate stress and plastic strain, taking into consideration the direction of loading and the previous plastic deformation. A typical stress-strain curve is shown in Figure 13. This curve presents the results of a uniaxial

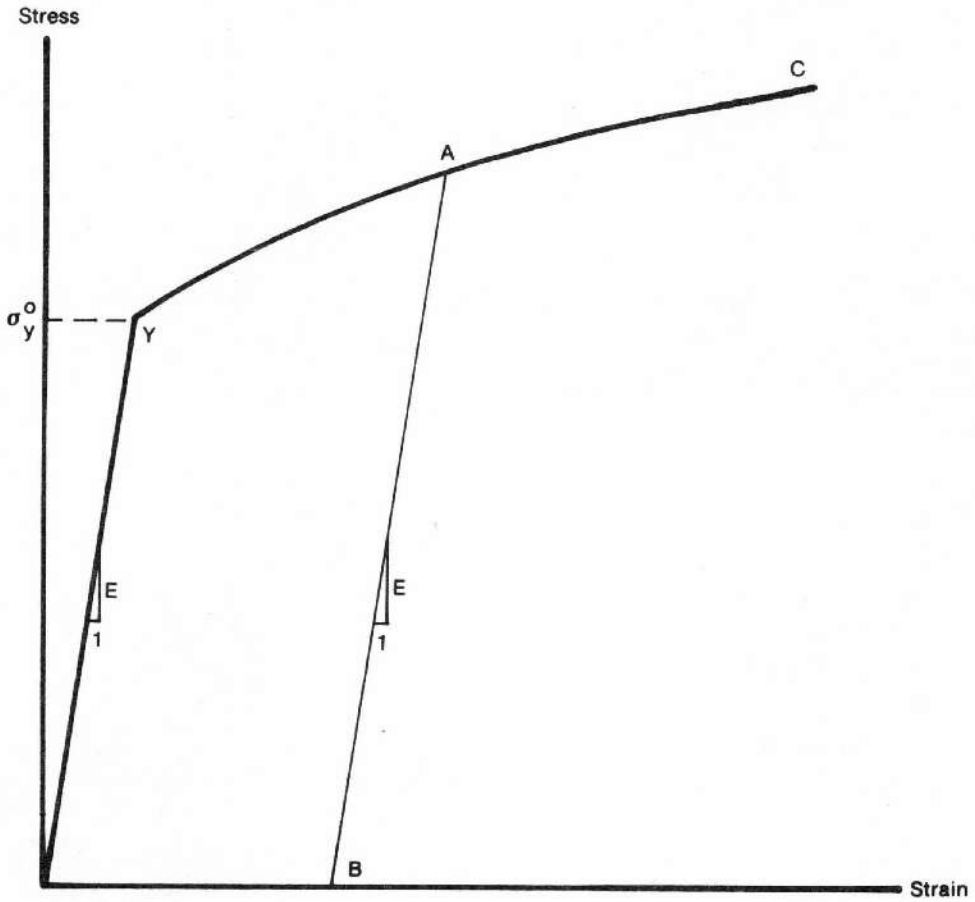

Figure 13. Idealized stress-strain behavior.

stress-strain experiment and may be interpreted beyond initial yield as the locus of work-hardened yield stresses. The equation of the curve is provided by the MATPRO package at each temperature.

To utilize this information, the usual idealization of the mechanical behavior of metals is made. Thus, linear elastic behavior is assumed until a sharply defined yield stress is reached, after which plastic (irrecoverable) deformation occurs. Unloading from a stress state beyond the initial yield stress, σ_y^o, is assumed to occur along a straight line having the elastic modulus for its slope. When the (uniaxial) stress is removed completely, a residual plastic strain remains, and this completely determines the subsequent yield stress. That is, when the specimen is loaded again, loading will occur along line BA in Figure 13, and no additional deformation will occur until point A is again reached. Point A is the subsequent yield stress. If $\sigma = f(\varepsilon)$ is the equation of the plastic portion of the stress-strain curve (YAC), then for a given value of plastic strain, the subsequent yield stress is found by simultaneously solving the pair of equations

$$\begin{cases} \sigma = f(\varepsilon) \\ \sigma = E(\varepsilon - \varepsilon^P) \end{cases} \tag{109}$$

which may be written as

$$\sigma = f(\frac{\sigma}{E} + \varepsilon^P). \tag{110}$$

This nonlinear equation may be solved efficiently by using Newton's iteration scheme

$$\sigma^{(m+1)} = f\left[\frac{\sigma^{(m)}}{E} + \varepsilon^P\right] \quad m = 0, 1, 2, \ldots \tag{111}$$

The initial iterate, $\sigma^{(o)}$, is arbitrary, and without loss of generality, is taken as 34.5 MPa. For any monotonically increasing stress-plastic strain relation, the iteration scheme in Equation (111) will converge uniformly and absolutely.

The computations of the stress-strain modeling are described below. The first computes strain as a function of plastic strain, temperature, and stress. The second computes stress as a function of plastic strain, temperature and plastic strain increments.

Values of plastic strain, ε^P, temperature and stress are used as follows:

1. For a given temperature, $\sigma = f(\varepsilon)$ is obtained from the MATPRO package.

2. The yield stress σ_y for given ε^P is obtained from Equation (111).

3. For a given value of stress, σ,

if $\sigma \leq \sigma_y$, $\varepsilon = \frac{\sigma}{E} + \varepsilon^P$

$$\varepsilon^P_{new} = \varepsilon^P_{old} \tag{112}$$

if $\sigma > \sigma_y$, $\varepsilon = f(\sigma)$

$$\varepsilon^P_{new} = \varepsilon - \sigma/E$$

$$d\varepsilon^P = \varepsilon^P_{new} - \varepsilon^P_{old}. \quad (113)$$

where E is computed using the MATPRO package.

Values of plastic strain, ε^P, temperature, and plastic strain increment, $d\varepsilon^P$, are used as follows:

1. For a given temperature, $\sigma = f(\varepsilon)$ is obtained from the matpro package.

2. The yield stress σ_y for given ε^P is obtained from Equation (111).

3. Given $d\varepsilon^P$ (see Figure 14),

$$\varepsilon^P_{new} = \varepsilon^P_{old} + d\varepsilon^P \quad (114)$$

Since $d\varepsilon^P > 0$, the new value of stress and strain must lie on the plastic portion of the stress-strain curve $\sigma = f(\varepsilon)$. So, σ and ε are obtained by performing a simultaneous solution, as before.

Rigid Pellet Fuel Deformation in FRACAS-I--This section describes the analytical models used to compute fuel deformation in FRACAS-I. Models are available to calculate length change and fuel

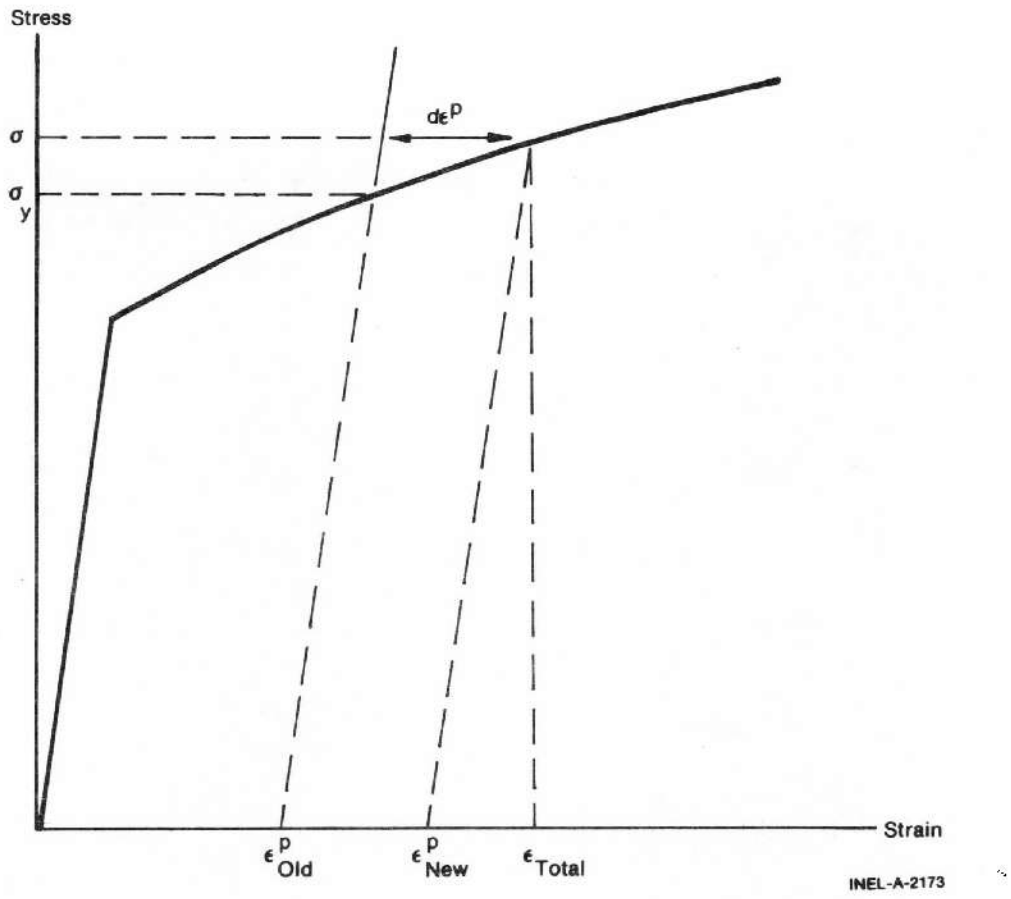

Figure 14. Computing STRESS.

radial displacement. Relocation is also considered in FRACAS-I, and is also discussed in this section. The effect of relocation, however, is included only in the thermal response and is not considered in the mechanical response of the fuel and cladding.

The assumptions made with respect to fuel deformation in FRACAS-I are that no pellet deformation is induced by fuel-cladding contact stress or thermal stress and that free-ring thermal expansion applies. Each individual fuel ring is assumed to expand

without restraint from any other ring, and the total expansion is the sum of the individual expansions.

Radial Deformation--Radial deformation of the pellet due to thermal expansion, irradiation swelling and densification is calculated with a free-ring expansion model. The governing equation for this model is

$$R_H = \sum_{i=1}^{N} r_i \left(1 + \alpha_{T_i} \Delta T_i + \varepsilon s_i + \varepsilon d_i\right) \tag{115}$$

where

R_H = hot-pellet radius (m)

α_{T_i} = coefficient of thermal expansion of the i-th radial temperature (1/K)

ΔT_i = average temperature of ith radial ring (K)

Δr_i = width of i-th radial ring (m)

N = number of annular rings

εs_i = swelling strain

εd_i = densification strain.

Axial deformation--Axial deformation of the fuel stack is calculated by summing the maximum ring axial expansions of each pellet. Maximum ring axial expansion of each pellet is calculated as the difference between the length of the ring with the maximum overall hot length and the cold length of that ring.

The calculation of the overall ring height includes consideration of a central dish, when present. The fuel stack length is thus calculated from

$$L_f = \sum_{j=1}^{M} (1 + \alpha_{T_i} \Delta T_i + \varepsilon s_i + \varepsilon d_i) L_j \qquad (116)$$

where

i = the ring with maximum axial length of the j-th node

L_f = hot length of the fuel stack (m)

M = number of axial nodes

L_i = length of the j-th radial ring (m).

Fuel Surface Relocation--Two closely related models are used to compute the effect of relocation. The fuel surface relocation model results in an effective pellet-cladding gap which is used in computing the gap conductance and the thermal gap. The space made available for cracks based on this model, is distributed inside the

pellet. This leads to the second relocation model which calculates an effective thermal conductivity across the cracked pellet. The effective thermal conductivity model was previously discussed in Section 2.3.7.1.

The amount of fuel surface relocation necessary to result in the proper gap closure versus power was studied by Coleman using FRAP-T3. These results are presented in Reference 25. The model which was developed from these results provides FRACAS-I with an effective fuel strain which is a function of the fuel rod cold-state geometry. This strain is treated the same as the other fuel radial strains (thermal expansion, swelling, and densification). With reference to Figure 15, the equation for the variable relocation

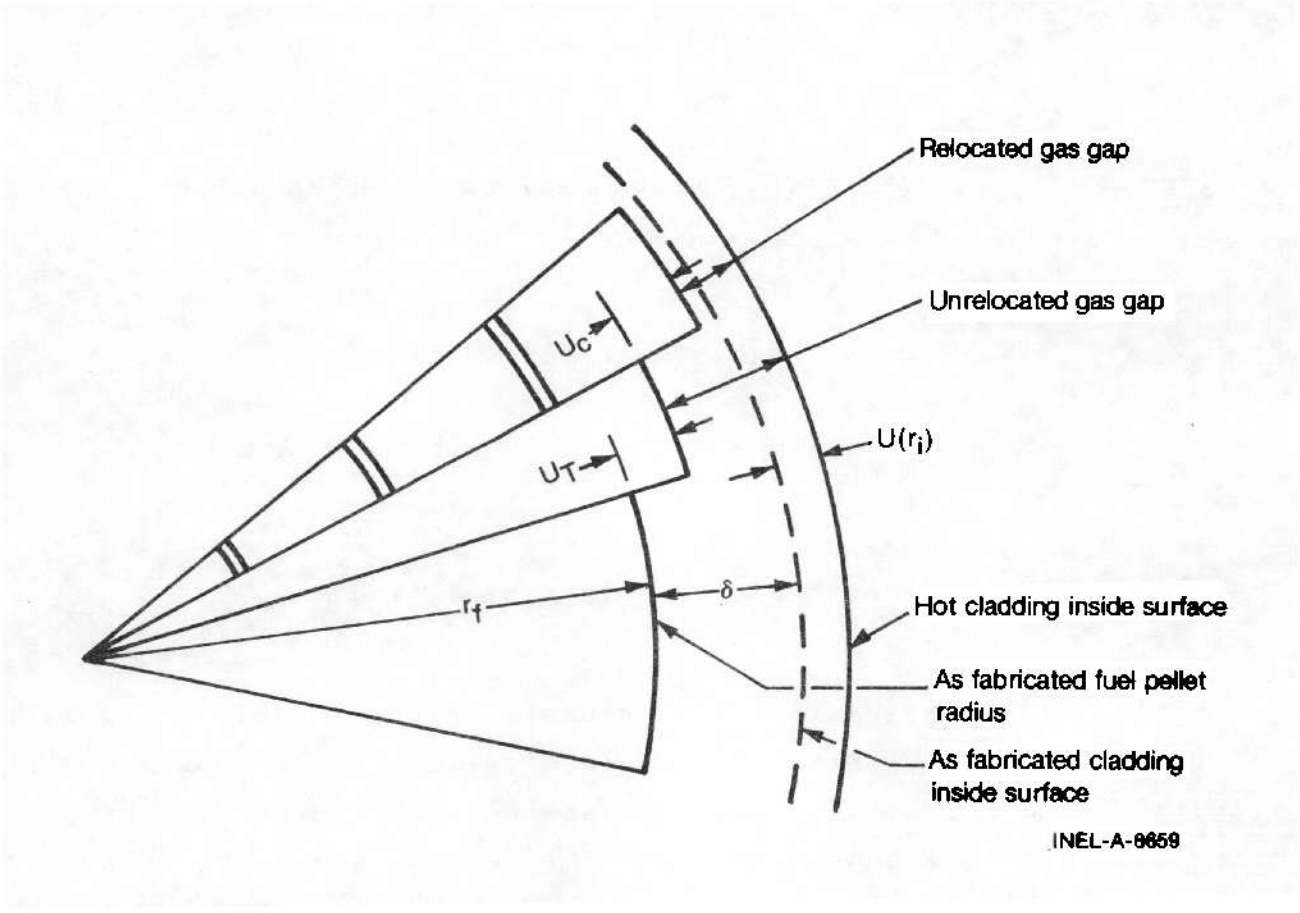

Figure 15. Fuel relocation.

model displacement is

1. Open Gap Case

$$U_c = \delta - 0.005\ r_f \tag{117}$$

2. Closed Gap Case

$$U_c = \delta - U_T - U(r_i) \tag{118}$$

where

U_c = radial displacement of fuel due to relocation (m)

U_T = radial displacement of fuel due to thermal expansion, irradiation swelling, and densification (m)

$U(r_i)$ = radial displacement of the cladding (m)

δ = as-fabricated fuel-cladding gap size (m)

r_f = as-fabricated pellet radius (m).

The fuel-cladding gap size used in the thermal and internal pressure calculations include the fuel relocation, while the fuel-cladding gap size used in the structural calculations does not. The fuel conductivity is modified according to Equation (51) to account

for the cracks formed by fuel relocation.

2.4.1.3 Deformable Pellet Deformation Model--The deformable pellet deformation model, FRACAS-II, is used to calculate the fuel rod deformation when stress effects on fuel deformation become important. This model computes the stress and strain distributions in both the fuel and cladding. Elastic and plastic strains in both the fuel and cladding are considered. The stresses and strains in the fuel and cladding are obtained by the transfer matrix approach. The plastic strains are obtained by the Method of Successive Substitutions, which was outlined in Section 2.4.1.1.

The method of obtaining the "pseudo-elastic" solution for fuel rod stresses and strains required at each plastic strain iteration in the Method of Successive Substitutions is described below.

The geometric model is a right circular cylinder (either solid or hollow) in a state of generalized plane strain. The applied loads are external pressure, internal pressure (if the cylinder is hollow), and axial force. The cylinder may consist of a single material, or may be a composite cylinder consisting of two layers of different materials. An arbitrary radial temperature distribution may be prescribed, and temperature dependent material properties may be used.

A single layer (homogeneous) cylinder is used to analyze the fuel and the cladding separately before contact occurs. A two-layered (composite) cylinder is used to analyze the fuel and cladding after fuel expansion results in firm contact between the fuel and the cladding. For the composite cylinder case, the stress and strain distributions are permitted to be discontinuous at the

interface between the layers, and the discontinuity in radial displacement and axial strain must be determined. (The discontinuity values are obtained from the displacements which exist in the fuel and cladding at the instant of fuel-cladding contact).

The method used to solve for the stresses, strains and displacements in the composite cylinder is the transfer matrix approach, as described in Reference 24, modified to consider the state of generalized plane strain. In addition, the technique has been extended to consider displacement discontinuities and both axial and radial cracks in the cylinder.

First, a complete homogeneous cylinder with no discontinuities, but with variable E, ν, and α (modulus of elasticity, Poisson's ratio, and coefficient of thermal expansion, respectively) is considered. Only radial variations in temperature, T, and material properties are considered. Generalized plane strain deformation is assumed, so that for all r,

$$\varepsilon_z = \text{constant} \tag{119}$$

The value of the constant axial strain, ε_z, is determined from the condition of axial force equilibrium,

$$\iint \sigma_z dA = F_z \tag{120}$$

where F_z is the resulting axial force. F_z is determined from the known internal and external pressures.

The governing equations of equilibrium and compatibility in the absence of any dislocations (displacement discontinuities) are given by

$$\frac{d\sigma_r}{dr} + \frac{\sigma_r - \sigma_\theta}{r} = 0 \tag{121}$$

$$\frac{d\varepsilon_\theta}{dr} + \frac{\varepsilon_\theta - \varepsilon_r}{r} = 0 \tag{122}$$

The elastic-plastic stress-strain relations are

$$\varepsilon_r = \frac{1}{E}\left[\sigma_r - \nu(\sigma_\theta + \sigma_z)\right] + \alpha_r T + \varepsilon_r^P + d\varepsilon_r^P \tag{123}$$

$$\varepsilon_\theta = \frac{1}{E}\left[\sigma_\theta - \nu(\sigma_r + \sigma_z)\right] + \alpha_\theta T + \varepsilon_\theta^P + d\varepsilon_\theta^P \tag{124}$$

$$\varepsilon_z = \frac{1}{E}\left[\sigma_z - \nu(\sigma_r + \sigma_\theta)\right] + \alpha_z T + \varepsilon_z^P + d\varepsilon_z^P \tag{125}$$

Substitution of Equations (123) and (124) into Equation (122) results in

$$\frac{d}{dr}\left\{\frac{\sigma_\theta}{E} - \frac{\nu}{E}(\sigma_r + \sigma_z) + \alpha T + \varepsilon_\theta^P + d\varepsilon_\theta^P\right\} + \frac{1+\nu}{E}\frac{(\sigma_\theta - \sigma_r)}{r} + \frac{\alpha_\theta T - \alpha_r T}{r} + \frac{\varepsilon_\theta^P - \varepsilon_r^P}{r} + \frac{d\varepsilon_\theta^P - d\varepsilon_r^P}{r} = 0 \tag{126}$$

Equations (121) and (126) relate the stresses as they vary across the cylinder. A number of node points are introduced along the

radius of the cylinder, and the stresses are evaluated only at the nodes. Thus Equations (119), (121), (125) and (126) can be written in finite difference form, and a set of recursion relations.

$$\begin{Bmatrix} \sigma_r \\ \sigma_\theta \\ \sigma_z \end{Bmatrix}_{i+1} = \begin{bmatrix} L(i) \end{bmatrix} \begin{Bmatrix} \sigma_r \\ \sigma_\theta \\ \sigma_z \end{Bmatrix}_i + \begin{Bmatrix} M(i) \end{Bmatrix} \tag{127}$$

are obtained. This matrix equation relates the stresses at node i-1 to those at node i. The matrices [L(i)] and [M(i)] depend only on the materials properties, geometry, and plastic strains.

By successive application of Equation (127), a relation between the stresses at any node and the stresses at node 1 (the node at the inside of the cylinder) can be obtained. This relation takes the form

$$\{\sigma\}_{i+1} = [a(i)]\ \{\sigma\}_i + \{B(i)\} \tag{128}$$

where

$$\{\sigma\} = \{\sigma_r, \sigma_\theta, \sigma_z\}. \tag{129}$$

The matrices [A(i)] and [B(i)] may be determined from [L(i)] and [M(i)], as follows:

$$[A(i)] = [L(i)]\ [A(i-1)] \tag{130}$$

$$\{B(i)\} = [L(i)]\ \{B(i-1)\} + \{M(i)\} \tag{131}$$

for i greater than 1, and

$$[A(1)] = [L(1)] \tag{132}$$

$$\{B(1)\} = \{M(1)\} \tag{133}$$

for i equal 1.

By recursion, [A(i)] and [B(i)] across the cylinder wall can be obtained with the result that

$$\{\sigma\}_N = [A(N-1)] \{\sigma\}_1 + \{B(N-1)\} \tag{134}$$

At the outside surface, $\sigma_r = -P_o$, where P_o is the external (coolant) pressure acting upon the cladding. Thus, the following condition can be obtained.

$$-P_o = A_{11}(N-1)\, \sigma_r(1) + A_{12}(N-1)\sigma_\theta(1) + A_{13}(N-1)\, \sigma_z(1) + B_1(N-1) \tag{135}$$

At the inside surface of the cylinder, one of the following conditions holds:

$$\begin{cases} \sigma_r(1) = -P_i, & \text{if } r_1 \neq 0 \\ \sigma_r(1) = \sigma_\theta(1), & \text{if } r_1 = 0 \end{cases} \tag{136}$$

Finally, the condition of axial equilibrium,

$$\iint \sigma_z dA = \sum_{j=1}^{n-1} \sigma_z(j)\, dA(j) = F_z \qquad (137)$$

must be satisfied. Using the recursion matrices, this becomes

$$\sum_{j=1}^{N-1} \sigma_z(j) dA_j = [0\ 0\ 1]\ \{[I]\ dA_1 + |A_1|\ dA_2 + \ldots + |A_{N-1}| dA_N\}\{\sigma_1\}$$

$$+ \{0 + \{B_1\}\ dA_2 + \ldots + \{B_{N-1}\}\ dA_N\}$$

$$\underline{\Delta}\ [C]\ \{\sigma_1\} + \{D\}. \qquad (138)$$

The axial force condition is the third component of this matrix equation, which can be written as

$$F_z = C_{33}\sigma_z(1) + D_j \qquad (139)$$

Equations (135), (136), (139) are solved simultaneously for the stresses at the inside node [σ], after which all other streses and strains can be determined from the recursion relations given in Equation (128).

Thus, once the transfer matrices [L(i)] and [M(i)] in Equation (127) are known for each annulus in the cylincer, finding the stresses throughout the cylinder becomes a straightforward procedure.

The advantage of using the transfer matrix approach in solving for fuel rod deformations is that different transfer matrices can be

used, depending on whether the fuel is cracked axially or radially, or both, and whether or not the cladding and fuel are in contact. The basic solution technique is not changed. The various transfer matrices required are illustrated below.

Homogeneous Cylinder--This section describes the transfer matrices for a homogeneous cylinder in which the radial displacements and axial strains are continuous. The temperature and material properties, however, may vary (radially) in an arbitrary manner.

As shown in Figure 16, the cylinder (either hollow or solid) is broken up into N-1 annular regions, with N node points, where r_i is the radius to the first node. (For a solid cylinder $r_i = 0$). Values of stresses, elastic strains, and plastic strains are found at each of the node points.

The derivatives are evaluated at the center of each annular region; that is, for the j-th annulus, at

$$r = 0.5\ (r_{j+1} + r_j) \tag{140}$$

Equations (121) and (126) are written for the midpoint of each annular region. Thus, for the j-th annulus,

$$\frac{d}{dr}\left(\frac{\sigma_\theta}{E}\right) = \left[\frac{\sigma_{\theta(j+1)}}{E\ (j+1)} - \frac{\sigma_{\theta(j)}}{E(j)}\right] \Bigg/ (r_{j+1} - r_j) \tag{141}$$

and

$$\frac{\sigma_\theta}{E} = \left[\frac{\sigma_\theta(j+1)}{E(j+1)} + \frac{\sigma_\theta(j)}{E(j)}\right] / 2 \qquad (142)$$

where function values at the midpoint are taken as the average of the function values at the endpoints. Denoting $\Delta r_j = r_{j+1} - r_j$,

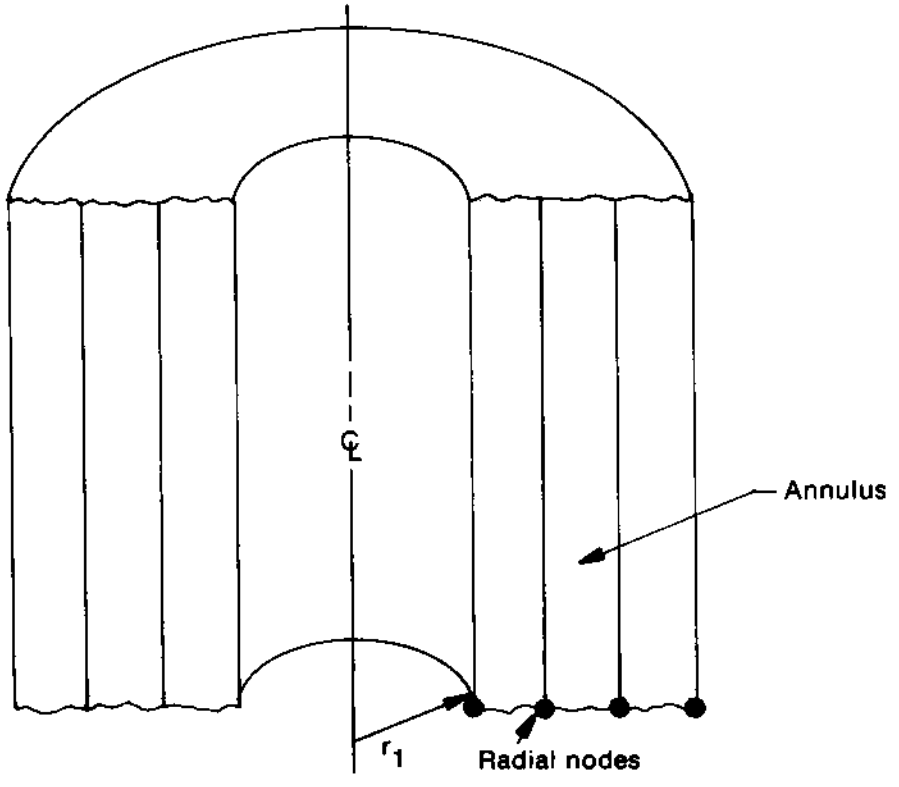

Figure 16. Node and annuli geometry.

Equations (121), (126), and (119) and (125) become

$$\left[\frac{1}{r_{j+1} - r_j} + \frac{1}{2\, r_{j+1}}\right] \sigma_r(j+1) + \left[\frac{-1}{2\, r_{J+1}}\right] \sigma_\theta(j+1)$$

$$= \left[\frac{1}{r_{J+1} - r_j} - \frac{1}{2r_j}\right] \sigma_r(j) + \left[\frac{1}{2r_j}\right] \sigma_\theta(j) \qquad (143)$$

and

$$\left\{\frac{-\nu\ (j+1)}{E(j+1)\ \Delta r(j)}\right\}\sigma_z(j+1) \quad + \left\{\frac{\nu(j)}{E(j)\ \Delta r(j)}\right\}\sigma_z(j)$$

$$+\left\{\frac{-\nu(j+1)}{E(j+1)\ \Delta r_j} \quad - \quad \frac{1+\nu(j+1)}{2\ E(j+1) r_{J+1}}\right\}\ \sigma_r(j+1)$$

$$+\left\{\frac{1}{E(j+1)\ \Delta r(j)} \quad + \quad \frac{1+\nu(j+1)}{2E(j+1)\ r_{J+1}}\right\}\ \sigma_\theta(j+1)$$

$$+\left\{\frac{+\nu(j)}{E(j)\ \Delta r(j)} \quad - \quad \frac{1+\nu(j)}{2\ E(j)\ r_j}\right\} \quad \sigma_r(j)$$

$$+\left\{\frac{-1}{E(j)\ \Delta r(j)} \quad + \quad \frac{1+\nu(j)}{2\ E(j)\ r_j}\right\} \quad \sigma_\theta(j)$$

$$+\left\{\left[\alpha_\theta T(j+1) + \varepsilon_\theta^P(j+1) + d\varepsilon_\theta^P(j+1)\right]\left(\frac{1}{\Delta r(j)} \quad + \quad \frac{1}{2\ r_{j+1}}\right)\right\}$$

$$+\left\{\left[\alpha_\theta T(j) \quad + \varepsilon_\theta^P(j) + d\varepsilon_\theta^P(j)\right] \quad \left[\frac{-1}{\Delta r(j)} \quad + \quad \frac{1}{2r_j}\right]\right\}$$

$$+ \quad \left\{\frac{-1}{2r_{j+1}} \quad \left[\alpha_r T(j+1) + \varepsilon_r^P(j+1) + d\varepsilon_r^P(j+1)\right]\right\}$$

$$+ \quad \left\{\frac{-1}{2r_j} \quad \left[\alpha_r T(j) \quad + \varepsilon_r^P(j) + d\varepsilon_r^P(j)\right]\right\} \quad = 0 \qquad (144)$$

and, finally

$$\frac{1}{E(j+1)} \left\{\sigma_z(j+1) - \nu(j+1) \left[\sigma_r(j+1) - \sigma_\theta(j+1)\right]\right\}$$

$$+\left[\alpha_z T + \varepsilon_z^P + d\varepsilon_z^P\right]_{j+1}$$

$$\frac{1}{E(j)} \left\{\sigma_z(j) - \nu(j) \left[\sigma_r(j) + \sigma_\theta(j)\right]\right\}$$

$$+\left[\alpha_z T + \varepsilon_z^P + d\varepsilon_z^P\right]_{j} \qquad (145)$$

For the j-th annulus, Equations (143), (144) and (145) may be compactly written as

$$[E(J)] \begin{Bmatrix}\sigma_r \\ \sigma_\theta \\ \sigma_z\end{Bmatrix}_{j+1} = [F(j)] \begin{Bmatrix}\sigma_r \\ \sigma_\theta \\ \sigma_z\end{Bmatrix}_{j} + \{G(j)\} \qquad (146)$$

where [E], [F] and [G] depend only on the material properties, plastic strains and thermal strains. The axial strains do not occur in the above. Multiplication of this equation by the inverse of [E] results in the equation

$$\begin{Bmatrix}\sigma_r \\ \sigma_\theta \\ \sigma_z\end{Bmatrix}_{j+1} = [L(j)] \begin{Bmatrix}\sigma_r \\ \sigma_\theta \\ \sigma_z\end{Bmatrix}_{j} + \{M(j)\}. \qquad (147)$$

Since neither [E] nor [F] depend on the plastic strains, the matrices $[E]^{-1}$ and [L] need to be found only once for each load

step. Hence only [E] [G] need to be recomputed at each step of the iteration in the Method of Successive Substitutions.

Transfer Matrix Across a Surface of Displacement Discontinuity--One annulus of zero thickness is used as a surface of discontinuity. The radial displacement and axial strain across this discontinuity may be discontinuous. The displacements on each side of the surface are related by

$$u_r(k) = u_r(k+1) + \Delta u_r \tag{148}$$

$$\varepsilon_z(k) = \varepsilon_z(k+1) + \Delta\varepsilon_z \tag{149}$$

where k is the annulus corresponding to the surface of discontinuity. In addition, the radial stress must be continuous, so that

$$\sigma_r(k) = \sigma_r(k+1) \tag{150}$$

Then by use of the compatability equations and $\varepsilon_\theta = u_r/r$, Equations (148), (149) and (150) can be written in matrix form as

$$[P]_{k+1} \{\sigma\}_{k+1} = [P]_k \{\sigma\}_k + [Q] \tag{151}$$

The inverse of [P] is easily evaluated explicitly, so that the appropriate transfer relations across the fuel-cladding interface are

$$\{\sigma\}_{k+1} = [P]^{-1}_{k+1} [P]_k \{\sigma\}_k + [P]^{-1}_{k+1} \{Q\} \quad (152)$$

which is in the form of Equation (128). Similar transfer relations are used for different combinations of axial and radial crack patterns.

2.4.2 The PELET/RADIAL Model. This section describes the RADIAL model, which estimates the thermal/mechanical state of the fuel during a time step, and the PELET model, which calculates the incremental elastic-plastic cladding deformation at the end of the time step. The interconnection between RADIAL and PELET was indicated in Section 2.2.2 and is described in detail in Appendix C.

2.4.2.1 The RADIAL Model--The principles by which hydrostatic stress and free area distribution are derived from in-reactor data were described in Section 2.2.2. The free area is that portion of the (r,θ) area circumscribed by the cladding which is not occupied by fuel. Part of this area resides in the fuel-cladding gap, and the remainder in the fuel cracks. These same principles and assumptions are applied in the RADIAL model (where current temperatures and powers are treated as data) to converge on values for the hydrostatic stress and free area partition for each axial node for the current time step.

This convergence is accomplished as follows. It is required to bring the quantity (PRG-PRF) below some criterion, where PRG and PRF are the (hydrostatic) stresses in the fuel-cladding gap and fuel cracks, respectively. These two variables can be independently calculated via the Mikic Model given an estimate of total free area, that is, the area which results from the fuel and cladding temperature and expansion plus an estimate of the current local fuel-cladding gap size. Choices for the fuel-cladding gap size are

constrained. They must be less than about 3σ, where σ is the standard deviation of the fuel-cladding gap roughness (1/2 peak height). The value of σ is fixed in RADIAL as 1/5 of the as-fabricated fuel-cladding gap size. (Changes to this gap size occuring from densification, creep, and swelling are taken into account.) The problem is to find some rule for successive variations of fuel-cladding gap size so that convergence is achieved. The method used is sketched in Figure 17. The original set of gap size-stress values from the previous time step is varied up and down producing three cases and three values for (PRF-PRG). A parabolic fit through these values gives an estimated fuel-cladding gap size where (PRF-PRG) = 0. The process is then repeated, using the last three values of (PRF-PRG). Convergence is rapid. The effective values for fuel elastic moduli can then be estimated via empirical correlations which will now be described.

The values deduced for the effective radial and axial moduli from in-reactor data have been found to correlate particularly well with certain parameters: the radial modulus correlates well with estimated local crack area and the deduced effective axial modulus correlates well with the calculated local total free area. The specific rods examined are listed in Table 2. Note that they span the range (in terms of cold free area) of U.S. power reactor fuel rod designs. This is emphasized in Figure 18. Plots of deduced elastic moduli versus void area are shown in Figures 19 and 20. The respective void areas are expressed as percent of total area within the cladding. Note that both moduli exhibit distinct separation according to cold free volume, in addition to having strong dependence on the change in void area with increasing power. This segregation is not a measurement anomaly; replicate rods from various tests produced highly similar results. In addition, rod 6 in test IFA-513 and Rod 1 of test IFA-432, although identical in design, are different in fill gas composition and hence, in power-

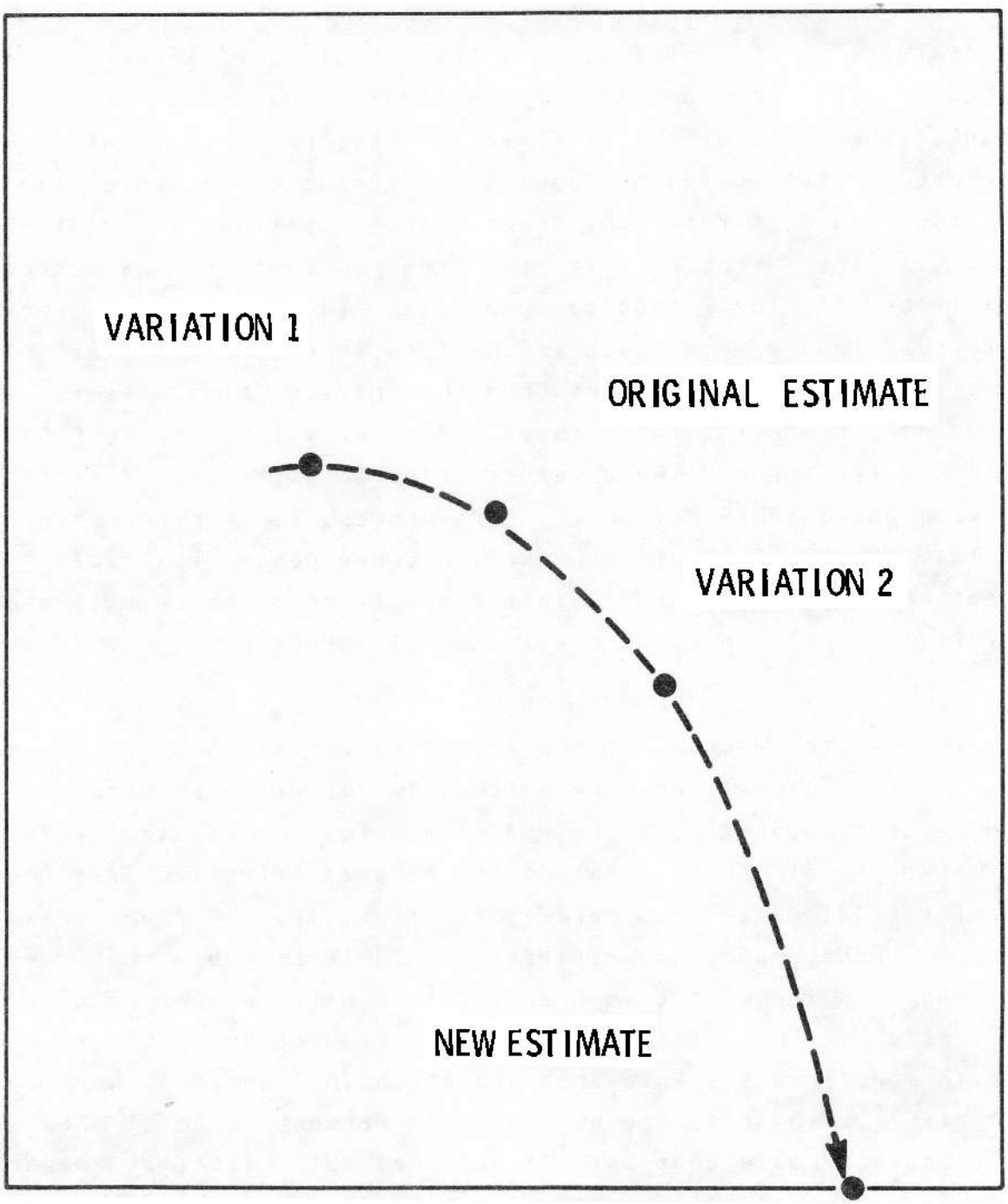

Figure 17. Convergence method for determining gap size and interfacial (hydrostatic) pressure.

TABLE 2. RODS EXAMINED FOR FUEL ELASTIC MODULUS CORRELATIONS (ALL 10% ENRICHED)

Halden Reactor Assembly Number	Rod Number	Fuel Pellet Diameter (mm)	Diametral Gap (m)	Fill Gas Composition
432	1	10.68	230	He
432	2	10.52	380	He
432	3	10.83	75	He
513	6	10.68	230	He,Xe(77%,23%)

temperature relationship. Their correspondence on both plots attests to both the adequacy of the correlating parameters and the reality of segregation according to initial void area.

These facts provide a basis for correlating effective moduli with current free void and its partition. The elements of these correlations (identical in logic for both moduli) are best shown schematically. In Figures 21 and 22 limit lines are shown for the radial and axial elastic moduli, respectively. These represent upper and lower (zero- and high-power) limits on the moduli as a function of crack and total void area, respectively.

A hypothetical path for a particular fuel rod during ascension to power is traced on each plot given in Figures 21 and 22. As power and temperature increase, the void fraction decreases. At

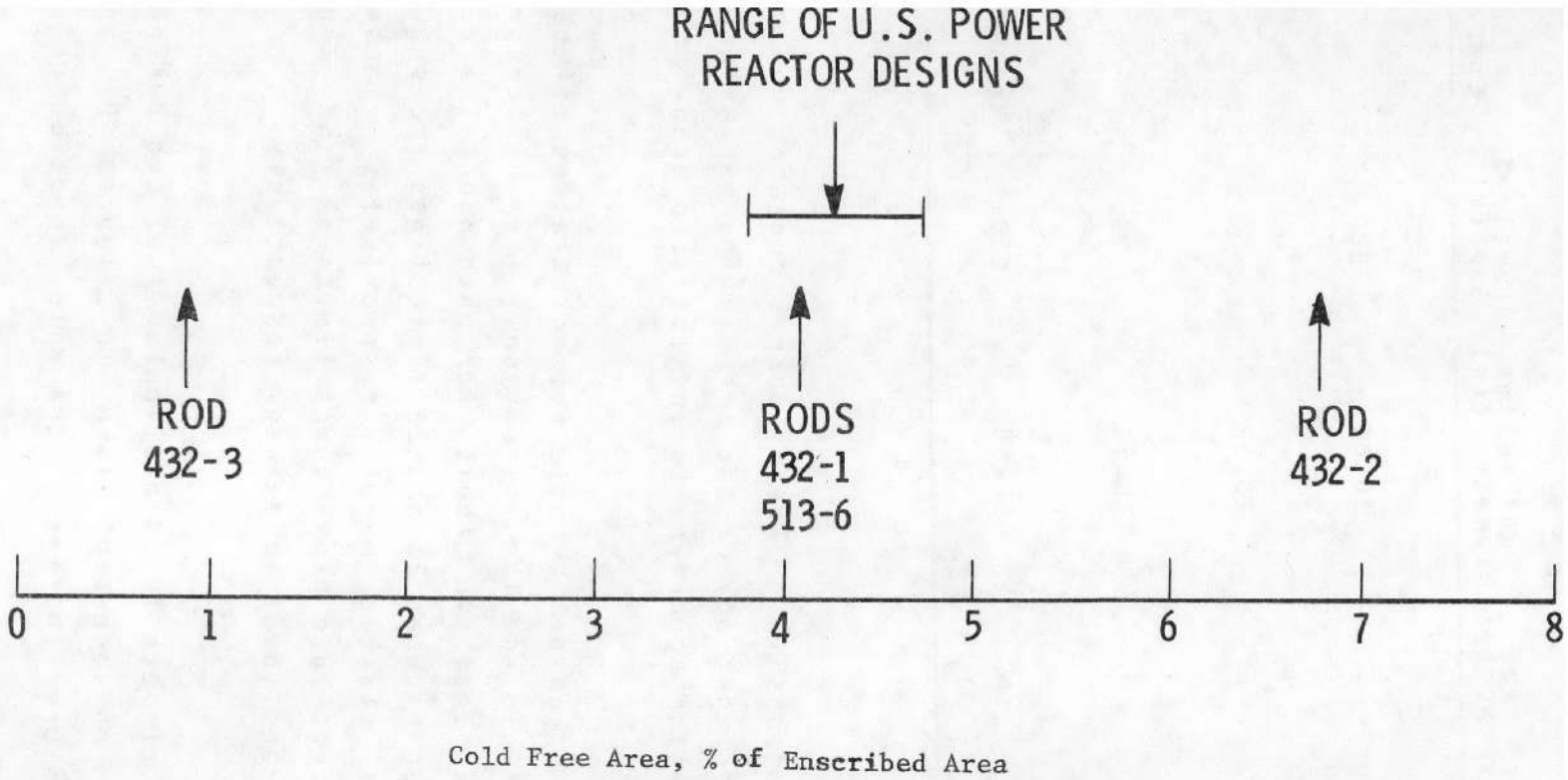

Figure 18. Range of test rods examined in terms of free area within the cladding.

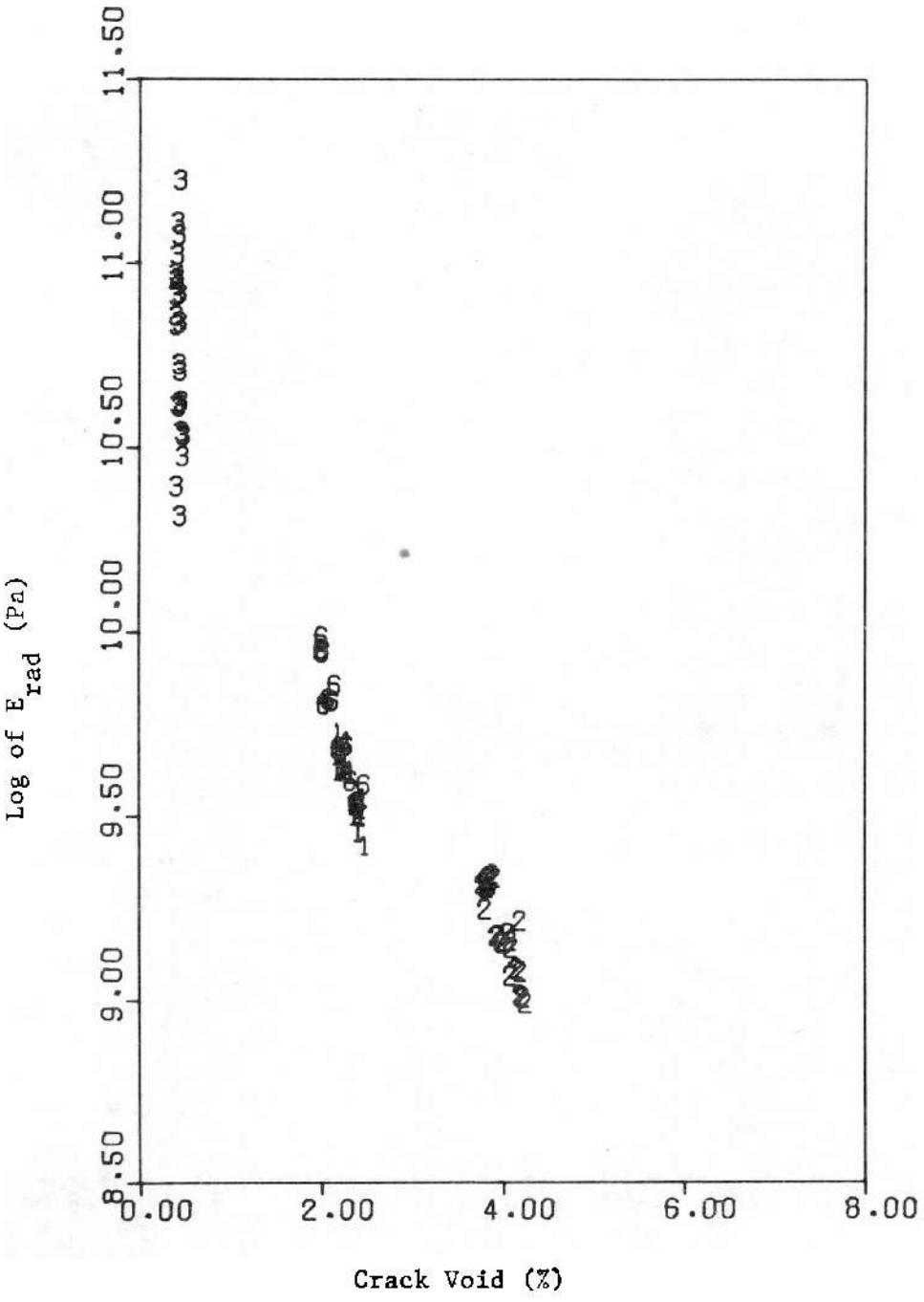

Figure 19. Radial elastic modulus as a function of fuel available void (data points identified by rod number).

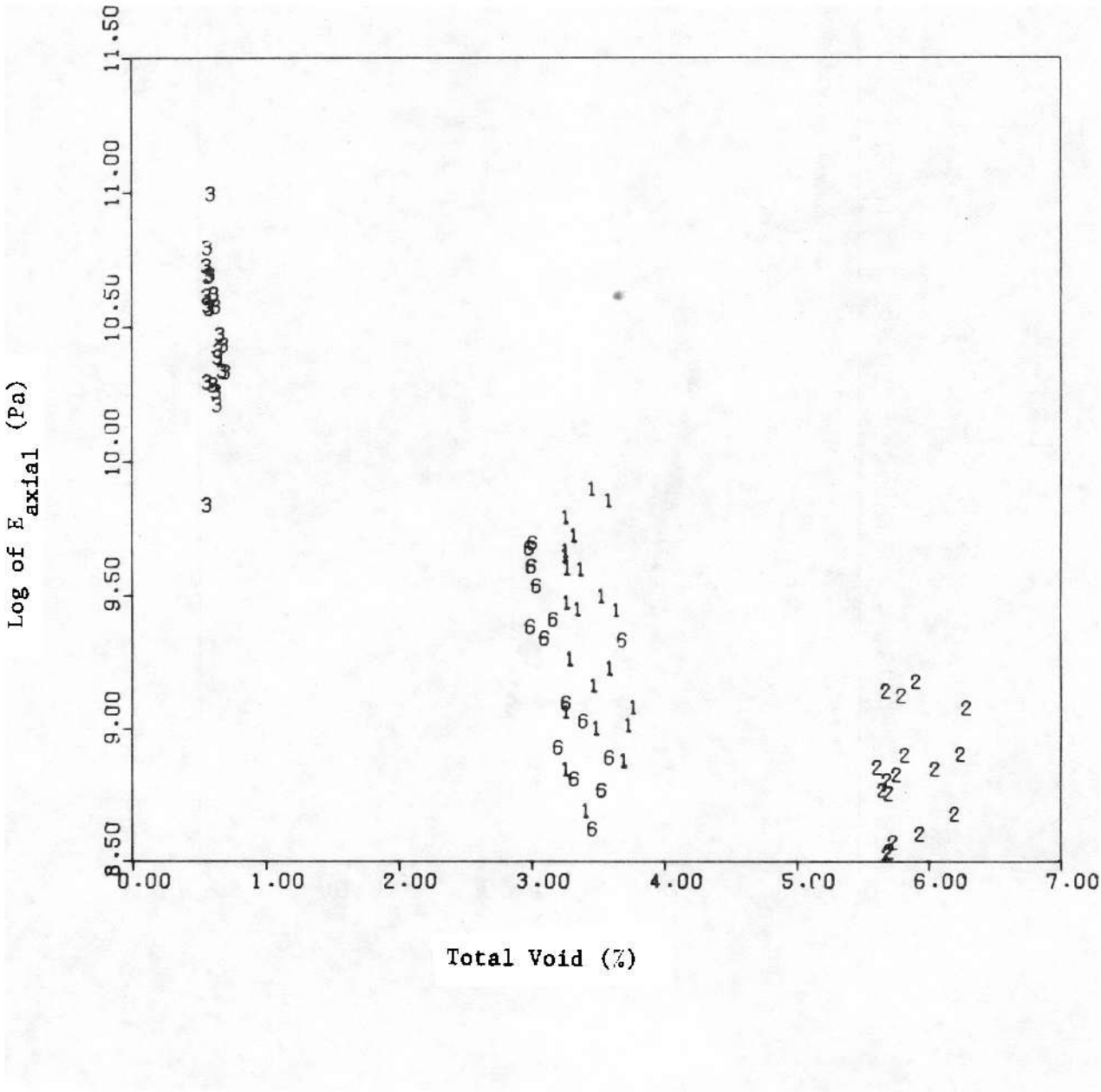

Figure 20. Axial elastic modulus as a function of total available void (data points identified by rod number).

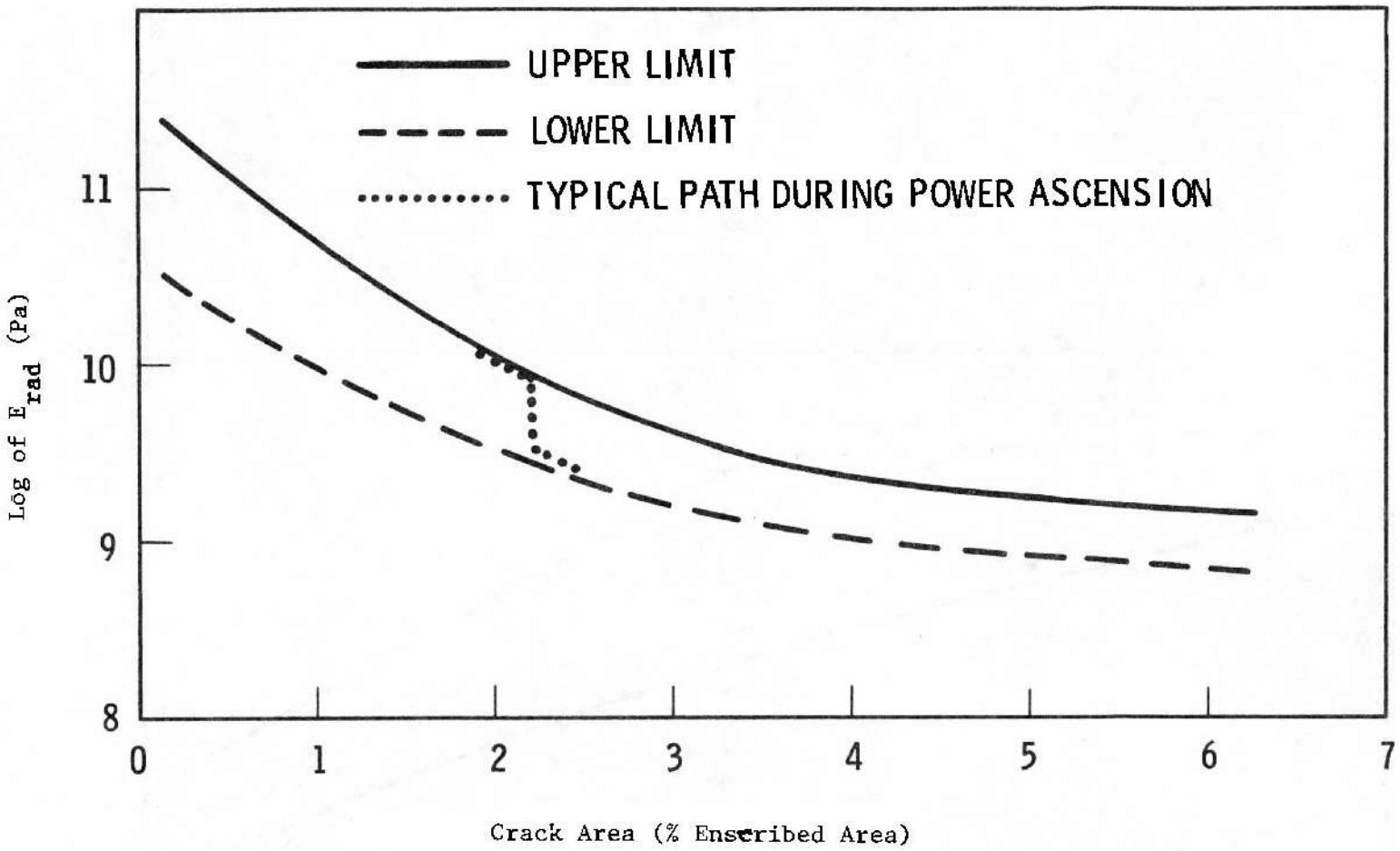

Figure 21. Upper and lower limits of the fuel radial modulus as a function of current crack area.

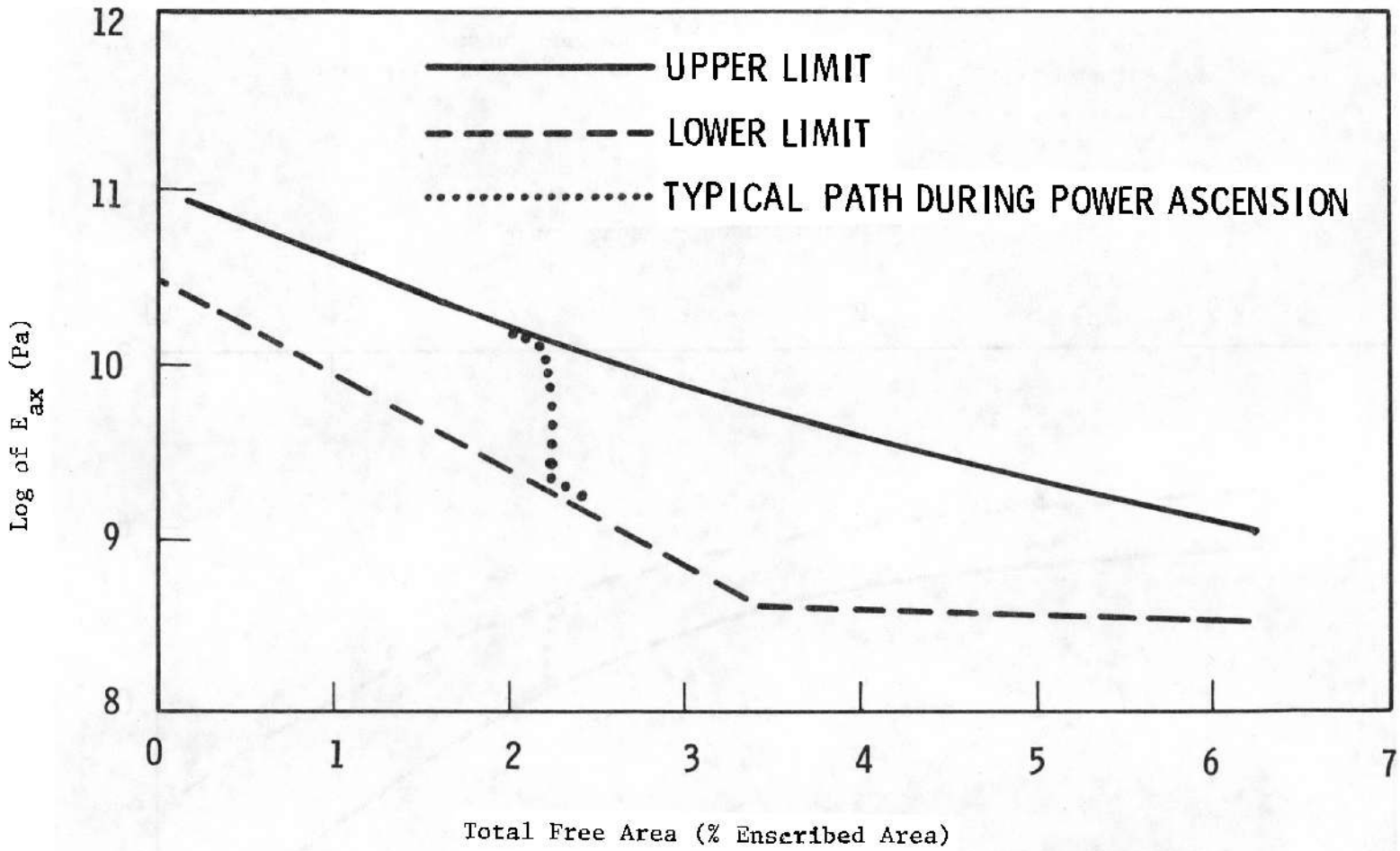

Figure 22. Upper and lower limits for the fuel axial modulus as a function of current total free area.

first, the modulus is allowed to respond to decreasing void fraction by traveling only along the lower limit curve. However, with a continually decreasing void, the modulus is allowed to travel toward the upper limit curve and is constrained to follow that curve having intersected it. The criteria governing departure from the lower limit curve and travel toward the upper limit curve is discussed below.

From cladding elongation data, a distinct change in slope for elongation versus power plots was observed at about the point where 15% of the total (cold) free void is estimated to be consumed by fuel thermal expansion. Accordingly, this is established as the point of departure from the lower limit curve. Similarly, it has been observed that the slopes of the cladding elongation versus power curves tend to increase only until fuel volume average temperature exceeds the temperature at the departure point by about 280 K. Accordingly, the ratio $\frac{\overline{T} - \overline{T}_D}{280}$ defines the fraction of the total distance between the two curves which the rod will attain. In the above, $\overline{T}$ is the current volume average fuel temperature and $\overline{T}_c$ is fuel average temperature at the time of departure from the lower-limit curve. These criteria apply to both moduli.

2.4.2.2 The PELET Package for Mechanical Analysis--PELET is a modification of the chained radial and axial finite element models used in the GAPCON-3[5] fuel performance code. The axial and radial models are "chained" in the sense that the axial stresses from the axial model constrain the radial calculations, which apply to representative slices of the fuel at each axial node. This section reviews both the original calculational procedure and the nature of the modifications made to it. This review is followed by a detailed

discussion of the basic models and solution procedures. Finally, the methods by which cladding creep and plasticity are handled in PELET are described.

Modifications to the GAPCON-3 Procedure--The GAPCON-3 procedure for finding the incremental elastic deformation and stress in the cladding is:

1. Representative thin slices of fuel rod (at midpoints of axial regions) are modeled by a series of axisymmetric triangular elements (see Figures 23 and 24). Incremental thermal strain on these elements is treated as initial strain, and translated into loads. These are combined with incremental pressure loads to find incremental stress in the elements.

2. The estimate of incremental fuel-cladding interfacial pressure (for regions in contact) is translated to radial loads which are applied to a comprehensive axial model of the total fuel rod (see Figure 25). Only axial stresses and strains are retained from this model.

3. The axial stresses within each axial region are translated to axial loads for a final pass through the radial models.

This chained radial-axial-radial procedure is modified in the PELET model in the following ways:

1. All axial regions are assumed to always be in contact. Therefore, radial model calculations are

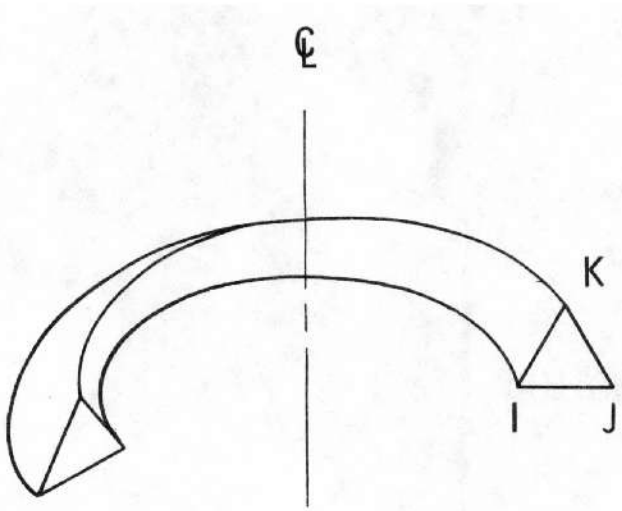

AXISYMMETRIC RING
FINITE ELEMENT

$$[K]\{q\} = \{f_a\} + \{f_a\} \ldots \{f_i\}$$

BASIC EQUATION

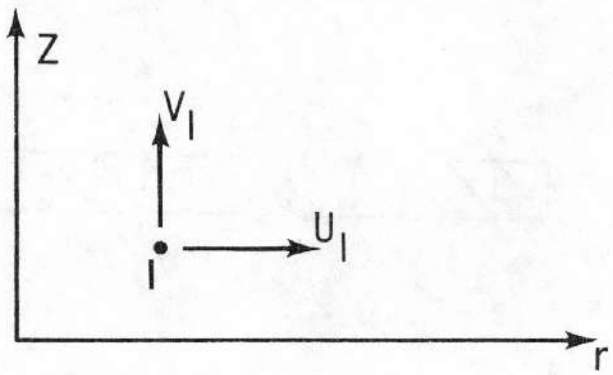

WHERE:

$[K]$ = STIFFNESS MATRIX FOR ELEMENT OR ELEMENTS

$\{q\}$ = NODE DISPLACEMENT VECTOR

$\{f_i\}$ = LOAD VECTOR OF NODAL APPLIED LOADS, THERMAL LOADS, CREEP AND PLASTICITY LOADS

Figure 23. Basic axisymmetric ring element used in the stress analysis models.

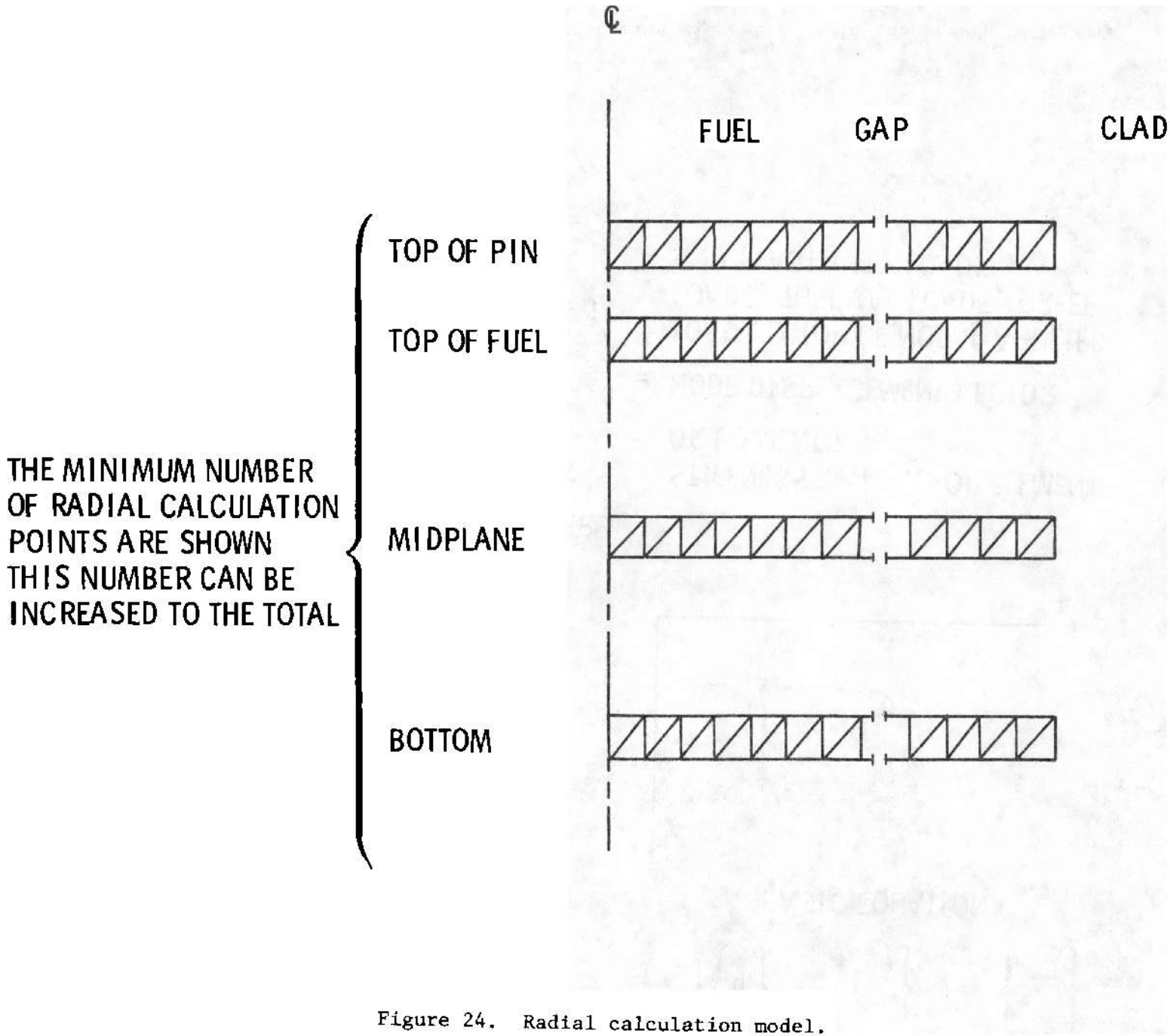

Figure 24. Radial calculation model.

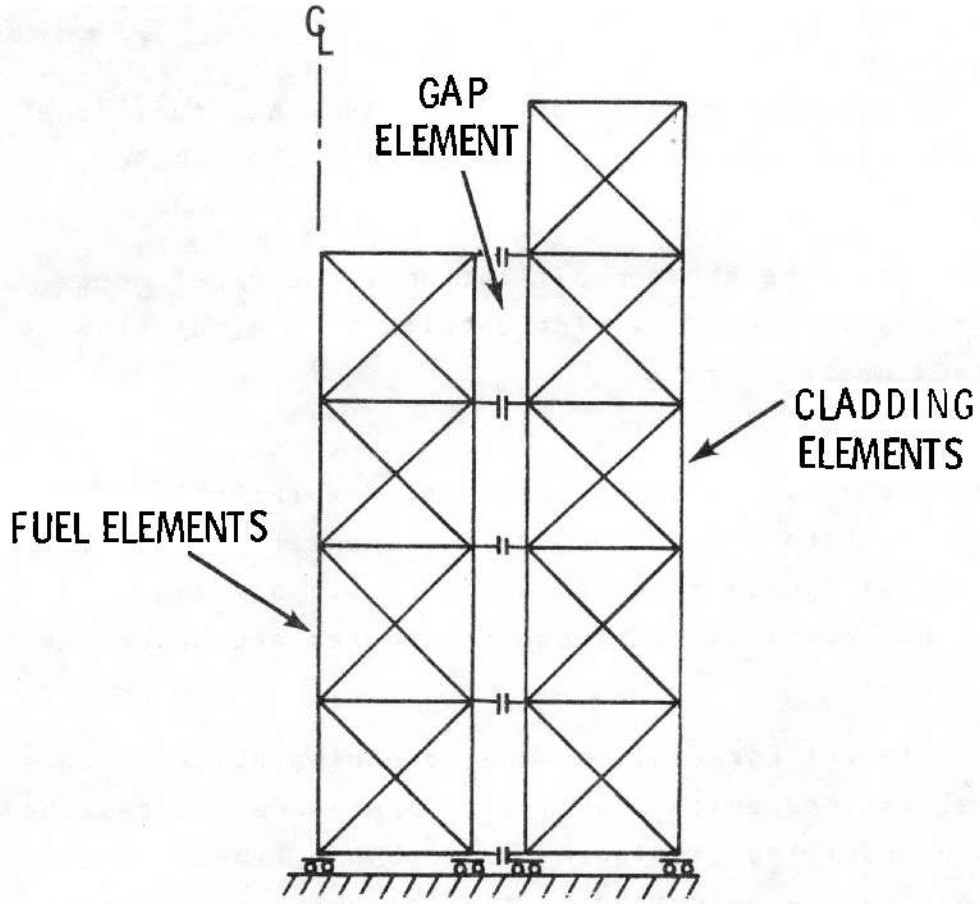

Figure 25. The axial mechanical analysis model using a quadrilateral element composed of four triangular elements. Cladding is accomplished by closure of the gap elements.

performed at all regions.

2. Next, the RADIAL model provides the estimate of incremental interfacial pressure; therefore, the first pass through the radial model has been eliminated.

3. The elastic moduli assigned to the fuel are altered (reduced) and are supplied to PELET by RADIAL.

Except for the above modifications, the PELET model functions in FRAPCON-2 as in GAPCON-3. The details of the solution procedure are discussed next.

Basic Models: Solution and Incrementation Procedures--The formulation solution procedures and incremental procedures for the radial and axial finite element models remain unchanged in PELET for FRAPCON-2. For completeness these procedures are described below.

Finite Element Formulation--the governing equation in a finite element matrix mechanical analysis procedure relates the applied loads to the resulting displacement through a linear transformation matrix. This can be described by the following equation:

$$[K]\,[q]_i = [f]_{external} + [f]_{creep} + [f]_{thermal} + [f]_{plastic} = [f]_i \qquad (153)$$

where

$[f]_{plastic}$ = incremental load vector due to plastic loads

$[f]_{external}$ = incremental load vector due to external loads

$[f]_{creep}$ = incremental load vector due to creep loads

$[f]_{thermal}$ = incremental load vector due to thermal loads

$[q]$ = nodal displacement vector for a given incremental load vector

$[K]$ = stiffness matrix or tranformation matrix relating applied loads and displacements.

The fuel-cladding system experiences strains resulting from displacements due to thermal expansion, internal and external pressure, and fuel-cladding interaction. Further displacement strains are incurred though creep and plasticity. In PELET these sources of strain are expressed as line loads $[f]_i$ at the element boundaries.

Changes in the element stresses and strains resulting from changes in the incremental load vectors $[f]_i$ are found by:

1. Translating thermal expansion and external load changes to incrmental nodal load vectors $[f]_i$.

2. Solving Equation (153) for the entire model to get the nodal displacements.

3. Translating the nodal displacements of each element to element strain.

4. Subtracting the initial strain. (See the following sections).

5. Calculating stress from strain.

6. Correcting for creep and plastic strains by translating these to nodal loads and repeating Steps 1 through 5.

The stiffness matrix for the entire model is assembled from the matrices for the individual elements, subject to compatibility of nodal displacements and to boundary conditions. Each element matrix is a 6 by 6 symmetric matrix, reflecting six degrees of freedom (radial and axial movement of the three corner node points). The matrices for all elements are identical algebraically, since all elements are identical structurally. The numerical values of the K from the different matrices are different for the following reasons.

1. The elements differ geometrically. (Nodes and internal degrees of freedom are always numbered counter-clockwise beginning at the lower left corner. For some elements $r_1 = r_3$ whereas for others $r_2 = r_3$, etc.).

2. The material properties will be evaluated at the element temperature which differs from element to element.

3. The dimensions of the elements will vary as deformation proceeds.

The single element shown in Figure 23 identifies the three triangular nodal points IJK. The figure indicates that for each node there are two displacements, u and v, corresponding to the radial and axial directions for a total of six displacements for a given element. The element stiffness matrix [K] is then a 6 by 6

matrix relating the six unknown displacements with six loads applied at the element nodes.

The derivation of Equation (153) is based on the minimization of the potential, or strain energy, in a continuum which can be specialized to a separate element. The strain energy can be written as shown in Equations (154), (155), and (156) using the concept of virtual strains and displacements and relating the strain energy of the body to the work done by body loads and surface loads:

$$\Pi = \int_{vol} dU - \int_{vol} xdV - \int_{surface} Tds \tag{154}$$

$$dU = \frac{1}{2} \{\varepsilon\}^T \{\sigma\}\, dV = \frac{1}{2} \{\varepsilon\}^T [C] [(\{\varepsilon\} - \{\varepsilon_o\})]\, dV \tag{155}$$

$$\Pi = \frac{1}{2} \int_{volume} \{\varepsilon^*\}^T [C] \{\varepsilon\} dV - \frac{1}{2} \int_{volume} \{\varepsilon^*\}^T [C]\{\varepsilon_o\}\, dV - \int_{volume} Xq^* dV - \int_{surface} Tq^* ds \tag{156}$$

where

$[\varepsilon]$ = strains (unknown and virtual)

$[\varepsilon_o]$ = initial strains (known thermal, creep, etc.)

$[C]$ = material matrix

X = body forces

= 0, for this application

T = surface tractions

q^* = virtual displacements

dU = internal energy.

The component parts of Equation (156) can be rewritten in terms of matrix notation for an element where internal stresses and strains are described in terms of element nodal values. Equation (157) defines a transformation matrix, [N], for an interpolation function which relates the displacements of the element nodal points [q] with the displacements internal to the element [u].

$$\{u\} = [N]\{q\} \tag{157}$$

An additional transformation matrix, [B], can be developed which relates the element nodal point displacements, [q], with the element strains, [ε], as defined in Equation (158).

$$\{\varepsilon\} + [B]\{q\} \tag{158}$$

By using Equation (158) and the material coefficient matrix, [C], the element strain matrix, [ε], and element displacement matrix, [q], can be related to the element stress matrix, [σ], as shown below

$$\text{or} \quad \{\sigma\} = [C]\{\varepsilon\}$$

$$\{\sigma\} = [C][B]\{q\} \tag{159}$$

The expression for describing the potential energy [Equation (154)] can be rewritten by direct substitution of Equations (157), (158), and (159) as

$$\Pi = \frac{1}{2}\int_{\text{volume}}\{q^*\}^T[B]^T[C][B]\{q\}dV - \frac{1}{2}\int_{\text{volume}}\{q^*\}^T[B]^T[C]\{\varepsilon_o\}dV$$

$$-\int_{\text{volume}}\{q^*\}^T[N]^T\{X\}dV - \int_{\text{surface}}\{q^*\}^T[N]^T\{d\}ds \qquad (160)$$

Using the variational principle for finding the minimum potential energy shown in Equation (154) and differentiating with respect to the virtual displacements, the expression can be rewritten in terms of the functional Π, the strain energy U and the external work W as shown in Equation (161).

$$\Delta\Pi = \Delta U + \Delta W = 0 \qquad (161)$$

Extracting the virtual displacement vector [q] from Equation (160) and performing the first variations indicated in Equation (161) with respect to the virtual displacements, Equation (162) is obtained.

$$0 = \int_{\text{volume}}[B]^T[C][B]\{q\}dV - \int_{\text{volume}}[B]^T[C]\{\varepsilon_o\}dV - \int_{\text{volume}}[N]^T\{X\}dV - \int_{\text{surface}}[N]^T\{T\}ds \qquad (162)$$

Equation (162) can be rewritten for this specific application by neglecting the body forces to obtain

$$\int_{\text{volume}} [B]^T[C][B]dV\{q\} - \int_{\text{volume}} [B]^T[C]\{\varepsilon_o\}dV - \int_{\text{surface}} [N]^T T\{ds\} = 0$$

or

$$[K]\{q\} = \{f_b\} + \{f_T\} \tag{163}$$

where

$$[K] = \int_{\text{volume}} [B]^T[C][B]dV = \text{(stiffness matrix for a single element)}$$

$$\{f_b\} = \int_{\text{volume}} [B]^T[C]\{\varepsilon_o\}dV = \text{(initial strain equivalent load vector)}$$

$$\{f_T\} = \int_{\text{surface}} [N]^T\{T\}ds = \text{(external applied surface forces translated into nodal loads)}$$

The matrices [B], [C] and [N] have yet to be defined for an axisymmetric constant strain triangular element.

For the case of interest, the initial strain term $[\varepsilon_o]$ takes the form of thermal, plasticity, and creep strains. Equation (153) can then be rewritten as

$$[K]\{q\} = \{f\}_{\text{thermal}} + \{f\}_{\text{plastic creep}} + \{f\}_{\text{external}} \tag{164}$$

which is identical to Equation (153).

The actual application of this procedure to a given problem

requires the selection of an element configuration (triangle, square, or rectangle) and the shape function [N] for describing the relationship between nodal point displacements [q] and displacements internal to the element [U].

In the case of FRAPCON-2, the element shape is a triangular ring. The triangular element is the least complicated of any of the special elements. The operation defined in Equation (163) indicates that the element formulation requires a volume integral to be performed. The axisymmetric triangular ring element allows integration as shown below.

$$[K] = 2\pi \iint [B]^T [C][B] r dr dz \tag{165}$$

An approximation to Equation (165) can be obtained by using centroidal values

$$[K] = 2\pi [\bar{B}]^T [C][\bar{B}] \bar{r} \, \Delta \tag{166}$$

where

Δ = cross sectional area of the triangle (the bar indicates evaluation at the element centroid).

Equation (166) has a further restriction in that the shape function [N] must be linear and does not require any additional nodal displacements other than at the element corners.

The shape function [N] can best be described by the geometry

shown by Figure 23 using the nodes IJK. The purpose of [N] is to provide a means of interpolating displacements within the boundary of the element defined by the nodal displacements of the element corners.

In general, the displacement of any node, I, can be broken into two components, u and v, as shown in Figure 23. A total displacement of six components is needed to complete the nodal displacement vector, Q. For a given element,

$$\{q\} = \begin{Bmatrix} u_I \\ v_I \\ u_J \\ v_J \\ u_K \\ v_K \end{Bmatrix} \tag{167}$$

Using a linear expression for u_I and v_I, Equation (168) can be written for all the nodes,

$$\begin{aligned} u_I &= \alpha_1 + \alpha_2 r_I + \alpha_3 Z_I \\ v_I &= \alpha_4 + \alpha_5 r_I + \alpha_6 z_I \\ u_J &= \alpha_1 + \alpha_2 r_J + \alpha_3 z_J \\ v_J &= \alpha_4 + \alpha_5 r_J + \alpha_6 z_J \\ u_K &= \alpha_1 + \alpha_2 r_K + \alpha_3 z_K \\ v_K &= \alpha_4 + \alpha_5 r_K + \alpha_6 z_K \end{aligned} \tag{168}$$

where

r_I = radial dimension of the nodal point I

z_I = axial dimension of the nodal point I

α = coefficient, to be determined

u_I = nodal displacement vector

v_I = nodal displacement vector.

Equation (168) can be solved for the α, and an expression can then be written for the displacements u and v of any point within the element at some location r and z [see Equation (169)]. This transformation between nodal point values and internal conditions is the interpolation function [N]

$$\begin{Bmatrix} u \\ v \end{Bmatrix} = \frac{1}{2\Delta} \begin{bmatrix} (a_I+b_Ir+c_Iz) & 0 & (a_J+b_Jr+c_Jz) & 0 & (a_K+b_Kr+c_Ka) & 0 \\ 0 & (a_I+b_Ir+c_Iz) & 0 & (a_J+b_Jr+c_Jz) & 0 & (a_K+b_Kr+c_Kz) \end{bmatrix} \begin{pmatrix} u_I \\ v_I \\ u_J \\ v_J \\ u_K \\ v_K \end{pmatrix} \quad (169)$$

where

Δ = area of the triangular cross section IJK

$a_I = r_Jz_K - r_Kz_J$

$a_J = r_Kz_I - r_Iz_K$

$a_K = r_Iz_J - r_Jk_I$

$b_I = z_J - z_K$

$b_J = z_K - z_I$

$$
\begin{aligned}
b_K &= z_I - z_J \\
c_I &= r_K - r_J \\
c_J &= r_I - r_K \\
c_K &= r_J - r_I
\end{aligned}
\tag{170}
$$

Equation (169) can be rewritten in the form used in Equation (157) as shown below.

$$
\begin{Bmatrix} u \\ v \end{Bmatrix} = [N]\{q\} \tag{171}
$$

The [B] matrix, defined by Equation (157), relates displacements to strains and can be developed by examining the strain terms which are defined for the axisymmetric condition as

$$
\{\varepsilon\} = \begin{Bmatrix} \varepsilon_r \\ \varepsilon_\theta \\ \varepsilon_z \\ \gamma_{rz} \end{Bmatrix} = \begin{Bmatrix} \dfrac{\partial u}{\partial r} \\ \dfrac{u}{r} \\ \dfrac{\partial v}{\partial z} \\ \dfrac{\partial u}{\partial z} + \dfrac{\partial v}{\partial r} \end{Bmatrix} \tag{172}
$$

or, noting that u and v are [q],

$$\{\varepsilon\} = [B]\{q\} \tag{173}$$

where $[\bar{B}]$ is evaluated at the element centroid (the bar denotes centroidal values for r denoted by $\bar{r}$),

$$[\bar{B}] = \begin{bmatrix} \frac{\partial N_I}{\partial r} & 0 & \frac{\partial N_J}{\partial r} & 0 & \frac{\partial N_K}{\partial r} & 0 \\ \frac{N_I}{\bar{r}} & 0 & \frac{N_J}{\bar{r}} & 0 & \frac{N_K}{\bar{r}} & 0 \\ 0 & \frac{\partial N_I}{\partial z} & 0 & \frac{\partial N_J}{\partial z} & 0 & \frac{\partial N_K}{\partial z} \\ \frac{\partial N_I}{\partial z} & \frac{\partial N_I}{\partial r} & \frac{\partial N_J}{\partial z} & \frac{\partial N_J}{\partial r} & \frac{\partial N_K}{\partial z} & \frac{\partial N_K}{\partial r} \end{bmatrix} \tag{174}$$

where

$$\frac{\partial N_I}{\partial r} = b_I \qquad \frac{\partial N_I}{\partial z} = c_I$$

$$\frac{\partial N_J}{\partial r} = b_j \qquad \frac{\partial N_J}{\partial z} = c_J$$

$$\frac{\partial N_K}{\partial r} = b_k \qquad \frac{\partial N_K}{\partial z} = c_K$$

$$\frac{N_I}{\bar{r}} = \frac{a_I}{\bar{r}} + b_I + \frac{c_I \bar{z}}{\bar{r}}$$

$$\frac{N_J}{\bar{r}} = \frac{a_J}{\bar{r}} + b_J + \frac{c_J \bar{z}}{\bar{r}}$$

$$\frac{N_K}{\bar{r}} = \frac{a_K}{\bar{r}} + b_K + \frac{c_K \bar{z}}{\bar{r}} \qquad (175)$$

The material matrix [C] can either be written for anisotsropic material properties or for isotropic conditions. PELET presently uses the latter condition in the cladding

$$[C] = \frac{E}{(1+\mu)\ (1-2\mu)} \begin{bmatrix} 1-\mu & \mu & \mu & 0 \\ \mu & 1-\mu & \mu & 0 \\ \mu & \mu & 1-\mu & 0 \\ 0 & 0 & 0 & \frac{1-2\mu}{2} \end{bmatrix} \qquad (176)$$

where

E = elasic modulus

μ = Poisson's ratio.

However in the fuel, the anisotropic form is used as follows

$$C = \frac{E_r}{(1+\mu_r)\ (1-\mu_r - 2\frac{E_r}{E_a}\mu_1^2)}$$

$$\begin{vmatrix} 1-\frac{E_r}{E_a}\mu_a^2 & \mu_r+\frac{E_r}{E_a}\mu_a^2 & \mu_a(1+\mu_r) & 0.0 \\ \mu_r+\frac{E_r}{E_a}\mu_a^2 & 1-\frac{E_r}{E_a}\mu_a^2 & \mu_a(1+\mu_r) & 0.0 \\ \mu_a(1+\mu_r) & \mu_a(1+\mu_r) & (1-\mu_r^2)\frac{E_a}{E_r} & 0.0 \\ 0.0 & 0.0 & 0.0 & \frac{(1+\mu_r)(1-\mu_r-2\frac{E_r}{E_a}\mu_a^2)}{2\frac{E_r}{E_a}(1+\mu_a)} \end{vmatrix} \quad (177)$$

where

$\bar{E}$ = elastic modulus

μ = Poisson's ratio

r = radial direction

a = axial direction.

By using Equations (169), (171), (172), (174), and (175), all of the matrix formulation terms previously defined can be found. It

is now necessary to develop the element stiffness matrix and load vectors for a single element. The implementation of this procedure for the radial and axial models is performed by formulating stiffness matrices for each individual element (XKBAR) and merging the separate matrices into a total stiffness matrix for the appropriate radial or axial model.

Assembly of the Global Stiffness Matrix-Radial Model--The assembly of individual finite elements into a total model involves careful accounting of the relative displacements or degrees of freedom (DOF) of each element. The radial model shown in Figure 24 has pairs of two triangular elements connected in series with additional pairs of elements. The merge operation of forming the global stiffness matrix from the element stiffness matrices consists of matching components in the individual stiffness matrices that involve common DOF from other elements and then summing them.

Each individual element has six DOF or two displacements at each of three corner nodes. A combined or global stiffness matrix may contain several hundred or thousand DOF. The individual matrices as well as the total global matrix are symmetric, banded and positive definite. The bandwidth is defined by the maximum number of DOF that interact with other DOF.

The fuel and cladding are assumed to be in contact, and a matrix for the total fuel-cladding system is formed by double-numbering the DOF common to the two material regions. Figure 26 illustrates the the final merged system and DOF numbering for it.

Figures 27 and 28 illustrates how the element stiffness components are assigned to the global stiffness matrix. Note that

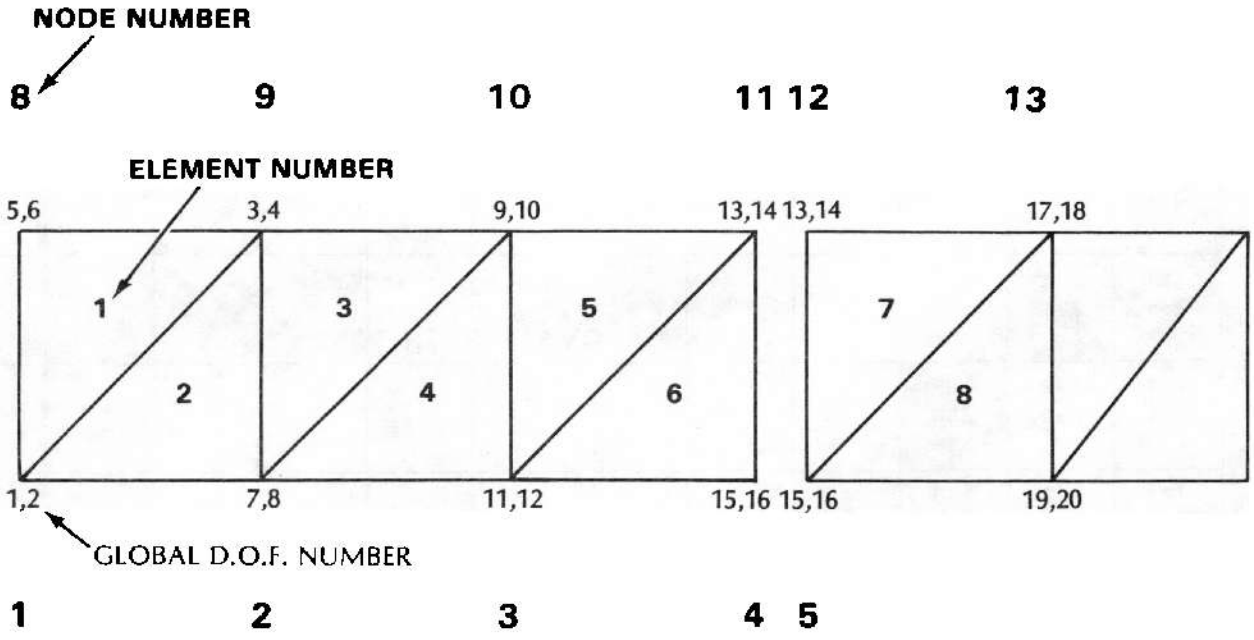

FUEL-CLAD COMBINED MODEL

Figure 26. Node and DOF numbering system for fuel-cladding combined radial model.

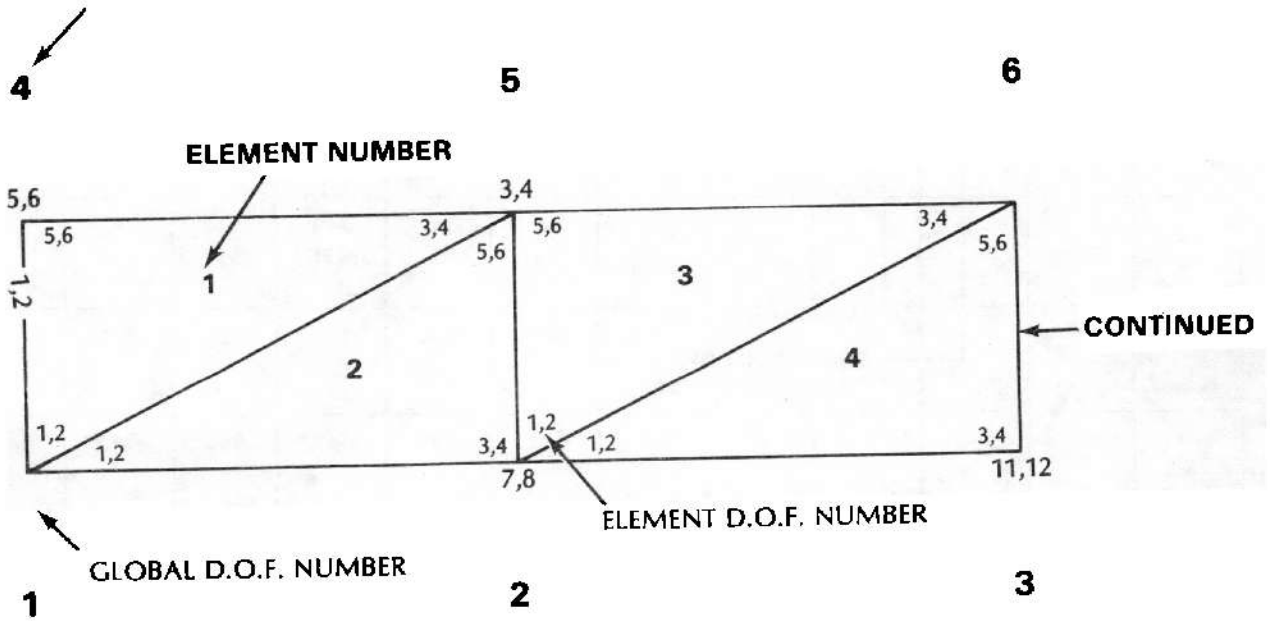

FUEL OR CLAD SEPARATE MODEL

Figure 27. Node and DOF numbering system for fuel or cladding separate radial model.

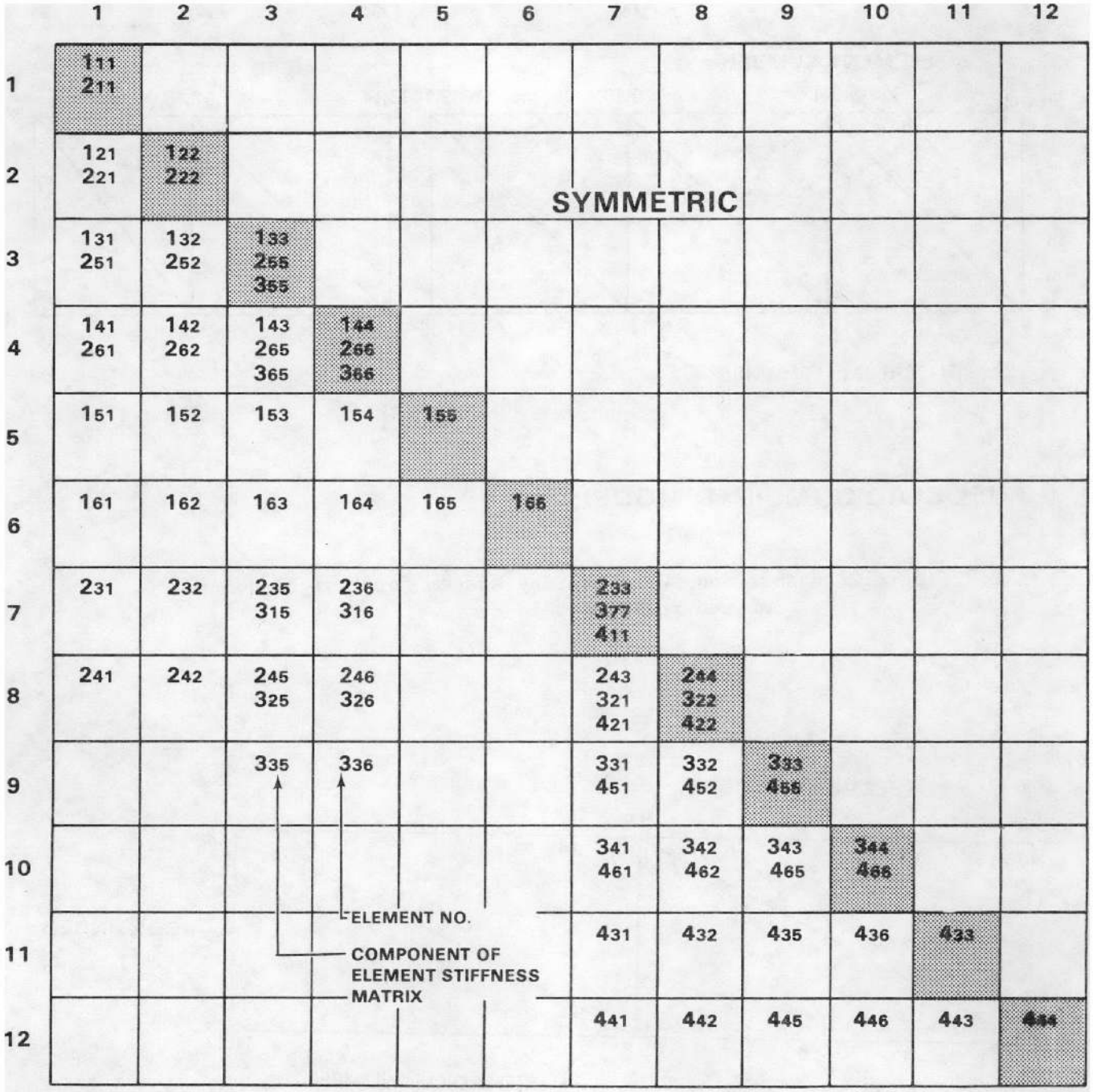

Figure 28. Global stiffness matrix for the four elements in Figure 27, global DOF numbers are along the outside.

node 1, for example, is shared by elements 1 and 2. Therefore, some components from elements 1 and 2 will be present in the global matrix in (global) DOF 1 and 2. Similarly node 5 is shared by elements 1, 2, and 3 so components from these elements would be expected to influence (global) DOF 3 and 4. The global stiffness matrix for the four elements shown in Figure 27 is presented schematically in Figure 28. An entry I is meant to indicate the jk-th component of the element stiffness matrix for element I. The diagonal components from contributing elements appear on the diagonal of the global matrix at the DOF those elements share. The assignment of the off-diagonal element components is more subtle, but in every case the shared DOF can be observed to be properly influenced by the contributing elements; e.g., DOF 4 has off-diagonal influence from elements 1, 2, and 3 only. Also the global stiffness matrix can be observed to be banded and symmetric. Because of the symmetry, only the main diagonal and either the upper or lower codiagonals need be retained. This greatly reduces the required computer core storage as compared with a square matrix of similar size.

Assembly of the Global Stiffness Matrix-Axial Model--The basic steps for calculating the element stiffness matrices used in the axial model are identical to the steps used in the radial model. The node and DOF numbering system for the axial model are shown in Figure 29. There is a renumbering of DOF in case of contact. The axial DOF for the boundaries of that region are to move together through the following procedure:

1. Let i and ii be the two axial degrees of freedom to be locked. In the global stiffness matrix, row ii is added to row i. To preserve symmetry, column ii is added to column i.

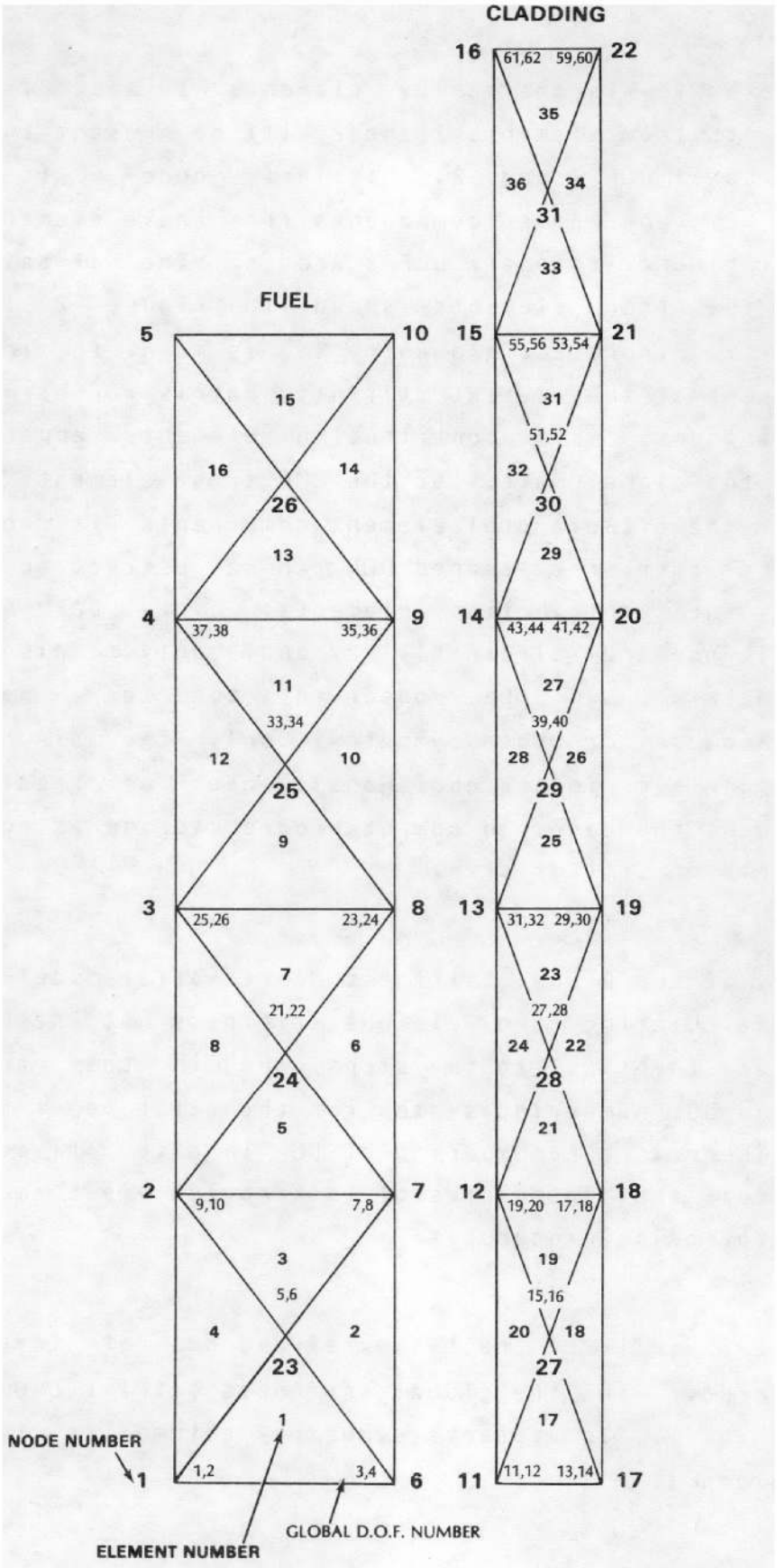

Figure 29. Node and DOF numbering system for fuel and cladding combined axial model.

2. Row and column ii are filled with zeros and a 1.0 is inserted on the diagonal at position (ii,ii).

3. Load ii is added to load i and load ii is filled with zeros.

4. In the solution, displacement ii will be zero and displacment i will represent the axial displacement in DOF i and ii. Arbitrarily set displacement ii through displacement i.

This procedure has been shown to collect all the proper influence from contributing elements and consists of a series of simple algebraic row and column operations.

Application of Boundary Conditions--The only boundary condition in the models is zero axial displacement along the bottom. Accordingly, the rows and columns corresponding to those DOF are set to zero in the global matrix, the diagonal term is set to one, and the corresponding load is set to zero. This forces the proper displacements to be zero.

Formulation of the Load Vector--The last step in the formulation of the problem is to transform the right-hand side of Equation (163) into a series of nodal loads (vector f).

The first load vector term in Equation (163) makes use of the [B] matrix to transform internal element initial strains into nodal loads,

$$2\pi \int_{\text{volume}} [B]^T[C]\{\varepsilon_o\} r dr d\theta = \{f\}_{\substack{\text{thermal}\\ \text{plastic}\\ \text{creep}}} \tag{178}$$

for centroidal values, this becomes

$$\{f\}_{\substack{\text{thermal}\\ \text{plastic}\\ \text{creep}}} = 2\pi \bar{r} \Delta [\bar{B}]^T[C]\{\varepsilon_o\} \tag{179}$$

The external load vectors, f_{external}, are developed by integrating the surface tractions, or pressures, and developing equivalent nodal loads

$$\int_{\text{surface}} [N]^T T ds = \{f\}_{\text{external}} \tag{180}$$

Because of the geometry used, the external loads become equivalent to line loads which are pressure driven. This leads to

$$\{f\}_{i_{\text{external}}} = \frac{\text{Pressure Acting on Element Face} * \text{Face Area}}{\text{Total Length of Nodal Line on Boundaries of Element Face (2 Nodes)}} * \text{Length of Node Line (i)} \tag{181}$$

The same result is obtained as if the total force on the exterior surface of the element had been lumped at its exterior nodes. This process of lumping is performed throughout the program.

Solution Procedure--Having formulated the global stiffness matrix and the loads, the remaining step is to solve for displacements and translate these into element stresses and strains. The solution routine takes advantage of the banded symmetric nature of the stiffness matrix.

Incrementation of Strains and Stresses--Incremental elastic strains and stresses are added to the total strain array after temperature convergence. Then creep/plastic strains are calculated and fed through the entire chain of radial and axial calculations to produce corrections to the stress and strain values. Automatic subdivision of the time step size may be done within this model to restrict the creep increment size. The solution is based on the concept that total strain can be described as

$$\varepsilon_T = \varepsilon_{elastic} + \varepsilon_{creep} + \varepsilon_{thermal} + \varepsilon_{plastic} \quad (182)$$

and that for any one incremental step, the strains and associated load vectors will be separated as follows:

$$\varepsilon_{T_i} = \varepsilon_{elastic_i} + \varepsilon_{thermal_i}$$

$$\varepsilon_{T_{i+1}} = \varepsilon_{elastic_{i+1}} + \varepsilon_{plastic_{i+1}}$$

$$\varepsilon_{T_{i+2}} = \varepsilon_{elastic_{i+2}} + \varepsilon_{creep_{i+2}} \quad (183)$$

---

a. The elastic stresses and strains for the i+1 and i+2 steps, change the elastic stress and strain distributions obtained as a result of the imposed plastic or creep strains. The total strain at the end of step i will be a sum of $\varepsilon_{Ti} + \varepsilon_{Ti+1} + \varepsilon_{Ti+2}$ with external loads and thermal loads from the ε_{Ti} increment and the plastic and creep effects from the i+1 and i+2 increments.

The stress state can be computed at the conclusion of a given time step or load step and the corrections to the stress distribution is as follows:

Thermal + Elastic

$$\{\sigma\}_i = [C]\{\varepsilon_T\} - [C]\{\varepsilon\}_{thermal}$$

Creep

$$\{\sigma\}_i = [C]\{\varepsilon_T\} - [C]\{\varepsilon\}_{creep}$$

Plastic

$$\{\sigma\}_i = [C]\{\varepsilon_T\} - [C]\{\varepsilon\}_{plastic} \quad (184)$$

where the total strain and stress vectors for the current point in time is a summation of the individual components.

$$\{\varepsilon_{total}\} = \sum_{i=1}^{n} \{\varepsilon_T\}_i \quad (185)$$

$$\{\sigma_{total}\} = \sum_{i=1}^{n} \{\sigma\}_i \quad (186)$$

Anisotropic Behavior--Anisotropy in plastic and creep deformation has a significant effect on the resulting deformation. The anisotropy model that is used is based on Hill's[26] concept of changing the definition of the effective stress and strain terms, and in addition, changing the coefficients in the Prandtl-Reuss equations. The modified Prandtl-Reuss equations

allocate the inelastic strain increment normal to the yield surface as a function of the stress and strain.

The definition of the anisotropy parameters change as a function of direction of testing. The equations for this application are referenced to the axial direction. This means that anisotropic strain characterizations should be based on uniaxial-axial material test results. A similiar set of equations can be developed for any of the other three directions.

For the isotropic case, the effective stress is given by

$$\sigma_e = \frac{1}{2}\left[(\sigma_{11}-\sigma_{22})^2 + (\sigma_{22}-\sigma_{33})^2 + (\sigma_{33}-\sigma_{11})^2\right]^{1/2} \qquad (187)$$

where

1 = axial direction

2 = hoop direction

3 = radial direction.

The effective strain is given by

$$d\varepsilon_e^P = \sqrt{\frac{2}{3}}\left[(d\varepsilon_{11}-d\varepsilon_{22})^2 + (d\varepsilon_{22}-d\varepsilon_{33})^2 + (d\varepsilon_{33}-d\varepsilon_{11})^2\right]^{1/2} \qquad (188)$$

The Prandtl-Reuss equations are

$$d\varepsilon_e^P = \frac{d\varepsilon_P}{\sigma_e} [\sigma_{11} - 1/2 (\sigma_{22} + \sigma_{33})]$$

$$d\varepsilon_e^P = \frac{d\varepsilon_P}{\sigma_e} [\sigma_{22} - 1/2 (\sigma_{11} + \sigma_{33})]$$

$$d\varepsilon_e^P = \frac{d\varepsilon_P}{\sigma_e} [\sigma_{33} - 1/2 (\sigma_{22} + \sigma_{11})] \quad (189)$$

For the case of anisotropy referenced to the axial direction, the effective stress is given by

$$\sigma_e = \left[\frac{R}{R+1} (\sigma_{11} - \sigma_{22})^2 + \frac{R}{P(R+1)} (\sigma_{22} - \sigma_{33}) + \frac{R}{R+1} (\sigma_{33} - \sigma_{11})\right]^{1/2} \quad (190)$$

where

$$R = \frac{\delta\varepsilon_{hoop}}{\delta\varepsilon_{radial}} \qquad \text{(obtained from a uniaxial axial test)}$$

$$P = \frac{\delta\varepsilon_{axial}}{\delta\varepsilon_{radial}} \qquad \text{(obtained from a uniaxial hoop test)}$$

$\delta\varepsilon$ = an increment of creep or plastic strain

The effective strain is given by

$$d\varepsilon_e^P = \frac{1}{G} [a_1(a_2 d\varepsilon_{11} - a_3 d\varepsilon_{22})^2 + a_2(a_3 d\varepsilon_{22} - a_1 d\varepsilon_{33})^2 + a_3(a_1 d\varepsilon_{33} - a_2 d\varepsilon_{11})^2]^{1/2} \quad (191)$$

where

$$G = \frac{R^2+R+PR}{P(R+1)^2}$$

$$a_1 = \frac{R}{R+1}$$

$$a_2 = \frac{R}{P(R+1)}$$

$$a_3 = \frac{1}{R+1}$$

The modified Prandtl-Reuss flow equations are

$$d\varepsilon^P_{33} = \frac{d\varepsilon_P}{\sigma_e}\left[\frac{P+R}{P(1+R)}\ \sigma_{33} - \frac{R}{P(1+R)}\ \sigma_{22} - \frac{1}{1+R}\ \sigma_{11}\right]$$

$$d\varepsilon^P_{22} = \frac{d\varepsilon_P}{\sigma_e}\left[\frac{R(P+1)}{P(R+1)}\ \sigma_{22} - \frac{R}{P(R+1)}\ \sigma_{33} - \frac{R}{R+1}\ \sigma_{11}\right]$$

$$d\varepsilon^P_{11} = \frac{d\varepsilon_P}{\sigma_e}\left[\sigma_{11} - \frac{R}{R+1}\ \sigma_{22} - \frac{1}{R+1}\ \sigma_{33}\right] \qquad (192)$$

For the case where the material is isotropic, R = 1, P = 1, and Equations (190), (191), and (192) become equal to Equations (187), (188), and (189).

Creep and Plasticity Equations--After the incremental elastic stresses and strains have been found and the total stress and strain arrays updated accordingly, incremental creep (generalized) strains are calculated and translated into loads, and thus, into stress-strain increments via the same procedure used for thermal strains.

An array of incremental strains is calculated by $d\varepsilon_e^P$ using eitner a strain hardening or time-hardening option (See Figure 30). The procedure is very general in nature and does not require a closed solution explicit in strain. The solution for a strain hardening calculation uses a modified Newton-Raphson iteration technique.

The modified Prandtl-Reuss equations are used to develop

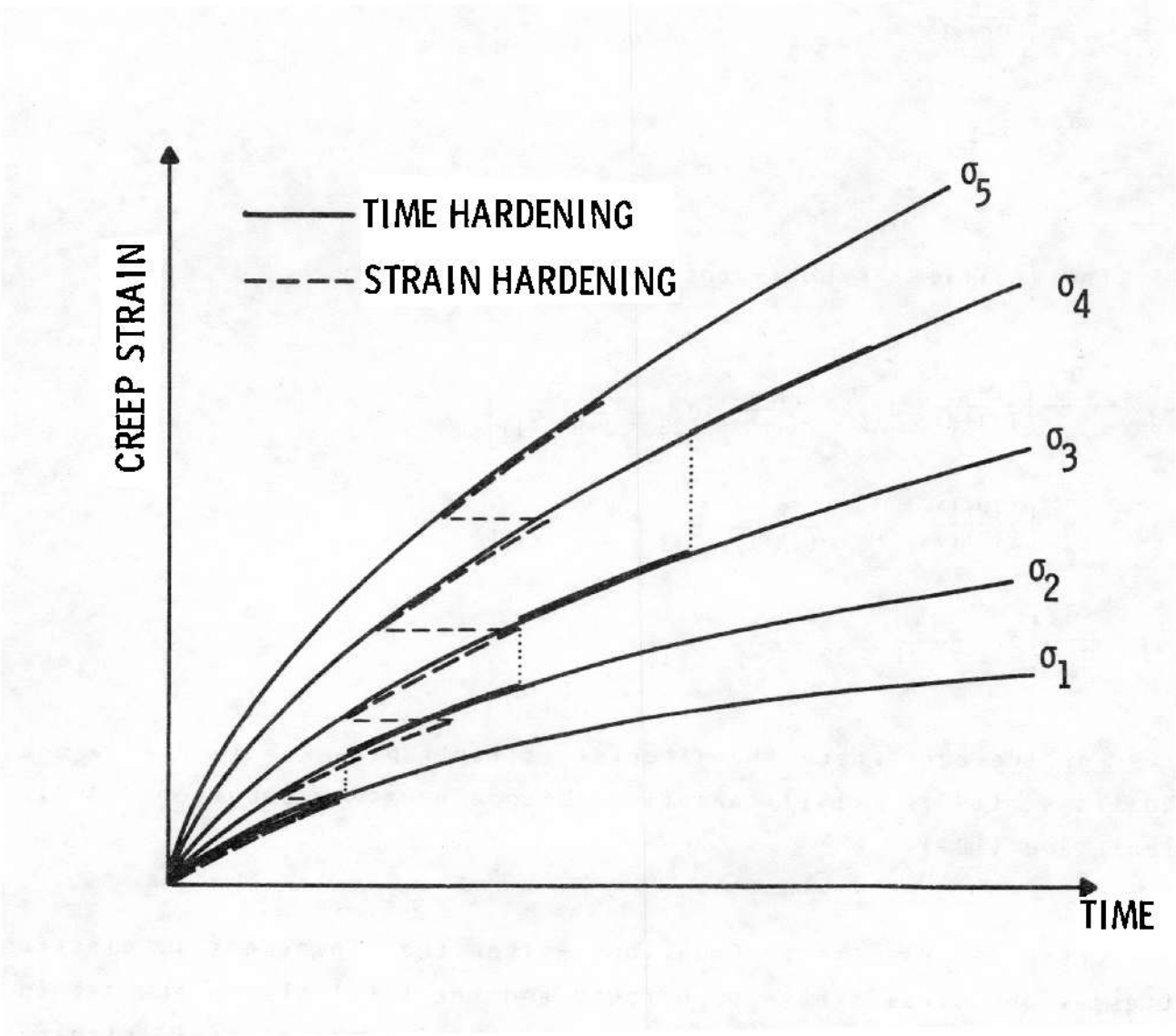

Figure 30. Comparison of strain hardening and time hardening options available.

initial strain vectors for each element $[\varepsilon_o]$. Using Equation (179), a set of of creep load vectors are developed that, when applied to the finite element structure, will cause it to deform. The computed strains are the total strains caused by the increments of creep strain. The corrections to the total stress state are found using Equation (184).

The creep equation used for zircaloy was developed by P.J. Pankaskie.[27]

$$\dot{\varepsilon} = A[1+\alpha\ k \exp(-k\ t)]\quad \exp(EAE)\quad [(1-f(\Delta T))\ \sinh(S_1\ \sigma) + [1+f(\Delta T)]\sinh(S_2\sigma)]/2 \tag{193}$$

where EAE is the effective activation energy consisting of the sum of a high temperature thermal activiation energy term, TAE, and a fast flux or low temperature activation energy term, FAE, as follows:

$$TAE = -[C\ (1-f(\Delta T)) + (D-0.038\ \sigma)\quad (1+f(\Delta T))]/2\ R\ T$$

$$FAE = 0.5\quad (E-F)\quad (1+f(\Delta T))$$

$$\phi > 0,\ E = n \cdot \ln\phi$$

$$\phi = 0,\ E = (C-0.044\sigma)\ [1 - \Delta T/(RT)]/(2RT_o)$$

$$\Delta T < 0,\ f(\Delta T) = -1$$

$$\Delta T \geq 0,\ f(\Delta T) = +1$$

α = 3310 (hr)

k = 0.0044 (hr^{-1})

A = 5.96 x 10^{14} (hr^{-1})

C = 63600.0 (cal/mole°K)

D = 9500.0 (cal/mole°K)

F = 65.77

ΔT = T_o-T, T_o + 640.0 exp(-7.18 x $10^{-7}\sigma$) (K)

n = 0.85

S_1 = 1.04 x 10^{-4} (psi^{-1})

S_2 = 1.0 x 10^{-5} (psi^{-1})

ϕ = fast flux - nvt ($E \gtrsim 1$ Mev)

σ = applied stress (psi)

Plasticity--The calculation of plastic strains is based on using the same initial strain method as is used for the creep calculation. The solution procedure, however, is implemented in a different manner and the criteria controlling the calculation are significantly altered.

The plasticity loop calculation is performed at the start of a creep loop. It is exercised when the stresses obtained from the just-completed elastic load step have driven the stresses in one or more elements above the yield stress. A test is made for each element based on the temperature and generalized strain in each element for that time.

As an example, consider the four-element cladding model shown

in Figure 27. For some loading conditions, the stresses for this four-element model are shown in Figure 31. At the conclusion of the just-completed elastic step, the stresses are shown to be above the yield stress curve. The stresses are then reduced back to the starting point shown by the stress conditions below the line. The total load step is then divided into substeps such that the first substep just brings the most plastic element to the yield surface. At this point, a second load substep is taken that will bring the second element to the yield surface. At the completion of this substep, a corrective plastic strain increment is computed using the initial strain load vector. The strain that is incurred by element 4 as it leaves the yield surface is considered as plastic for both the pseudo-elastic and plastic portions. This procedure is repeated until all four elements are plastic as is shown when

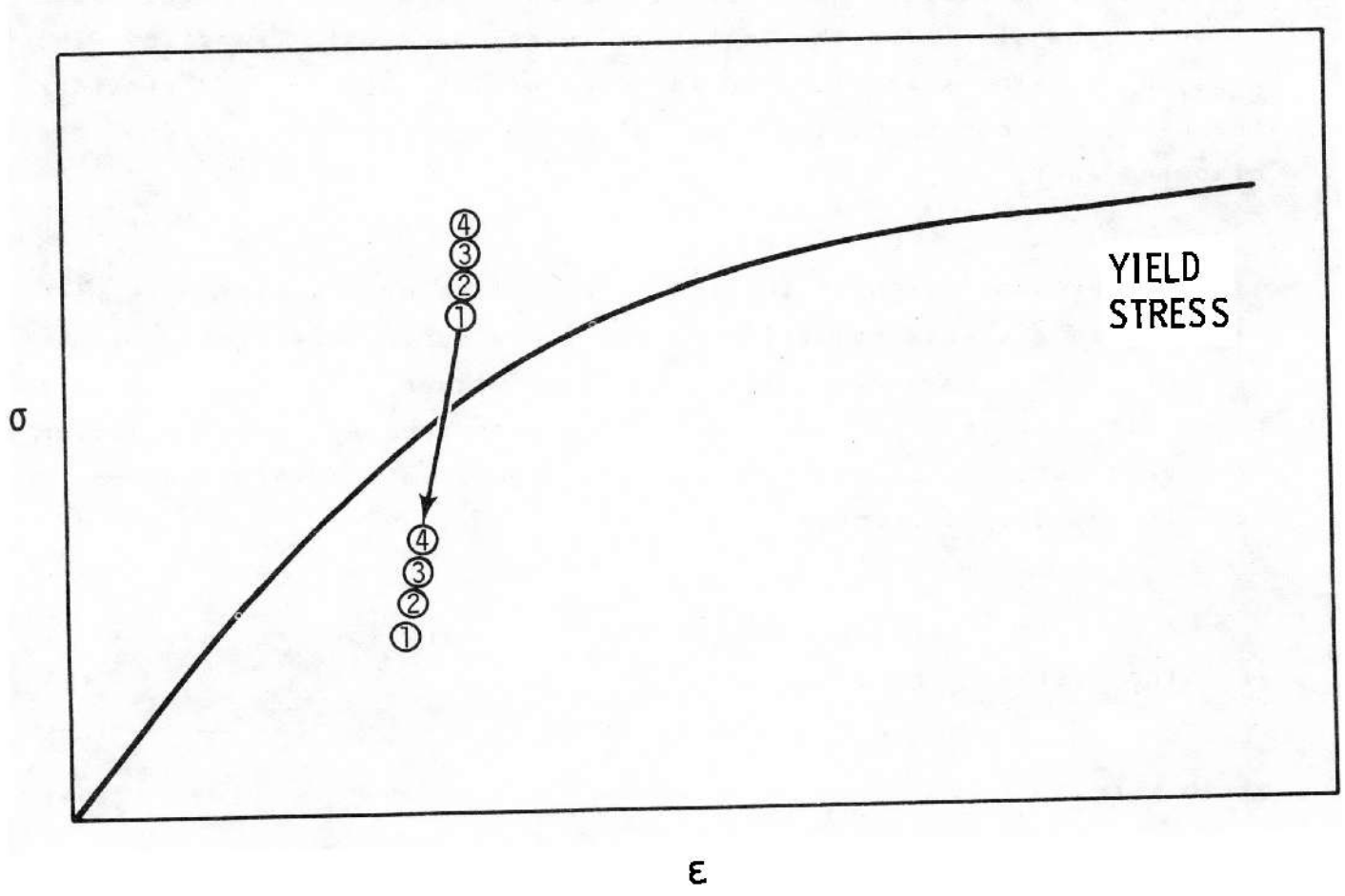

Figure 31. Elements 1, 2, 3 and 4 are plastic and are brought back prior subplastic state.

element 1 is brought to the yield surface. A corrective plastic load step is taken and then the final portion of the original load step can be taken driving all elements above the yield surface. This procedure is concluded with a final plastic load step to correct the stress back to the yield condition (see Figure 32).

In actual practice, the oscillation of the elements below the yield surface after a plastic corrective substep is less than 3.45 MPa out of 275.8 to 413.7 MPa. The actual spread between stresses decreases as more plastic substeps are taken and in the limit, elements 1 through 4 would be at the same stress at the conclusion of the load step if the material were perfectly plastic. The plastic strain is accumulated for each of the substeps and provides the basis for computing the plastic strain distributions through the cladding wall.

At the conclusion of the load step, all elements will have been returned to a stress condition on the yield curve or slightly below. At this time, a creep step is then taken in a normal manner completing the load and time step. For each substep, the solution procedure uses the chained radial and axial radial sequence to compute the displacements.

The yield stress (see Figure 33) for zircaloy is calculated from the following equation:

$$\text{yield stress} = C\,\sigma^{n} \qquad (194)$$

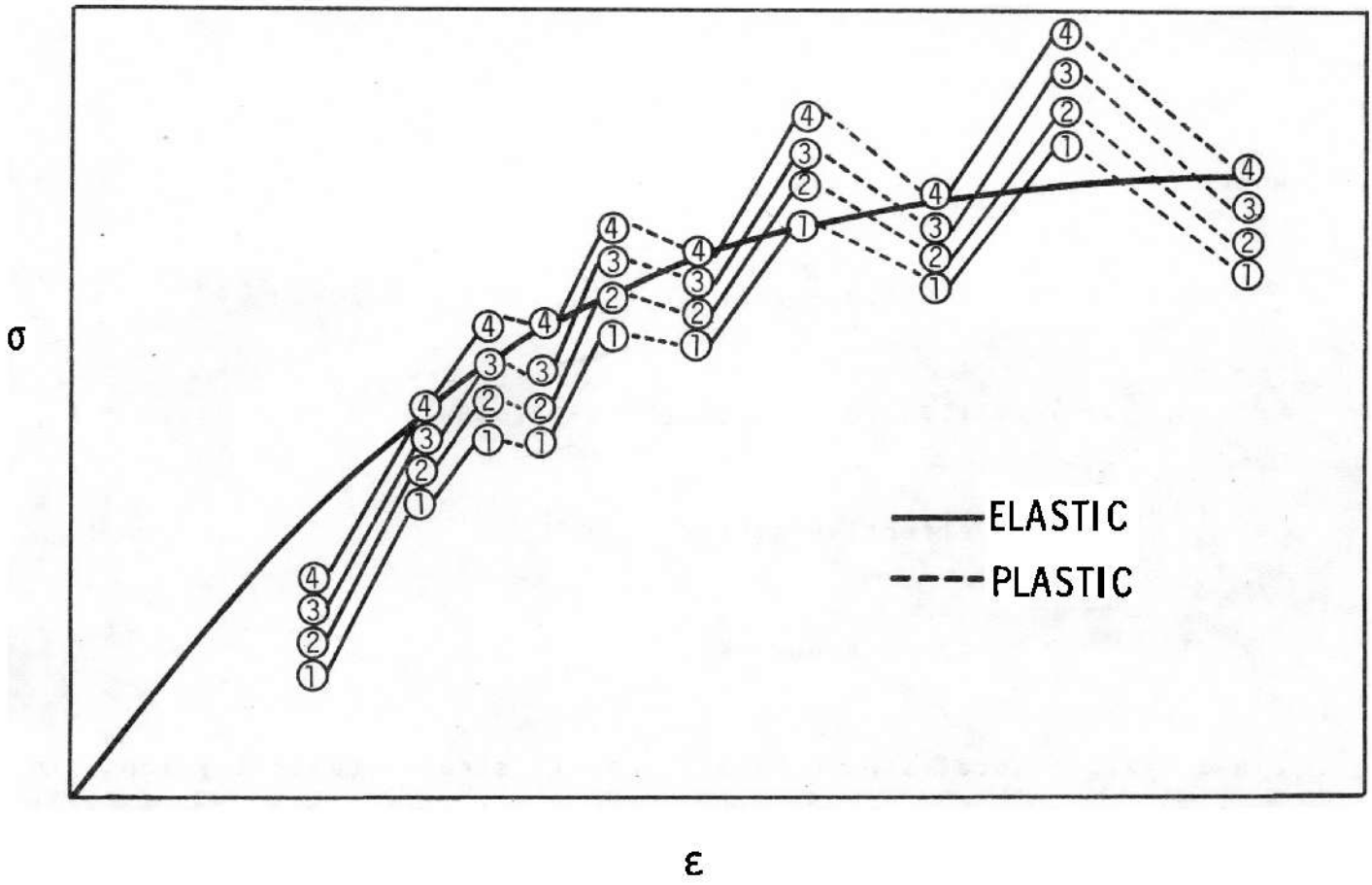

Figure 32. The plastic strain taken by alternating plastic elastic steps

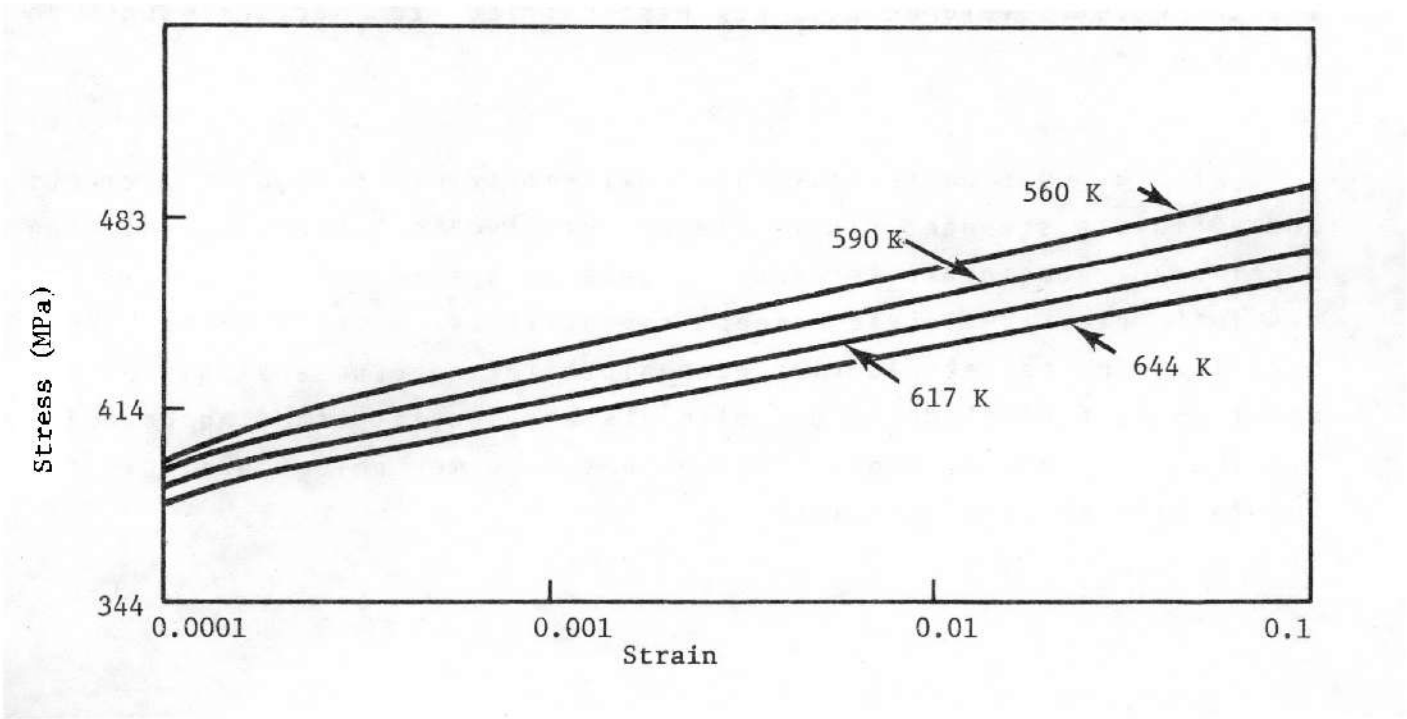

Figure 33. Yield stress versus strain used in GAPCON-3 calculations for temperature range 560 K to 644 K.

where

$C = 12860.0 - 146.5\ T + 0.1378\ T^2 - 7.28 \times 10^{-5}\ T^3$

$n = 1.75 \times 10 + 3.58 \times 10^{-2} T - 7.638 \times 10^{-4}\ T^2 - 4.95 \times 10^{-7}\ T^3$

σ = effective stress

T = temperature (K).

2.4.3 AXISYM Local Strain Model. Local strain concentrations in nuclear fuel rods are known to be potential sites for failure initiation. Assessment of such strain concentrations requires a two-dimensional analysis of stress and strain in both the fuel and the cladding during pellet-cladding mechanical interaction. To provide this capability in the FRAPCON-2 code, AXISYM, a finite element model developed at INEL, was modified to perform such an analysis.

AXISYM uses constant strain, axisymmetric, triangular elements and employs a standard finite element displacement formulation. The model can accomodate temperature dependent material properties and has full elastic-plastic creep capabilities. AXISYM has been modified for pellet-cladding mechanical interaction analysis by the addition of fuel-cladding gap elements and special cladding boundary constraints and provides for a detailed mechanical analysis for examination of local strains.

2.5 Fuel Rod Internal Gas Pressure Response

After the fuel rod temperature and deformation calculations have been completed, the pressure of the gas in the fuel rod is computed. To calculate the gas pressure, the temperature and volume of the gas are required. The thermal models discussed in Section 2.3 provide the temperature of the gas in the fuel rod plenum, fuel-cladding gap, and fuel voids. The deformation models discussed in Section 2.4 provide information for computing the volume of the fuel rod plenum, fuel-cladding gap, and fuel voids.

The fuel rod internal gas pressure model is based on the following assumptions:

1. Perfect gas law holds (PV = NRT).

2. Gas pressure is constant throughout the fuel rod.

3. Gas in the fuel cracks is at the average fuel temperature.

2.5.1 Fuel Rod Internal Gas Pressure. Fuel rod internal gas pressure is computed from the perfect gas law modified to permit different volumes of gas at different temperatures as given by

$$P = \frac{NR}{\sum \frac{V_i}{T_i}} \qquad (195)$$

where

P = system pressure of gas (Pa)

N = moles of gas in fuel rod (gm.mole)

R = universal gas constant (K.gm.mole)

V = the i-th volume (m^3)

T = temperature of gas in the i-th volume (K).

In FRAPCON-2, the different volumes considered are dish, crack, porosity, plenum, fuel-cladding gap and roughness volume. The choice of mechanics options, PELET or FRACAS, will result in the total void volume being apportioned between fuel cracks and fuel-cladding gap in different proportions.

Based on the above discussion, the detailed gas law becomes

$$P_g = \frac{M_g R}{\frac{V_P}{T_p} + \sum_{n=1}^{N} \left[\frac{\pi(r_{cn}^2 - r_{fn}^2)\,\Delta z_n}{T_{G_n}} + \frac{V_c \Delta z_n}{T_{cr}} + \frac{V_{por}\,\Delta z_n}{T_{por}} + \frac{V_{dsh} \Delta z_n}{T_{dsh}} + \frac{V_{rf} \Delta z_n}{T_{rf}} \right]} \quad (196)$$

where

P_g = internal fuel rod pressure (Pa)

M_g = moles of gas in fuel rod (gm.mole)

R = universal gas constant (K.gm.mole)

V_p = plenum volume (m^3)

n = axial node number

T = temperature of gas in plenum (K)

N = number of axial nodes into which fuel rod is divided for numerical solution

r_{cn} = radius of inside surface of fuel at axial node n (m)

r_{fn} = radius of outside surface of fuel at axial node n (m)

T_g = temperature of gas in fuel-cladding gap at axial node n (K)

Δz_n = fuel rod length associated with axial node n (m)

V_c = fuel crack volume per unit length of node n (m^2)

T_{cr} = temperature of the crack volume (K)

V_{por} = open porosity volume per unit length of node n (m^2)

T_{por} = temperature of node n porosity volume (K)

V_{dsh} = dish volume per unit length of node n (m^2)

T_{dsh} = temperature of node n dish volume (K)

V_{rf} = roughness volume per unit length of node n (m^2)

T_{rf} = temperature of node n roughness volume (K).

The gas pressure calculation, therefore, requires information on the gas inventory, void volumes, and the void temperatures which is provided by the following supportive models.

2.5.2 Fission Gas Production. Given production rates for the major diffusing gases, the burnup dependent total fission gas generated at axial elevation z is calculated as

$$GPT(z) = \frac{BU(z)\ VF(z)}{100\ A_v}\ (PR_{krypton} + PR_{helium} + PR_{xenon}) \quad (197)$$

where

GPT(z) = total fission gas producted at z (gm.mole)

BU(z) = burnup at z (fission/cc)

VF(z) = fuel volume (cc)

A = Avogadro's Number

PR = fission gas production rate (atoms/100 fissions) for krypton, xenon, and helium; values of 4.5, 25.5, and 0.3, respectively, are assumed.

All the fission gas produced, however, is not released. A portion is trapped in the fuel and a portion is released to the fuel-cladding gap volume. Only the released portion is used to calculate the rod internal gas pressure. The gas release fraction is calculated as discussed in the following sections.

2.5.3 Fuel Rod Gas Release. Gas release models in FRAPCON-2 account for not only fission gas release (krypton, xenon, and helium) but also nitrogen release. The nitrogen is released from the fuel lattice where it is trapped during the fuel fabrication process. Fission gas release in FRAPCON-2 includes five model options: ANS-5.4,[28] Beyer-Hann,[29] MacDonald-Weisman,[30] FAST-GRASS, and GRASS.[31] Each of these release models is discussed below.

2.5.3.1 ANS-5.4 Gas Release Model--The ANS-5.4 fractional fission gas release is calculated (on a local basis only) as a function of time and fuel temperature and burnup. The fuel is divided into radial and axial nodes according to the proposed ANS standard. A user requirement is that the time step sizes be such that the burnup increments do not exceed 2000 MWd/MTU.

The modeling is divided into two main sections, one for release

of stable isotopes and the other for release of short-lived isotopes. There are high and low temperature models for both the stable and radioactive fission products. The release is calculated using both the high and low temperature models, and the larger release value is used.

The stable fission gas (high temperature model) cumulative total release fraction for a fuel volume after time step K is defined as

$$F_K = 1 - \left\{ \sum_{i=1}^{K-1} [B_i(\tau_i g_i - \tau_{i+1} g_{i+1})/D_i'] + B_K \Delta t_K g_K \right\} / \sum_{i+1}^{K} B_i \Delta t_i . \tag{198}$$

with

$$\tau_i = \sum_{j=1}^{K} D_j' \, \Delta t_j \tag{199}$$

$$g_i = g(\tau_i) = 1 - 4\sqrt{\tau_i/\pi} + 3\tau_i/2 \qquad \text{for } \tau_i \leq 0.1 \tag{200}$$

$$g_i = g(\tau_i) = \frac{1}{15\tau_i} - \frac{6}{\tau_i}\left(\sum_{n=1}^{3} \frac{\exp(-n^2\pi^2\tau_i)}{n^4\pi^4} \right) \quad \text{for } \tau_i > 0.1 \tag{201}$$

$$D_i' = [(D_o/a^2) \exp(-Q/RT_i)] \times 100^{Bu_i/28000} \tag{202}$$

where

F_K = local cummulative fractional gas release through time step K

B_i = local fission gas production rate during the i-th time step

Δt = length of i-th time step (s)

Q = 72,300 (cal/mole)

R = 1.987 (cal/mole.K)

T_i = temperature during the i-th time step (K)

Bu = accumulated local burnup (MWd/MTU) at the midpoint of the i-th time step

D_o/a^2 = 0.61 (s)

K = current time step.

Equation (198) is rewritten in the code as

$$F_K = 1 - \frac{\sum_{i=2}^{K} \left(\frac{B_i}{D_i} (\tau_i g_i - \tau_{i+1} g_{i+1}) \right)}{\sum_{i=2}^{K} B_i \Delta t_i} \qquad (203)$$

with

$$\tau_{K+1} = g_{K+1} = 0 \qquad (204)$$

The low temperature model for the stable fission gas release is dependent only on fuel burnup. The fractional fission gas release is

$$F = 1 \times 10^{-7} Bu \qquad (205)$$

where

Bu = rod average accumulated burnup (MWd/MTU).

The high temperature model for radioactive fission gas release assumes that power and temperature have remained constant for several half-lives. The fractional release is a function of time and fuel temperature and burnup, and is also dependent on half-life. The release fraction for isotope i is

$$F_i = \frac{3}{1-\exp(-\mu_i\tau_i)} \left[\frac{1}{\sqrt{\mu_i}} \left[\text{erf}\left(\sqrt{\mu_i\tau_i}\right) - 2\sqrt{\mu_i\tau_i/\pi}\exp\left(-\mu_i\tau_i\right)\right] - \frac{1 - (1+\mu_i\tau_i)\exp(-\mu_i\tau_i)}{\mu_i}\right] \quad \text{for } \tau_i \leq 0.1 \tag{206}$$

and

$$F_i = \left[\frac{1}{\sqrt{\mu_i}} \coth\left(\sqrt{\mu_i}\right) - \frac{1}{\mu_i}\right] - \frac{6\mu_i}{\exp(\mu_i\tau_i)-1}\left(\sum_{n=1}^{3} \frac{1-\exp\left(-n^2\pi^2\tau_i\right)}{n^2\pi^2\left(n^2\pi^2+\mu_i\right)}\right) \quad \text{for } \tau_i > 0.1 \tag{207}$$

with

$$\mu_i = \lambda_i/D' \tag{208}$$

$$\tau_i = D't \tag{209}$$

where

λ_i = decay constant for isotope i (1/s)

t = total accumulated irradiation time (s)

D' = $[(D_o/a^2) \exp(-Q/RT)] \times 100^{(Bu/2800)}$

erf = error function

Bu = total accumulated burnup (MWd/MTU)

T = temperature (K) for previous four half-lives.

The low temperature radioactive fission gas release for isotope i is defined by

$$F_i = (1/\lambda_i)\,[1 \times 10^{-7} \sqrt{\lambda_i} + 2 \times 10^{-12} P] \qquad (210)$$

where

P = specific power (MWd/MTU)

λ_i = decay constant for isotope i (1/s).

2.5.3.2 Beyer-Hann Gas Release Model--The Beyer-Hann gas release model is an empirical correlation based on carefully selected data sets wherein maximum fuel temperatures were measured or could be estimated. Reference 28 discusses the development of the basic model, which identifies discreet constant release rates from three different temperature zones in the fuel. The temperature boundaries of these zones and their assigned release rates are shown in Table 3. The release rates were assigned from a statistical correlation of results from seven well-qualified irradiation tests, plus agreement with microcoring results on irradiated fuel pellets.

TABLE 3. ASSIGNED TEMPRATURE BOUNDARIES AND RELEASE FRACTIONS

Region	Temperature Bounds (k)	Release Fraction
1	1473 to 1673	0.050
2	1673 to 1973	0.141
3	1973 to 3073	0.807

In addition tc the high-temperature gas release indicated in Table 3, a low-temperature gas release rate has been added, which has been simplified from the original formulation in Reference 29. The low temperature release rate is a simple linear function of fuel burnup, reaching a maximum of 1.0% at 20,000 MWd/MTU.

Finally, the NRC-recommended gas release enhancement factor for high burnup fuel (greater than 20,000 MWd/MTU) has been added as an option. This correlation takes the form

$$F_{corr} = F_{old} + (1 - F_{old})\, Y \qquad (211)$$

where

F_{old} = uncorrected fractional release rate

F_{corr} = corrected fractional release rate.

The function Y has the form

$$Y = \frac{1 - \exp A\ (Bu - 20{,}000)}{1 + B/F_{old} \exp C(Bu - 20{,}000)} \qquad (212)$$

where A, B, and C are constants and have the values

A = 4.36×10^{-5}

B = 0.665

C = 1.107×10^{-5}.

A convention ceveloped by Soulhier and Notley[32] is used in the application of the Beyer-Hann model. As burnup proceeds, the identity of the time step in which the last highest release fraction was attained must be maintained. If the current release fraction is greater than the last highest value, then the total current inventory is released at the current (all-time high) rate. If this is not the case, then only the inventory produced since the attainment of the last higher release value is available for release.

2.5.3.3 MacDonald-Weisman Gas Release Model--The MacDonald-Weisman fission gas release model considers the release determined by escape of gas from the fuel matrix and release of trapped gas from grain boundaries or dislocations. The model presented in Reference 19 is repeated here. If k^1 represents the portion of

fission gas that escapes without being trapped, then

$$dn_i = k^1 p dt \tag{213}$$

where

dn_i = gas released directly in time dt (moles)

dt = the time increment (s)

p = the gas production rate (moles/s).

If the probability of trapped particle release per unit time is k, and the number of moles trapped is C, then the trapped moles released in dt is $dn_2 = k\ C\ dt$. Only a fraction, k^1, of the gas released from traps reaches the surface, thus the total gas released is $dn = k^1\ k\ c\ dt + k^1\ p\ dt$.

If C is replaced by (pt - n), and integration is performed, one obtains

$$n = p\ t = \frac{1 - k^1}{k^1 k}\ [1 - \exp\ (k^1 kt)]. \tag{214}$$

At constant power, the total fractional release is

$$F = n/(pt) = 1 - (1 - k^1)\ \frac{1 - \exp(-Kt)}{Kt} \tag{215}$$

where $K = k^1 k$. The constants, k and k^1, have been evaluated from

data as functions of fuel temperature and density in the form

$$A \exp (-B/T - Cd + D) \tag{216}$$

where

T = fuel temperature (K)

d = fuel density (percent of theoretical density)

and for k and k^1, respectively,

A = 0.25, 1.0

B = 11894.0, 6916.7

C = 0.0, 0.333

D = 0.0, 33.95.

The preceding formulation is extended to variable power time histories by assuming reactor operation is described by a series of constant power steps. The number of moles released, n, during the i-th interval is then

$$\Delta n_i = n_i - n_{i-1} = P_i \left\{ \Delta t_i - \frac{1 - k_i^1}{K_i} \left[1 - \exp(-K_i \Delta t_i) \right] \right\}$$

$$+ C_{i-1} \left[1 - \exp(-K_i \Delta t_i) \right] \qquad (217)$$

The first terms represent the release during t had the initial concentration been zero. The last term is additional release due to previously produced gas. Since the total release from time zero is n, the fraction of total gas produced which is released is

$$F = \left(\sum_{i=1}^{m} \Delta n_i \right) \Big/ \left(\sum_{i=1}^{m} p_i \Delta t_i \right) \qquad (218)$$

This fraction is used along with the total gas production (see Section 2.5.2) to obtain the gas inventory.

2.5.3.4 GRASS and FAST-GRASS Gas Release Models--GRASS is a highly mechanistic gas release model which accounts for bubble formation, migration, coalescence, channeling and eventual release. The model was developed at Argonne National Laboratory (ANL) and is described in documentation provided by ANL.[31] FAST/GRASS is an abbreviated version of GRASS which was designed to run more efficiently.

2.5.4 Nitrogen Release. The release of nitrogen initially present in fuel material from fabrication occurs as a result of a diffusion transport mechanism. The model proposed by Booth[33] is used, given

the following assumptions:

1. The initial concentration of diffusing substance, C, is uniform throughout a sphere of radius, a.

2. Transport of material does not occur from the external phase (gaseous nitrogen) back into the initial carrier medium.

The governing equation is

$$r \frac{\partial C}{\partial t} = D \frac{\partial^2 (Cr)}{\partial r^2} \tag{219}$$

where

r = radial location (m)

C = concentration of diffusing substance

t = time (s)

D = diffusion coefficient

with

C = 0.0 when r = a

$C = C$ when $t = 0$.

By applying a series solution method, the fractional release of the diffusing substance (nitrogen) can be approximated based on the value of B

$$B = \pi^2 D_{N_2}(T)t \tag{220}$$

where

$D_{N_2}(T)$ = temperature dependent diffusion coefficient for nitrogen

t = time from the start of diffusion (s).

Then, when $B > 1$, the fraction of nitrogen released as of time, t, equals

$$F_{N_2} = 1 - 6 \exp(-B/\pi^2) \tag{221}$$

and, when $B \leq 1$,

$$F_{N_2} = 6 \left[D_{N_2}(T)t/\pi\right]^{0.5} - 3D_{N_2}(T)t. \tag{222}$$

From the experimental data of Ferrari [34,35]

$$D_{N_2}(t) = (1 \times 10^{-12}) \exp(G) \tag{223}$$

where

$$G = 20202.0 \left(\frac{1.0}{1673.0} - \frac{1.0}{T}\right) \quad (224)$$

2.5.5 Fuel Rod Void Volumes. Void volumes computed by FRAPCON-2 include the pellet dishing, the fuel-cladding gap, the volume crack, the plenum, the open porosity, and the roughness volume. These are calculated as indicated below.

2.5.5.1 Pellet Dish Volume--The volume between pellets is calculated and included as part of the overall volume in the internal gas pressure model. The interpellet volume is calculated at each time step as the difference between the cold-pellet and hot-pellet geometries.

Figure 34 shows (a) a cold-pellet interface configuration and (b) an exaggerated hot-pellet interface configuration. The void volume available for internal fill gas is defined by the cross hatched areas (A and B in the figure).

2.5.5.2 Fuel-Cladding Gap Volume--The fuel-cladding gap volume is calculated by considering the area between two concentric cylinders. The outer cylinder is assumed to have a diameter equal to the diameter of the cladding inside surface based on plastic deformation. The inside cylinder is assumed to have a diameter equal to the diameter of the relocated fuel pellet.

2.5.5.3 Fuel Crack Volume--As the fuel expands, extensive

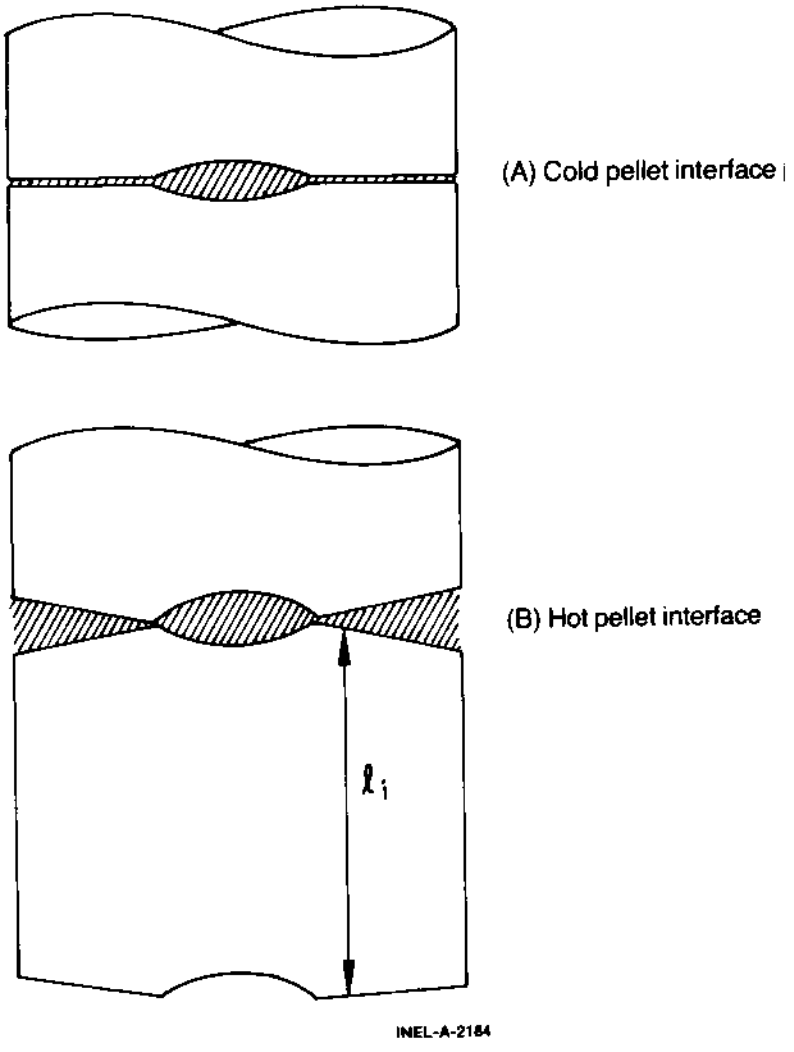

Figure 34. Dish void volume.

cracking occurs due to the high thermally-induced stresses resulting in a relocated fuel surface. If FRACAS is used, this crack volume is computed as

$$V_c = V_{eg} - V_{TX} - V_g \qquad (225)$$

where

V_c = fuel crack volume per unit length (m^2)

V_{eg} = fuel volume per unit length defined by expanded radial nodes including thermal expansion, swelling, and densification (m^2)

V_{TX} = the computed fuel-cladding gap volume per unit length based on the relocated fuel surface (m^2)

V_g = the volume per unit length within the thermally expanded cladding (m^2).

However, if PELET is the option being executed, the crack volume is calculated as

$$V_{cr} = V_{rfs} \text{ VFF}/100.0 \quad (226)$$

where

V_{cr} = fuel crack volume per unit length (m^2)

V_{rfs} = fuel volume (contained within the relocated fuel surface) per unit length (m^2)

VFF = void fraction within fuel (%).

2.5.5.4 Plenum Volume--The plenum volume is calculated from geometry considerations of the thermally expanded cladding and the thermal expansion, densification, and swelling of the fuel. The volume of the hold-down spring is considered.

2.5.5.5 Open Porosity Volume--A portion of the initial fabrication porosity is open to free gas flow which is given by the expressions

$$V_{por} = 0.0 \qquad \text{when } G_{den} \geq 94.0 \tag{227}$$

$$V_{por} = 1.97 \times 10^{-8} (94.0 - G_{den}) \qquad \text{when } 91.25 < G_{den} < 94.0 \tag{228}$$

$$V_{por} = 2.77 \times 10^{-4} - 3.818\, G_{den} - 1.43 \times 10^{-8}\, G_{den}^2 + 2.497 \times 10^{-10}\, G_{den}^3 \qquad \text{when } G_{den} < 91.25 \tag{229}$$

where

V_{por} = porosity volume per unit length (m^2)

G_{den} = DEN - 1.25

DEN = fuel density (percent of theoretical density).

2.5.5.6 Roughness Volume--The roughness of the surface of the fuel and cladding result in a small void volume accounted for by

$$V_{rough} = \frac{5.27 \times 10^{-5} \pi D_p}{V_f} \quad (230)$$

where

V_{rough} = roughness volume per unit length (m^2)

D_p = initial pellet diameter (m)

V_f = geometric fuel volume per unit length (m^2)

The gas pressure response resulting from the above models feeds back into the mechanical and temperature response models in the iteration scheme.

2.6 Fuel Rod Failure Models

A set of models has been developed for FRAPCON-2 to predict the probability of failure of zircaloy cladding under a variety of steady state and transient conditions. Collectively, these models form the FRAIL-5 (FRAP Integrity Limit) package. This package interfaces only with the FRACAS-I mechanics option.

Each model has the capability of predicting a different mode of zircaloy fuel rod cladding failure. Probabilities of failure are calculated for each failure mode, then appropriately combined to

yield a net probability of failure for the fuel rod cladding. The failure models considered by FRAIL-5 are cladding melt, eutectic melt, excess oxide, excess ballooning, cladding collapse, overstress, crack growth, overstrain, fatigue, stress-rupture and flow blockage. Not all of the failure models in FRAIL-5 are applicable to steady state. Only the steady state failure models are discussed below.

2.6.1 Model for Cladding Melt. The cladding melt model predicts cladding failure whenever the MATPRO melt temperature or a melt temperature supplied by the user is exceeded. The probability for failure is set to one when this condition exists.

2.6.2 Model for Eutectic Melt. The cladding eutectic melt model predicts cladding failure when (TCOOL/2 + TCLAD)/1.5 > 1233 K where TCOOL is the coolant temperature and TCLAD is the average clad temperature (K). The probability for failure is set to one when this condition exists.

2.6.3 Model for Excess Oxide. If the thickness of the cladding oxide layer is greater than 17% of the original cladding wall thickness, failure of the cladding is assumed to occur. If the oxide layer thickness is less than 17% of the original wall thickness, the probability for failure is assumed to be zero.

2.6.4 Model for Overstress. The assumptions in the overstress failure model are:

1. Overstress failure must be modeled using true hoop stress.

2. The true hoop stress at failure is a function of temperature, cold work and fast neutron fluence.

3. The cladding cross section is circular, although the inside and outside surfaces are not necessarily concentric.

4. The cladding axial radius of curvature is infinite.

5. Wall thinning is the primary deformatin that causes an an increase in true stress.

6. The cladding is incompressible.

The overstress model uses the cladding mechanical limits model described in Reference 3. This model uses a correlation between circumferential temperature variation (for which the overstress model assumes a 50 K variation) and circumferential strain to compute local wall thinning. The local wall thinning is then used to convert the true burst stress to an effective true burst stress for idealized symmetric deformation. The overstress model compares this with the effective true hoop stress from the current time step which is computed by

$$\bar{\sigma}_{\theta} = \text{HSTRESS} * (1 + \text{HSTRAN})/(1 + \text{STRANR}) \qquad (231)$$

where

HSTRESS = the engineering hoop stress (MPa)

HSTRAN = the hoop strain (MPa)

STRANR = the radial strain (MPa).

For the purpose of the FRAIL-5 subcode, the probability of failure as a function of stress and temperature is needed. This is obtained by assuming a distribution of failure stress about the mean failure stress.

The beta distribution function was found to be most representative of the failure stress data. The beta distribution is limited to a finite interval and may be adjusted to include all available data. For a given temperature, values of stress which lie above the defined interval result in failure (probability of one), while values which fall below the interval result in no failure (probability of zero). Because the beta distribution is defined only on the interval 0 to 1, it is necessary to normalize both the failure stress and the standard deviation of the failure stress to this interval. By a simple variable tranformation, the normalized failure stress is found from the expression

$$\overline{x} = \frac{\overline{\sigma}_{\theta F} - B}{T - B} \qquad (232)$$

where

$\bar{x}$ = normalized failure stress (MPa),

and B and T define the interval of available failure stress data. This interval was chosen to be three standard deviations above and two standard deviations below the mean failure stress, so that for a given temperature, the available test data are included in the interval.

The normalized standard deviation is found from the equation

$$s = s' \frac{\partial \bar{x}}{\partial \bar{\sigma}_{\theta F}} = \frac{s'}{T - B} \qquad (233)^{36}$$

where

s' = normalized standard deviation; that is, standard deviation of x

s = standard deviation of $\bar{\sigma}_{\theta F}$.

The cumulative beta distribution, obtained by integration of the frequency distribution function, is used to determine the probability of failure as a function of stress and temperature.

2.6.5 Model for Crack Growth. The well-known phenomenon of stress corrosion cracking (SCC) is an important contributor to stress

rupture and is considered in this failure model. A literature search for quantitative data explaining the SCC phenomenon has resulted in only two data sets which can be used in model development.[37, 38] All other literature was of a qualitative nature. Two quantitative papers used a fracture mechanics approach to explain the SCC phenomenon. This section briefly explains the fracture mechanics approach. Adaptations were made to the method to assure compatability with FRAIL-5. The adaptations are also presented.

References 36 and 37 state that the SCC phenomenon can be described by the crack growth equation

$$\frac{da}{dt} = CK_I^4 \qquad (234)$$

where

K_I = stress intensity factor

C = material constant (m/s)

a = crack length (m)

t = time (s).

Here, the crack length is measured through the cladding wall. The axial and tangential components of crack length are not considered by Equation (234).

The stress intensity factor, K_I, may be found from the equation

$$K_I = \sigma_\theta Y \sqrt{a} \qquad (235)$$

where

σ_θ = applied tensile hoop stress (MPa)

Y = fracture mechanics flaw geometry factor.

The material constant, C, in Equation (234) was found to be dependent on temperature and iodine concentration. The experimentally determined correlation for C was found to be

$$C = 1.32 \times 10^{-7} I_2^{3/4} \exp\left(\frac{-35900}{RT}\right) \qquad (236)$$

where

I_2 = iodine concentration (mg/dm)

T = temperature (K)

R = gas constant (cal/mol.K).

For a given temperature and iodine concentration there is a critical stress intensity factor, K_{ISCC}, below which SCC will not occur. This implies that there exists a threshold stress below

which SCC will not occur. This threshold stress is given by

$$\sigma_{threshold} = \frac{K_{ISCC}}{Y \sqrt{a}} \tag{237}$$

This threshold stress may also be found from the following empirical relationship

$$\sigma_{threshold} = \frac{(2710 - 3T)\ I_2^{-3/16}}{Y \sqrt{a}} \tag{238}$$

where all variables are as previously defined.

Knowing the crack velocity given by Equation (234), the crack length can be determined at any point in time. This crack length may then be compared to the critical crack length in order to determine if the fuel rod has failed. The critical crack length is defined as the critical depth necessary to cause instantaneous failure by stress rupture.

All variables necessary to calculate the crack length are made available to FRAIL-5 from MATPRO and the FRAPCON-2 code, with the exception of a, the initial crack depth, and Y, the flaw geometry factor. Until a more exact determination of these variables can be made, the following values are assumed. The initial flaw in the cladding is assumed to be a pit-shaped flaw, 12.7 mm in depth. For pits, Y = 1.29. These values of Y and a were found most frequently in the lot of stress-relieved tubing used in the experiments described in References 36 and 37.

The critical crack length may be found, as suggested in References 36 and 37, from the expression

$$\frac{a_c}{w} = 1 - \frac{\sigma}{\sigma_B} \qquad (239)$$

where

a_c = critical crack length (m)

w = cladding thickness (m)

σ = applied hoop stress (MPa)

σ_B = burst strength (MPa).

Because the frequency distribution function of the burst strength is known, the frequency distribution of a_c/w may be calculated. By knowing the probability frequency distribution of a_c, it is possible to obtain a probability of failure due to SCC from a knowledge of the calculated crack length.

2.6.6 Model for Overstrain. The assumptions used in the overstrain failure model are

1. The mean failure strain can be correlated with temperature by least-squares fitting to the failure strain data base.

2. The distribution of the failure strain about the mean

failure strain can be approximated by a beta probability distribution.

3. The failure strain is not a function of the hydrogen, oxygen, cesium, or iodine content of the cladding.

The overstrain failure model calculates the probability of failure as a function of strain and temperature. The strain at failure is assumed to be distributed according to the beta distribution. The upper and lower limits are set at +2 and −2 standard deviations, respectively, from the mean failure strain. The standard deviation is 16% of the mean failure strain.

The mean failure strain as a function of temperature is obtained from the cladding strain at rupture model described in Refereice 37. The effects of cold work and irradiation level are taken into account

2.7 Uncertainty Analysis Option

An uncertainty analysis option has been developed for FRAPCON-2 so that a user may easily obtain estimates of the uncertainty in calculated code outputs. The option has specifically been designed so that the user may perform an uncertainty analysis on a FRAPCON-2 case in a understandable and systematic manner. The option further provides for a sequential development of analysis complexity by allowing the user to restart and continue an analysis from intermediate points. One goal of the option is to provide to all users a straightforward technique based on sound methodology for estimating code uncertainties.

2.7.1 Uncertainty Methodology. The uncertainty analysis option is based on the response surface method. Any of the output variables of a computer code may be termed a response. There is some functional relationship between a response and the input variables. In the space of the input variables, this relationship defines a surface, and hence the term response surface. When the code is rather simple, this surface may be determined analytically over the entire range of the input values. More often, as in the case of FRAPCON-2, the surface may be known only through the code, as the range of inputs and problem types is very large. Thus, the complete true response surface cannot be determined analytically. The response surface method of uncertainty analysis is based on a systematic sampling of the true surface which is then approximated by a polynomial equation in the independent (input) variables. In effect, the true surface is approximated by a smooth surface.[39]

The polynomial equation approximating the true surface is derived as follows. Let $Y(x_i)$ denote the code response as a function of $x_i = x_1, x_2, \ldots, x_K$ inputs. The Taylors series expansion about any point is then given by

$$Y(x_i) = Y(\mu_i) + \sum_{i+1}^{K} \frac{\partial Y(\mu_i)}{\partial x_i} (x_i - \mu_i) + 1/2 \sum_{i=1}^{K} \frac{\partial^2 Y(\mu_i)}{\partial_i^2} (x_i - \mu_i)^2 + \sum_{\substack{i,j \\ i<j}}^{K} \frac{\partial^2 Y(\mu_i)}{\partial x_i \partial x_j} (x_i - \mu_i)(x_j - \mu_j) + \text{higher order terms} \quad (240)$$

Truncating the Taylors series at second order terms, the desired polynomial equation is obtained by identifying the coefficients of the polynomial with the partial derivatives of the series expansion. The coefficients are estimated from sample values

of the true response surface obtained by perturbing the nominal inputs. For a second order polynomial to reasonably approximate the true surface, the region of the surface being sampled must be small enough so that large irregularities are not present. Experience has shown that a range of plus and minus one standard deviation ($\pm 1\sigma$) in the input variable uncertainties will usually satisfy this requirement for FRAPCON-2.

The polynomial approximation to the true response surface may be used to examine the behavior of the true surface in the region of the sample space without the burden of excessive cost. In particular, the polynomial can be used to study the propagation of errors through the code and their effect on the uncertainty in computed outputs. Thus, an estimate of response uncertainty and the relative contributions of input variables to this certainty may be obtained using the response surface method.

Once the user has selected a base case problem and made a choice of output responses and input variables, the following procedures will be followed by the code to obtain the desired final results, the estimates of response uncertainties.

1. An experimental design will be chosen. This is simply a pattern for perturbing the independent variables of the case. The pattern is obtained in matrix format where the columns correspond to inputs and the rows correspond to the individual analysis that must be performed. The case is run as many times as the design dictates, each time varying the input variable perturbations according to the pattern.

2. The response surface equations are then generated at each FRAPCON-2 time step using the information derived from step one. Basically, a multiple regression routine used with certain simplifications arising from the orthogonal properties of the experimental design.

3. The response surface equations are used to generate uncertainty distributions for the response parameters. Second order error propagation analysis is used to estimate the means and variances of the responses.

4. Finally, estimates of the fractional contributions to the response variances are made to indicate the relative importance of individual input variables.

2.7.2 Uncertainty Application. The uncertainty analysis option in FRAPCON-2 is essentially identical to that in FRAP-T5[40]. The only difference lies in expanded input and response lists that reflect the differences in the two codes. The user is referred to Reference 41 for detailed discussions of the development and assessment of the method. The purpose of this section is to suggest possible use of the option and specific limitations of the method of which the user should be aware.

Obviously, the most important feature of the option is the ability to determine the uncertainty in code outputs that result from propagating uncertainties in inputs through the code. Equally important for code development, however, is the ability to determine the relative contributions to the overall uncertainty of each input variable. This can lead to studies on the need for specific code development or experimental programs. For example, if it is found

that fuel thermal conductivity uncertainty contributes 80% of the uncertainty in cladding temperature but fuel Poisson's ratio contributes less than 1%, then future work should be directed at refining the uncertainty in fuel thermal conductivity.

Another use of the option is a traditional sensitivity analysis. Here the user should be aware that the interpretation of the perturbations that define the experimental design as one standard deviation is not made until the very last step of the analysis. At that point the interpretation is necessary in order to infer information about the uncertainty distribution of the output responses. If the user is willing to forego this inference, then the perturbations making up the experimental design can in fact be arbitrary. If, for example, the user wishes to study the sensitivity of a particular response to 10% deviations in a family of input variables, this analysis is entirely possible. The output coefficients of the response equation can be interpreted as sensitivity coefficients given in units comparable to the responses. The coefficients can be ranked by absolute magnitude and this ranking represents the sensitivity of the response to each input. Thus traditional sensitivity studies may easily be executed.

Occasionally, the user must be prepared to question the validity of results produced by the option. The estimates of response uncertainty are based on approximations (the response surface equations) to the true code output. The accuracy of these estimates therefore depends directly on the degree to which the equations really do approximate the true code output. An often used method to evaluate this is to examine the distribution of residuals formed by taking the differences between the code predictions and the response surface equations. At present, the code fits a full model equation to the data, resulting in very small

residuals. The best method is to examine residuals from data not used to fit the equations. This entails generating more computer data. However, the nominal case is always run and only used in equation fitting for quadratic analyses. The user is therefore advised to compare the nominal case with the response equations. If the true code output is actually linear, the mean will equal the nominal. The difference between the two may be taken as some measure of the quality of the linear response equation approximation.

3. GENERAL CODE DESCRIPTION

3.1 Code Structure and Solution Routine

FRAPCON-2 is a large and complex code that contains over 200 subroutines. The hierarchy of subroutines, their function and their interrelation are discussed in detail in Appendix C. This section discusses the code structure, solution scheme and the major subroutines involved in the solution scheme.

3.1.1 Code Structure. The FRAPCON-2 subroutines have been grouped in packages, not all of which need to be compiled for every run. These packages are listed in Table 4. Note that every execution requires the FRPCON package and the MATPRO package; the former contains the driver routine, the setup routines, and the thermal models. Using only these two packages restricts one to the FRACAS-I mechanical modeling option and precludes selection of the GRASS or FAST-GRASS fission gas release models.

The other packages listed in Table 4 correspond to the models of the same name discussed in Section 2.

TABLE 4. MAJOR FRAPCON-2 PACKAGES

Package	Description
FRPCON	The main section of the code, including all of the thermal models; also includes the uncertainty analysis routines, the FRAIL cladding failure model, and the FRACAS-I mechanics model.
FRACAS-II	Contains the subroutines comprising the FRACAS-II deformable pellet mechanics model.
PELET	Contains all of the subroutines that comprise the PELET/RADIAL mechanics model.
AXISYM	Contains the subroutines comprising the detailed finite element mechanics model.
MATPRO	The MATPRO material properties package.
GRASS	Contains the subroutines which comprise the GRASS fission gas release model.
FAST-GRASS	Contains the subroutines which comprise the FAST GRASS fission gas release model.

3.1.2 Solution Scheme. Figure 35 shows a flowchart of FRAPCON-2 beginning with case setup, following through the convergence loops and ending with output. Each major section of this sequence will be discussed, together with the subroutines involved. To aid this discussion, Figure 36 presents an abbreviated outline of the main subprogram, FRPCON, arranged in the same order as the flowchart. Major subroutines appear in the figure as do the major FORTRAN loops.

The first portion of the flowchart has to do with case setup and initialization. This includes reading the input data, the dynamic dimensioning procedure, initializing variables, and an initial problem description output. The subroutines listed in Table 5 are involved in the setup and initialization.

Next, the code enters the first of four major loops in the FORTRAN coding, the Time Step Loop. The Time Step Loop encompasses virtually all of the remainder of the FRAPCON-2 code. In each execution of the Time Step Loop, the code solves for the thermal and mechanical equilibrium of the fuel rod at a new point along the rod power versus time history input by the user. Those subroutines which are executed only once per time step are listed in Table 6.

Three additional loops exist in the code. The next loop encountered within the Time Step Loop is the Gas Release Loop. This loop is cycled until the value for calculated rod internal gas pressure (dependent on temperature, volume, and fission gas release) converges. Subroutines called from within this loop are listed in Table 7.

The next inner loop in the coding is the Axial Node Loop. For

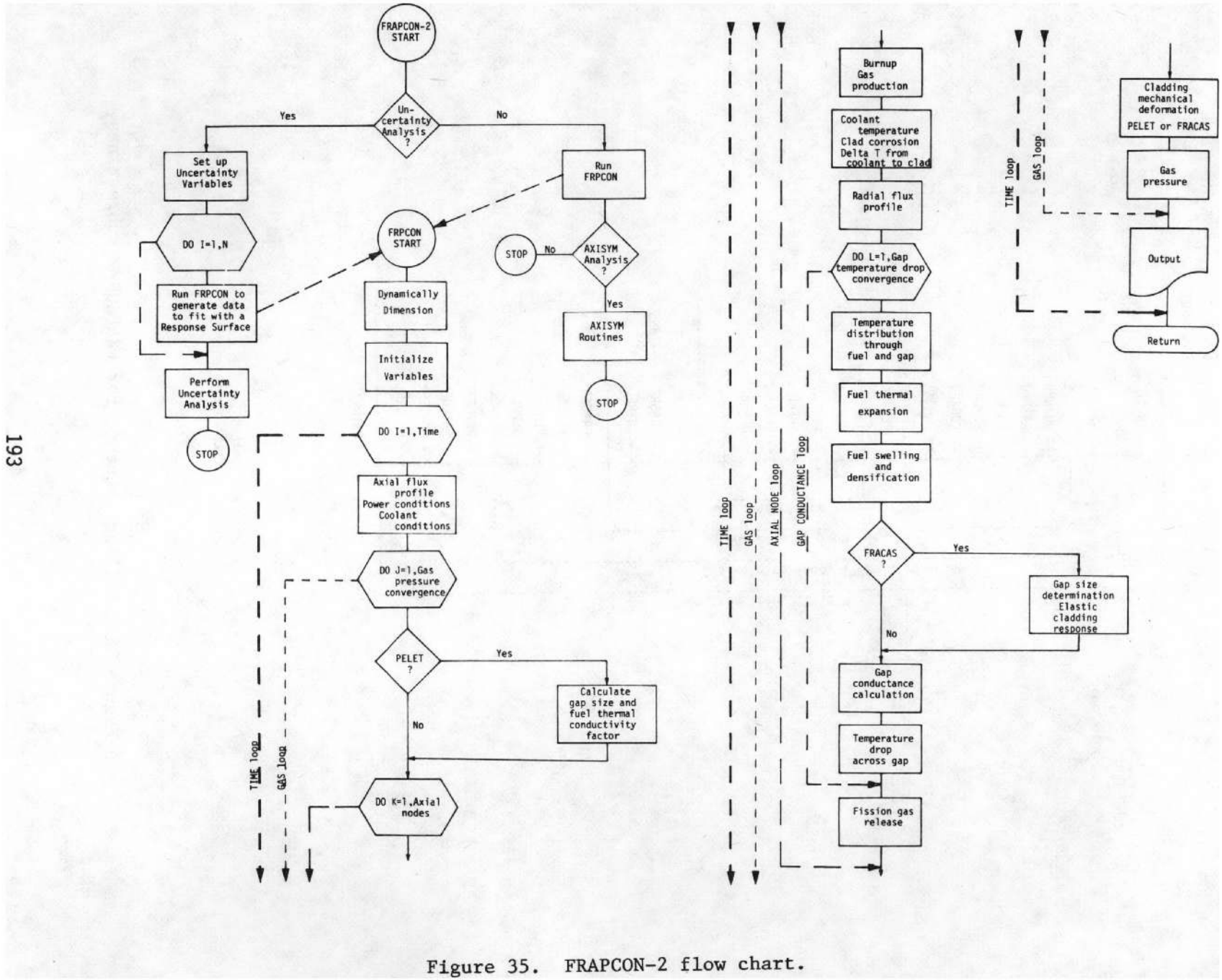

Figure 35. FRAPCON-2 flow chart.

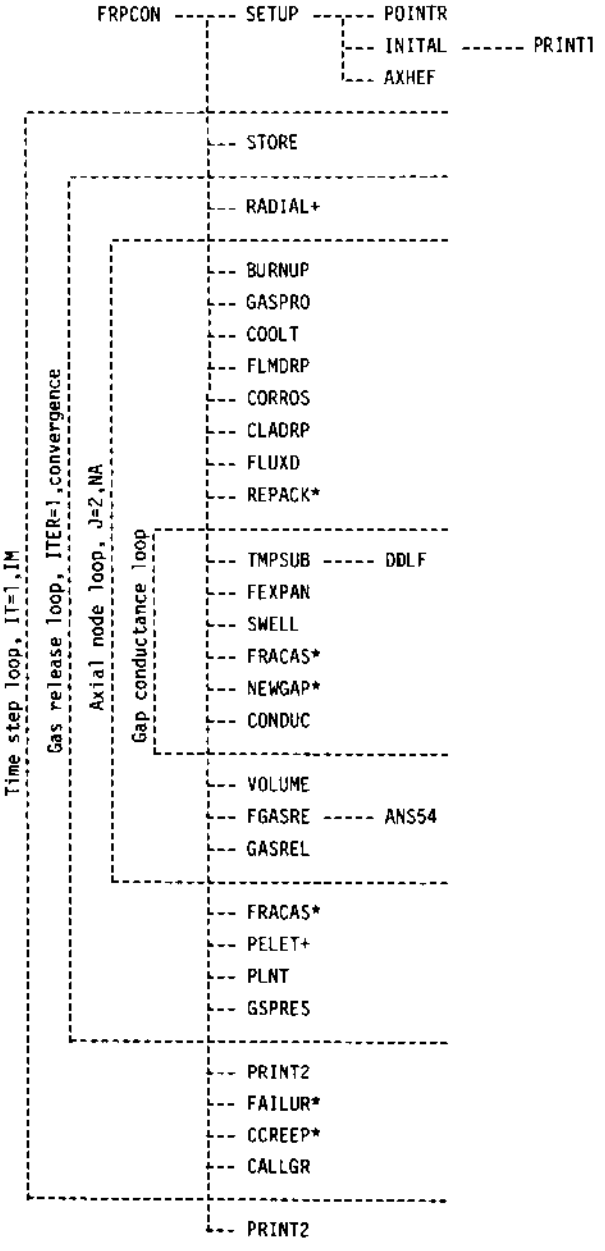

Figure 36. Calling sequence for FRAPCON-2 subroutines.

TABLE 5. INITIALIZATION SUBROUTINES

Subroutine	Description
SETUP	Reads the data input pertaining to the problem size requirements.
POINTR	Performs the dynamic dimensioning procedure.
INITAL	Reads the remaining problem description input and initializes the variables.
PRINT1	Generates the output reflecting the initial conditions and specifications of the fuel rod and lists the proposed power history.
AXHEF	Calculates the axial power profile as it affects the axial regions of the fuel rod and also any varying axial power profile changes.

TABLE 6. SUBROUTINES IN THE TIME STEP LOOP

Subroutine	Description
STORE	Stores variable values as necessary to account for history dependency.
PRINT2	Generates output for the code that presents converged values for all of the axial nodes for both thermal and mechanical solutions.
FAILUR	A package of subroutines which calculate the probability of cladding failure based on an analysis of the FRACAS-I generated cladding conditions.
CCREEP	The cladding creep portion of the FRACAS mechanics model.
CALLGR	Calls the GRASS or FAST-GRASS fission gas release packages.

TABLE 7. SUBROUTINES IN THE GAS RELEASE LOOP

Subroutine	Description
RADIAL	If the PELET mechanical package is used, RADIAL is called to calculate the fuel thermal conductivity degradation factor, the effective gap size, the fuel cladding interface pressure, and the effective elastic modulus of the cracked fuel in each axial region.
FRACAS	The FRACAS-I and FRACAS-II fuel-cladding mechanical response models are both controlled by this subroutine. This loop calculates the time independent permanent deformation.
PELET	The chained axial-radial finite element model that calculates the cladding mechanical response.
PLNT	Calculates the current plenum gas temperature and volume.
GSPRES	Calculates the rod internal gas pressure.

every pass through the Gas Release Loop, the Axial Node Loop sequences through each of the axial regions defined by the input. The subroutines controlled by this loop are listed in Table 8.

The innermost loop is the Gap Conductance Loop. This loop iterates on each axial node until thermal equilibrium in the radial direction is achieved. Thermal equilibrium is signified by a converged value for the calculated temperature drop from the fuel outer surface to the cladding inner surface. The subroutines listed in Table 9 comprise the Gap Conductance Loop.

At the completion of all the time steps, and before returning to the driver package, a final call to PRINT2 is made. This call results in the printing of a summary table for the entire power history of the rod.

3.2 Code Results

FRAPCON-2 generates fuel rod response information as a function of fuel rod fabrication information, boundary conditions, and power history. This information is provided to the user in the form of printed output and in the form of plots (optional). The capability also exists to supply this information for steady state initialization of the FRAP-T5 or FRAP-T6 computer codes. The information provided to the transient fuel rod analysis code consists of permanent burnup effects such as cladding creepdown, fuel swelling, fuel densification and fission gas inventory. This section presents the important response parameters, the plotting package and information on the FRAPCON link with FRAP-T.

TABLE 8. SUBROUTINES IN THE AXIAL NODE LOOP

Subroutine	Description
BURNUP	Calculates the local fuel burnup.
GASPRO	Calculates the fission gas production.
COOLT	Calculates the coolant temperature.
FLMDRP	Calculates the temperature drop from the cladding surface to the coolant.
CORROS	Calculates the corrosion on the cladding surface.
CLADRP	Calculates the temperature drop from the cladding inside surface to the cladding outside surface.
FLUXD	Calculates the radial flux depression.
REPACK	Relocation model for the FRACAS mechanics models.
VOLUME	Calculates the void, fuel, and cladding volumes present in the rod.
FGASRE	McDonald-Weisman and Booth Diffusion fission gas release models.
ANS54	ANS-5.4 fission gas release model.
GASREL	Beyer-Hann fission gas release model.

TABLE 9. SUBROUTINES IN THE GAP CONDUCTANCE LOOP

Subroutine	Description
TMPSUB	Calculates the radial temperature distribution through the fuel.
COLF	Solves the equations for the radial heat balance.
FEXPAN	Fuel thermal expansion routine.
SWELL	Calculates fuel swelling and fuel densification.
FRACAS	If the FRACAS mechanics models are used, this subroutine calculates the new position of the cladding due to deflection caused by internal gas pressure changes.
NEWGAP	Calculates the new fuel-cladding gap size (used with the FRACAS mechanics models only).
CONDUC	Calculates new values for the gap conductance and the fuel-cladding gap temperature drop.

3.2.1 Fuel Rod Response. FRAPCON-2 provides the calculated fuel rod thermal, mechanical and pressure response data. The results are presented in three forms: an axial region printout, a power-time step printout, and a summary page printout.

The axial region printout presents local information on power, time, time step and burnup. Also presented are rod radial temperature distribution, coolant temperature, cladding stresses and strains (both recoverable and permanent), gap conductance, fuel-cladding interfacial pressure, and coolant film heat transfer information.

The power-time step printout presents rod burnup, void volumes and associated temperatures, mole fractions of constituent gases and release fractions, total moles of rod gas, and rod gas pressure. Also this printout presents stresses, strains, temperatures and stored energy as a function of axial region.

The summary page printout presents time-dependent information about the hot axial region. This includes temperatures of the cladding, fuel-cladding gap, and fuel; fuel-cladding interfacial pressure; cladding stress and strain; fuel outside diameter; gap conductance and gas pressure; zircaloy oxide thickness; and hydrogen uptake.

3.2.2 Plot Package. The FRAPCON-2 plotting package is made up of subroutines which make use of the IGS graphics system. The plot information is stored on unit TAPE17 by FRAPCON-2 and is processed by the plot package which generates the curve information on unit TAPE10. TAPE10 can be used to generate the plots on computer system devices such as a FR80 microfiche plotter, a microfilm plotter, and

a CALCOMP plotter.

3.2.3 FRAP-T Initialization. FRAPCON-2 contains subroutine RESTFS which, when the flag NTAPE is set to 1, stores sets of history dependent information for each power-time step. This information is stored on unit TAPE1 and is for FRAP-T initialization. This gives the user the ability to model the fuel rod response of a rod which experiences significant burnup prior to some transient excursion.

3.3 Features of FRAPCON-2

FRAPCON-2 has been designed with special features to aid the user. The code has been dynamically dimensioned so that the code may be implemented on computers with limited core storage. The code also has a restart feature which allows for modeling power histories which require more than 100 power-time pairs (the maximum number of power-time pairs which can be input for any single run is limited to 100).

3.3.1 Dynamic Dimensioning. FRAPCON-2 has been dynamically dimensioned so that a minimum amount of core storage is required for any given fuel modeling process. Those parameters which are a function of the problem size are dimensioned to the exact size required by the axial and radial nodalization and the number of power-time steps. The user can set the core size based on the number of axial and radial nodes and the number of time steps.

3.3.2 FRAPCON-2 Restart. In the event that a user requires more than 100 power-time steps for the analysis of the behavior of a fuel rod, the capability exists to restart the code. This allows the

user the freedom to model the steady state behavior of a fuel rod in as much detail as is deemed necessary. When NRESTR is set to 1, FRAPCON-2 stores information for a FRAPCON-2 restart on unit TAPE2. This information can then be used to continue an analysis which requires more than 100 power-time pairs. The restart option is not available when the PELET mechanical modeling option is chosen.

4. REFERENCES

1. EG&G Idaho Inc., Quarterly Technical Progress Report on Water Reactor Safety Programs Sponsored by the Nuclear Regulatory Commission's Division of Reactor Safety Research, October-December 1976, NUREG/CR-0512, TREE-1298, January 1979, p. 43.*

2. EG&G Idaho Inc., Quarterly Technical Progress Report on Water Reactor Safety Programs Sponsored by the Nuclear Regulatory Commission's Division of Reactor Safety Research, January-March 1980, NUREG/CR-1400, EGG-2031, April 1980, pp. 19-20.*

3. D. L. Hagrman et al., MATPRO-Version 11 (Revision 1): A Handbook of Materials Properties for Use in the Analysis of Light water Reactor Fuel Rod Behavior, NUREG/CR-0497, TREE-1280, Rev 1, February 1980.*

4. D. R. Coleman et al., FRAP-S3: A Computer Code for the Steady State Analysis of Oxide Fuel Rods - Model Assessment Report, NUREG/CR-0786, TREE-1352, R4, April 1979.*

5. D. D. Lanning et al., GAPCON-THERMAL-3 Code Description, PNL-2434, January 1978.

6. EG&G Idaho, Inc., Quarterly Technical Progress Report on Water Reactor Safety Programs Sponsored by the Nuclear Regulatory Commission's Division of Reactor Safety Research, July-September 1978, NUREG/CR-0412, TREE-1294, October 1978, pp. 45-49.**

7. M. P. Bohn, FRACAS: A Subcode for the Analysis of Fuel Pellet-Cladding Mechanical Interaction, TREE-NUREG-1028, April 1977.

8. B. B. Mikic, Thermal Contact Conductance: Theoretical Considerations, International Journal of Heat Mass Transfer, Volume 14, pp. 205-214.

9. R. E. Willford et al., The Analysis of Fuel Relocation for the NRC/PNL Halden Assemblies IFA-431, IFA-432,and IFA-513, NUREG/CR-0588, PNL-2709, April 1980*

10. C. R. Hann et al., Data Report for the NRC/PNL Halden Assembly IFA-432, NUREG/CR-0560, PNL-2673, 1978.**

11. D. D. Lanning and M. E. Cunningham, Startup Data Report for NRC/PNL Halden Assembly IFA-513, NUREG/CR-0862, PNL-2948, July 1979.*

12. M. E. Cunningham, D. D. Lanning, and S. D. Montgomery, A Procedure for the Qualitative Interpretation of Fuel Centerline Thepmocouple Response to Step Power Decreases, NUREG/CR-1012, PNL-3096, October 1979.*

13. F. Dittus and L. M. K. Boelter, Heat Transfer in Automobile Radiators of the Tubular Type, University of California Publications in Engineering, 2, 13, 1930 pp. 443-461.

14. W. H. Jens and P. A. Lottes, Analysis of Heat Transfer, Burnout, Pressure Drop, and Density Data for High-Pressure Water, ANL-4627, 1951.

15. F. Kreith, Principles of Heat Transfer, 8th Edition, Scranton: International Book Company (1964).

16. C. E. Beyer et al., GAPCON-THERMAL-2: A Computer Program for Calculating the Thermal Behavior of an Oxide Fuel Rod, BNWL-1898, November 1975.

17. A. M. Ross and R. L. Stoute, Heat Transfer Coefficients Between UO_2 and Zircaloy-2, CRFD-1075, AECL-1552, June 1962.

18. A. C. Rapier, T. M. Jones, and J. E. McIntosh, The Thermal Conductance of Uranium Dioxide/Stainless Steel Interfaces, International Journal of Heat Mass Transfer, Volume 6, pp. 397-416, 1963.

19. N. Todreas and G. Jacobs, Thermal Contact Conduction in Reactor Fuel Elements, Nuclear Science and Engineering, Volume 50, p. 283, 1973.

20. J. E. Garnier and S. Begej, Ex-Reactor Determination of Thermal Gap and Contact Conductance Between Uranium Dioxide: Zircaloy-4 Interfaces, NUREG/CR-0330, PNL-2696, April 1979.*

21. B. A. Finlayson, The Method of Weighted Residuals and Variational Principles, New York: Academic Press, 1972.

22. W. H. McAdams, Heat Transmission, 34th Edition, New York: McGraw-Hill Book Company, Inc., 1954.

23. R. W. Garner et al., Gap Conductance in Test Series-2 Test Results Report for Tests GC 2-1, GC 2-2, and GC 2-3, NUREG/CR-0300, TREE-1268.**

24. A. Mendelson, Plasticity: Theory and Applications, New York: The MacMillan Company, 1968.

25. D. R. Coleman and E. T. Laats, FRAP-T3, A Computer Code for the Transient Analysis of Oxide Fuel Rods - Model Assessment Report, NUREG/CR-0555, TREE-1320, February 1979.*

26. R. Hill, A Theory of the Yielding and Plastic Flow of Anisotropic Metals, Proceedings of the Royal Society of London, Vol 143A, pp. 281-297, 1948.

27. P. J. Pankaskie, Irradiation Effects on the Mechanical Properties of Zirconium on Dilute Zirconium Alloys: A Review, BN-FA-618, July 1976.

28. W. N. Rausch and F. E. Panisko, ANS54: A Computer Subroutine for Predicting Fission Gas Release, NUREG/CR-1213, PNL-3077, August 1979.*

29. C. E. Beyer, C. R. Hann, Prediction of Fission Gas Release From UO_2 Fuel, BNWL-1875, November 1974.

30. J. Weisman et al., Fission Gas Release from UO_2 Fuel Rod with Time Varying Power Histories, ANS Transactions, 12, 2 November 1969.

31. J. Rest, GRASS-SST: A Comprehensive Mechanics Model for the Prediction of Fission Gas Behavior in UO_2 Based Fuels During Steady State and Transient Conditions, NUREG/CR-0202, ANL-78-53, June 1978.**

32. R. Soulhier and M. J. F. Notley, Effect of Power Changes on Fission Product Gas Release from UO_2 Fuel, Nuclear Applications, Volume 5, p. 296.

33. A. H. Booth, A Method of Calculating Fission Gas Diffusion from UO_2 Fuel and Its Application to The X-2 Loop Test, AECL-496, CRDC-721, 1957.

34. H. M. Ferrari, Nitrogen Release from UO_2 Pellets at Elevated Temperatures, Nuclear Science and Engineering, 17, 4, December 1963.

35. H. M. Ferrari, Diffusion of Nitrogen in Uranium Dioxide, Journal Of Nuclear Materials, 12, 2, 1964.

36. P. R. Bevington, Data Reduction and Error Analysis for the Physical Sciences, New York: McGraw-Hill Book Company, 1969.

37. P. H. Kreyns, G. L. Spahr, J. E. McCauley, An Analysis of Iodine Stress Corrosion Cracking of Zircaloy-4 Tubing, WAPD-TM-1248, February 1976.

38. R. P. Tucker, P. H. Kreyns, J. J. Kearns, The Effects of Internal Surface Flaws, Iodine Concentration and Temperature on the Stress Corrosion Cracking Behavior of Zircaloy-4 Tubing, WAPD-TM-1248, February 1976.

39. R. L. Plackett and J. P. Burman, The Design of Optimum Multifactorial Experiments, Biometrika, 33, p. 305-325, 1946.

40. L. J. Siefken et al., FRAP-T5: A Computer Code for the Transient Analysis of Oxide Fuel Rods, NUREG-CR-0840, TREE-1281, June 1979.*

41. J. P. C. Kleijnen, Statistical Techniques in Simulation - Part II, Marcel Dekker, Inc., Publisher 1975.

*Available for purchase from the NRC/GPO Sales Program, U.S. Nuclear Regulatory Commission, Washington, DC 20555, and the National Technical Information Service, Springfield, VA 22161,

**Available for purchase from the National Technical Information Service, Springfield, VA 22161.

APPENDIX A

INPUT AND OUTPUT DESCRIPTION

APPENDIX A

INPUT AND OUTPUT DESCRIPTION

Appendix A describes the input necessary to run FRAPCON-2 and how to interpret the output data. The makeup of the input data deck consists of:

1. Uncertainty analysis option card

2. Uncertainty NAMELIST IN (if uncertainty analysis option is chosen)

3. Title card for the job being run

4. NAMELIST FRPCN

5. NAMELIST FRPCON

6. NAMELIST EMFCPN (if evaluation model option is chosen)

7. Plot input.

The standard input includes the uncertainty analysis option card, the title card, and two NAMELISTs, FRPCN and FRPCON. Optional input includes the NAMELIST IN, NAMELIST EMFCPN, and the plot input.

Section 1. of this appendix describes the standard input, which is in NAMELIST format. Section 2. describes the optional

input. Section 3. presents the output format and Section 4. describes the control language necessary to run the code on the CDC CYBER computer.

1. STANDARD INPUT

1.1 USE OF NAMELIST.

The standard input to FRAPCON-2 is in the form of two NAMELISTs, FRPCN and FRPCON. The use of NAMELIST input requires that the user follow a prescribed input format. Within certain restrictions, however, great flexibility is provided for designing an input deck.

The input format requires that:

1. The first character on every card be left blank.

2. The first card of a NAMELIST data set must contain a "$" in column 2, immediately followed by the appropriate NAMELIST name.

3. The last entry of a data set must be a "$".

4. The data items must be separated by commas (the comma should follow <u>immediately</u> after the <u>constant</u>).

The form of the data items in an input record is

<u>Symbolic_Name</u> = <u>Constant</u>,

The symbolic name may be a variable name or an array element name. Subscripts must be integer numbers. The constant may be an integer or real number.

1.2 DATA DECK FORMULATION.

The cards necessary to create a standard input deck for FRAPCON-2 include the uncertainty analysis option card, the title card, NAMELIST FRPCN, and NAMELIST FRPCON.

The uncertainty analysis card is used to input the choice of whether or not the uncertainty analysis option is to be run. If the option is to be used , a "1" is placed in Column 5 and NAMELIST IN follows. If the option is not to be used, a "0" is placed in Column 5. If the uncertainty analysis option is not used, the uncertainty analysis card is followed by the title card(s). There is no limitation on the length of the title or the number of title cards used, but only the first 40 characters of the first card will be printed by the code. The title card is followed first by NAMELIST FRPCN, and then by NAMELIST FRPCON. Evaluation models are used if the value of the variable IMSWCH is not equal to zero. If plot options are chosen, additional cards are added after NAMELIST FRPCON.

What follows is a description of the variables comprising NAMELIST FRPCN. These variables are used by the code to describe the physical space in the computer where information will be stored.

NAMELIST $EPRCN

Variable Name	Description and Restriction	Default Value
IAXSYM	Controls AXISYM option; use only with MECHAN=3 =1, AXISYM is used =0, AXISYM is not used	0
IM	Number of power-time steps (greater than 1)	-
MECHAN	Controls choice of mechanical model =1, PELET-RADIAL =2, FRACAS-1 =3, FRACAS-II	0
NA	Number of axial regions (may vary from 3 to 18)	-
NC	Number of radial nodes in cladding; used only if MECHAN=1 (greater than 1)	4
NF	Number of radial nodes in fuel; used only if MECHAN=1 (greater than 1)	5
NR	Number of radial nodes in fuel; used for thermal calculations (recommended value is 11)	11

Variable Name	Description and Restriction	Default Value
NGASR	Controls choice of gas release model = −2, FAST/GRASS or GRASS = −1, Booth diffusion = 0, Maclonald-Weisman = 1, Beyer-Hann with NRC high burnup correction factor = 2, Beyer-Hann without NRC high burnup correction factor ≥ 6, ANS-5.4; NGASR is used as the number of radial regions in the fuel for the gas release calculations	

When choosing values for the variables in NAMELIST FRPCN the user must consider that more detailed modeling will result in increased computer core storage requirements and increased running time. Those variables which directly influence the running time and core storage requirements include IM, NA, AND NR (NF and NC if MECHAN=1). The influence of the MECHAN and NGASR option choices is best determined by trial for the specific problem being modeled.

The card immediately following the $END card of NAMELIST FRPCN will be the first card of NAMELIST FRPCON. NAMELIST FRPCON contains the actual rod parameters, power history, etc., and consists of the variables listed below. The user has the option to input English or SI units. Each input variable lists the appropriate English or SI unit in the variable description. These must be input with those units.

NAMELIST FRPCON

Variable Name	Description and Restrictions	Default Value
COMP	Plutonium oxide content of fuel (weight percent)	0
CPL	Plenum length (in.,m)	-
DCI	Inside diameter of cladding (in.,m); input a value for each axial region if IVARDM = 2	-
DCO	Outside diameter of cladding (in.,m); input a value for each axial region if IVARDM = 2	-
DE	Equivalent heated diameter (in.,m); input a value for each axial region if IVARDM = 2	-
DELTAZ	Array containing lengths of axial segments (in.,m); variable only if IVARDM = 1	-
DEN	Fuel density as percent of theoretical; 10.97 gm/cc is assumed theoretical density	-
DISHSD	Dish shoulder width; pellet radius minus dish radius (in.,m)	-

Variable Name	Description and Restriction	Default Value
DP	Diameter of pellet (in.,m); input a value for each axial region if IVARDM = 2	-
DSPG	Outside diameter of spring (in.,m)	-
DSPGW	Diameter of spring wire (in.,m)	-
ENRCH	Fuel enrichment (weight percent)	-
FA	Axial power profile peak-to-average ratio =1.0, if QMPY = average >1.0, if QMPY = peak	1.0
FGPAV	Initial fill gas pressure (psia, N/m^2)	-
FLUX	Fast neutron flux (neutrons/m^2.s)	$6x10^{17}$
GO	Mass flow rate (lb/hr.ft^2 kg/s.m^2) see NSP; if go=0, cladding surface temperature=TW at all axial nodes	0
HDISH	Depth of pellet end dish (in.,m)	-
HPLT	Height of pellet (in.,m)	-

Variable Name	Description and Restriction	Default Value
ICM	Index for cladding material =2, zircaloy-2 =4, zircaloy-4	-
IDXGAS	Index for initial fill gas composition =1, helium =2, air =3, nitrogen =4, fission gas =5, argon =6, user specifies mole fractions, see AMFAIR, etc.	-
IMSWCH	Switch to control use of the evaluation models; use only if MECHAN=2 = 0, use no EM models = 1, use all EM models =-1, individual models specified by user; see NAMELIST EMFPCN in optional input section	0
IPLANT	Switch to specify the radial power profile =-1, User inputs radial power profile (See RAPOW) = 0, Code uses FLUXD subroutine Radial power profile from LASER tables, if IPLANT = 1,2,3,4 1=PWR, uranium enriched, 6 >ENRCH> 2.0 2=BWR, uranium enriched, 3.5 >ENRCH> 1.5 3=PWR, plutonium enriched, 10 >ENRCH> 2.0 4=BWR, plutonium enriched, 6 >ENRCH> 1.5	-

Variable Name	Description and Restriction	Default Value
IQ	Index for axial power shape =0, user input (see FA,QF) =1, cosine shape calculated by code CMPY must be average powers; see FA	0
IVARDM	Index for axially depenoent dimensions =0, no variation =1, axial length variation; DELTAZ input as array =2, variable radial dimensions; DCI, DCO, DP, DE, BUIN input as arrays	0
JDLPR	Index for output control (when NOPT=0) =1, peak power axial node only =1, all axial nodes	0
JN	Number of entries (maximum of 40) in each set of QF and X tables (omit if IQ=1)	-
JST	Array controlling choice of axial power shape for each time step (IQ must = 0) Shape 1 is described by the first X and QF arrays Shape 2 is described by the second X and QF arrays. etc., maximum of 8 shapes	1,1,1, etc.

Variable Name	Description and Restriction	Default Value
NOPT	Output option =0, full output =3, summary page output	0
NSP	Switch for time dependent parameters =0, constant parameters =1, P2, TW, and GB must be input as arrays versus time array	0
NUNITS	Specifies input unit type =0, metric units =1, English units	0
P2	System pressure (see NSP) (psia, N/m^2)	-
QF	Axial power profile factors; up to 8 shapes containing JN entries for each shape; May be normalized to peak or average power; see FA, IQ, QMPY	-
QMPY	Linear heat rating array versus time array (kW/ft,kW/m). QMPY values may be either peak or average powers. If MECHAN=1,QMPY should not change more than 5.0 kW/m (1.5 kW/ft) per time step.	-
RC	Radius of pellet annulus (in.,m)	0.0

Variable Name	Description and Restriction	Default Value
ROUGHC	Arithmetic mean roughness of cladding surface (in.,m)	4.5×10^{-5}
ROUGHF	Arithmetic mean roughness of fuel surface (in.,m)	8.5×10^{-5}
TIME	Table of accumulated times corresponding to GMPY array, time to end of step (days, first value greater than 0.0)	-
TOTL	Fuel stack height (ft,m)	-
TW	Inlet water temperature (°F,K); see NSP	-
VS	Total number of spring turns	-
X	Table of axial elevations corresponding to GF entries (ft,m); must range in ascending order from 0.0 to TOTL, for up to 8 shapes, omit if IQ=1	-

The following variables, also contained in NAMELIST FRPCON, are basically input options rather than requirements. The user may wish to use the default values for most of these variables.

Default Name	Description and Restriction	Default Value
AMFAIR	Absolute mole fraction of air; used only if IDXGAS = 6	0.0
AMFARG	Absolute mole fraction of argon; used only if IDXGAS = 6	0.0
AMFFG	Absolute mole fraction of fission gas; used only if IDXGAS = 6; use only if AMFKRY = 0.0 and AMFKE = 0.0	0.0
AMFHE	Absolute mole fraction of helium; used only if IDXGAS = 0	0.0
AMFH2	Absolute mole fraction of hydrogen; used only if IDXGAS = 6	0.0
AMFH2O	Absolute mole fraction of steam; used only if IDXGAS = 6	0.0
AMFKRY	Absolute mole fraction of krypton; used only if IDXGAS = 6	0.0
AMFN2	Absolute mole fraction of nitrogen; used only if IDXGAS = 6	0.0
AMFXE	Absolute mole fraction of xenon; used only if IDXGAS = 6	0.0

Variable Name	Description and Restriction	Default Value
BETA	Variable not currently used.	0.0
BUIN	Initial fuel burnup (MWd/MTU,MWs/kg); also consider inputting AMFFG; may be axially dependent array if IVARDM = 2	0.0
CATEXF	Texture factor: fraction of cladding cells with basal poles parallel to the tube axis	0.05
CLDWKS	Cold work of the cladding, fraction	0.2
CP	Anisotropy coefficient; used with MECHAN=1	1.0
CR	Anisotropy coefficient; used with MECHAN=1	1.0
CRDT	Initial crud thickness (mil,m)	1.0
CRDTR	Crud building rate (mil/hr,m/s) only if ICOR=2	1.4×10^{-4}
CREPHR	Creep step size for FRACAS-I and FRACAS-II (hrs)	10.0
CTMAX	Maximum clading temperature attained by the fuel rod, axial array (F,K)	386.33 etc.

Variable Name	Description and Restriction	Default Value
DENG	Ratio of pellet immersion density to geometric density	0.75
FOTMIL	Fuel oxygen to metal ratio	2.0
GRNSIZ	Initial fuel grain size (μm)	5.0
ICOR	Index for crud model =0, constant crud; no temperature drop if boiling =1, constant crud; temperature drop if boiling =2, varying crud; temperature drop if boiling	0
ITREST	Restart index (time-power step to begin a restart, use only with FRACAS options)	0
LINKT	Version number of FRAP-T code for which restart tape is to be written (5 or 6)	5
NFROD	Number of like fuel rods being analyzed	1
NOFAIL	Controls the use of cladding failure models used with FRACAS-I =0, failure probability considered =1, failure probability not considered	1

Variable Name	Description and Restriction	Default Value
NPCYCL	Number of previous power cycles	0
NPLTAB	Parameter on plot abcissa =0, time =1, rod average power =2, local burnup	0
NPRINT	GRASS print index =1, no GRASS output =4, full GRASS output	
NREAD	FRAPCON restart read =0, no restart read =1, read restart tape	0
NRESTR	FRAPCON restart write =0, no restart write =1, write restart tape	0
NTAPE	FRAP-T restart =0, no restart data stored =1, data stored each time step for FRAP-T use	0
NUCFC	User specified collapse failure criterion =0, collapse mode is not considered =1, collapse mode is considered	0

Variable Name	Description and Restriction	Default Value
QEND	Normalized heat flux from top	0.3,
PPMH2O	Fuel initial water content (ppm)	0.0
PPMN2	Fuel initial nitrogen content (ppm) of fuel stack to plenum, one value for each axial power profile; see QF	15.0 etc.
RAPOW	Radial power profile, applied at boundaries of equal volume rings in order from surface to center; 11 values are required, normalized to an average value of 1.0, used only if IPLANT = -1	1,1, etc.
RSNTR	Absolute change in fuel density due to thermal resintering (kg/m^3)	0.0
SGAPF	Fission gas atoms produced per 100 fissions	30.0
TSINT	Fuel sintering temperature (°F,K)	2912.
UBFS	User specified balloon failure strain	$1.x10^9$
UMELT	Cladding failure melting temperature (°F) =0, MATPKG value is used >0, input value is used	0.0

Variable Name	Description and Restriction	Default Value
UOFD	Cladding oxide failure depth criterion (percent)	17.0

2. OPTIONAL INPUT

The optional input is comprised of three groups, the uncertainty analysis input, the evaluation model input, and the plot input.

2.1 UNCERTAINTY OPTION.

As noted previously, the uncertainty option is used when a "1" is placed in column 5 of the uncertainty analysis card. When the option is selected for use, the uncertainty analysis option card is followed by the NAMELIST IN. The variables contained in IN are described below.

NAMELIST IN

Variable Name	Description and Restrictions	Default Value
FACTOR(K)	Flag for additive or multiplicative uncertainty factors. =0, additive =1, multiplicative (default)	-

Variable Name	Description and Restriction	Default Value
C(I,J,K)	Uncertainty factors. Factors are described by polynomials of up to third order in temperature (I) in four temperature ranges (J) for approximately 50 factors (K). Values are one standard deviation. Multiplicative factors should be input as a decimal fraction. For example, an uncertainty factor of 1.25 indicating a one sigma uncertainty of 25 should be input as 0.25. The code will add the 1.00 when used	0.0 etc.
TL(J,K)	Upper temperature limits describing ranges applicable to uncertainty factor polynomials. If no temperature range uppermost limit, enter 0.	0
LRES(N)	List of responses from Table A-1. Order is not important. Individual responses may be listed more than once. For example, a given response may be desired at more than one axial node. Not to exceed 100 total responses.	0
NODE(N)	List of axial nodes corresponding LRES(N). List must match LRES(N) one for one.	1

Table A-1. DEFAULT UNCERTAINTY FACTORS

LFAC	Source	Additive (A) or Multiplicative (M)*	Factor	Temp. Range (K)
1.	Fuel specific heat	M	1.02 1.012+1.6E-5xT 2.06	T<500. 500.<T<3000. 3000.<T
2.	Fuel thermal conductivity	A	0.2	-
3.	Fuel emissivity	M	1.10	-
4.	Fuel thermal expansion	A	0.253-6xT 0.00125	T<500. 500.<T
5.	Fuel elastic modulus	A	0.3E11 (Pa)	-
6.	Poisson's ratio	A	0.094	-
7.	Fuel creep	-	(TBD)**	-
8.	Fuel fracture strength	A	0.19 (Pa)	-
9.	Fuel swelling	M	1.50	-
10.	Fuel restructuring	-	(TBD)	-
11.	Fuel densification	-	(TBD)	-
12.	Fission gas release	-	(TBD)	-
13.	Cladding specific heat	A	10.(J/kg.K) 10. 25. 100.	T<300. 300.<T<1090. 1090.<T<1300. 1300.<T
14.	Cladding thermal conductivity	A	1.01 (W/m.K)	-
15.	Zirc oxide emissivity	A	0.10	-

Table A-1. (Continued)

LFAC	Source	Additive (A) or Multiplicative (M)*	Factor	Temp. Range (K)
16.	Zirc oxide thermal conductivity	A	1.20	-
17.	Cladding axial thermal expansion	M	1.20 1.50	T<1073. 1073.<T
18.	Cladding diametral thermal expansion	M	1.20 1.50	T<1073. 1073<T.
19.	Cladding elastic modulus	M	1.10 1.20	T<1083. 1083.<T
20.	Cladding strength Coefficient	A	29.E6 (Pa)	-
21.	Cladding circumferential	A	0.08 -0.91+1.25 E-3xT 0.11	T<800. 800.<T<1170 1170.<T
22.	Cladding Meyer hardness	-	(TBD)	-
23.	Cladding creep rate	-	(TBD)	-
24.	Cladding Poisson's ratio	A	0.025	-
25.	Cladding oxidation	M	1.175 1.065	T<1523. 1523<T.
26.	Gas thermal conductivity	M	1.25	-
27.	Gas viscosity	M	1.25	-
28.	Gap heat transfer	M	1.25	-
29.	Alpha-Beta transition temperature	A	10.(K)	-

Table A-1. (Continued)

LFAC	Source	Additive (A) or Multiplicative (M)*	Factor	Temp. Range (K)
30.	Pellet stack height	M	1.001	-
31.	Cladding outer diameter	M	1.001	-
32.	Fuel density	M	1.0067	-
33.	Pellet shoulder radius	M	1.034	-
34.	Pellet dish depth	M	1.034	-
35.	Pellet height	M	1.001	-
36.	Pellet dish volume	M	1.034	-
37.	Pellet outer radius	M	1.001	-
38.	Cladding inner radius	M	1.001	-
39.	Cladding outer radius	M	1.001	-
40.	Cladding roughness	M	1.100	-
41.	Fuel roughness	M	1.100	-
42.	Amount of gas in rod	M	1.034	-
43.	Plenum volume	M	1.001	-
44.	Cold pressure	M	1.034	-

Table A-1. (Continued)

LFAC	Source	Additive (A) or Multiplicative (M)*	Factor	Temp. Range (K)
45.	Mole fractions of of gas components	-	(TBD)	-
46.	Unused	-	-	-
47.	Initial temperature estimate	-	(TBD)	-
48.	Power history	M	1.050	-
49.	ANS decay heat curve	M	1.067	-
50.	Unused	-	-	-
51.	CHF factor	M	1.080	-
52.	Unused	-	-	-
53.	Unused	-	-	-
54.	Unused	-	-	-
55.	Jnused	-	-	-
56.	Jnused	-	-	-
57.	Unused	-	-	-
58.	Unused	-	-	-
59.	Unused	-	-	-
60.	Jnused	-	-	-
61.	Plenum length	-	(TBD)	-
62.	Equivalent heated diameter	-	(TBD)	-

Table A-1. (Continued)

LFAC	Source	Additive (A) or Multiplicative (M)*	Factor	Temp. Range (K)
63.	Diameter of spring, outside	-	(TBD)	
64.	Diameter of spring wire	-	(TBD)	-
65.	Fuel enrichment	-	(TBD)	-
66.	Mass flow rate	-	(TBD)	-
67.	system pressure	-	(TBD)	-
68.	Axial heat Normalization Factors	-	(TBD)	-
69.	Fuel stack height	-	(TBD)	-
70.	Inlet water temperature	-	(TBD)	-
71.	Total spring turns	-	(TBD)	-
72.	Initial fuel burnup	-	(TBD)	-
73.	Texture factor	-	(TBD)	-
74.	Cold work	-	(TBD)	-
75.	Weight percent PuO_2	-	(TBD)	-
76.	Initial crud thickness	-	(TBD)	-
77.	Crud buildup rate	-	(TBD)	-
78.	Porosity correction	-	(TBD)	-

Table A-1. (Continued)

LFAC	Source	Additive (A) or Multiplicative (M)*	Factor	Temp. Range (K)
79.	Fast neutron flux	-	(TBD)	-
80.	Initial grain size	-	(TBD)	-
81.	Fuel initial water content	-	(TBD)	-
82.	Fuel initial nitrogen content	-	(TBD)	-
83.	Normalized heat flux at top of fuel stack	-	(TBD)	-
84.	Pellet core radius	-	(TBD)	-
85.	Fission gas atoms per 100 fissions	-	(TBD)	-
86.	Fuel sintering temperature	-	(TBD)	-
87.	Cladding oxide failure criterion	-	(TBD)	-
88.	Unused	-	-	-
89.	Unused	-	-	-
90.	Unused	-	-	-
91.	Unused	-	-	-
92.	Unused	-	-	-
93.	Unused	-	-	-
94.	Unused	-	-	-
95.	Unused	-	-	-

Table A-1. (Continued)

LFAC	Source	Additive (A) or Multiplicative (M)*	Factor	Temp. Range (K)
96.	Unused	-	-	-
97.	Unused	-	-	-
99.	Unused	-	-	-
100.	Unused	-	-	-

* Additive (A) or Multiplicative (M) refers to the manner in which the factor was applied. That is, percentage uncertainties were multiplicative whereas absolute uncertainties additive.

** (TBD) - to be determined.

Variable Name	Description and Restriction	Default Value
LFAC(N)	List of factors from Table A-2 to be included in the analysis. Order is important. Example, (LFAC)= 2, 4, 8, 5, 6, the analysis will include these five factors in this order in the experimental design and confounding arrays.	0
LTYPE	Type of analysis desired. =1, linear =2, linear plus foldover =3, linear plus quadratic =4, linear plus foldover plus quadratic	1
LPB	Placket-Burman design flag =0, fractional factorial design =1, Placket-Burman design	0
AMU(L,K)	First four dimensionless central moments of the uncertainty factor distributions assumed to apply over all temperature ranges. Normal distribution is default.	0
IPRINT	Flag for additional experimental design including design generators and one and two factor aliases. =0, no =1, yes	0

Table A-2. Responses

LRES	Response
1	Zircaloy oxide thickness (M)
2	Net permanent fuel deformation (m)
3	Cladding plastic hoop strain
4	Cladding plastic axial strain
5	Cladding plastic radial strain
6	Cladding peak temperature during operation (K)
7	Open porosity
8	Fuel burnup (MWd/MTU)
9	Fuel centerline temmperature (K)
10	Fuel surface temperature (K)
11	Cladding inner surface temperature (K)
12	Cladding outer surface temperature (K)
13	Internal gas pressure (Pa)
14	Radial gas gap (m)
15	Gram-moles gas in the rod
16	Mole fraction of rod gases
17	Cladding residual hoop strains
18	Cladding residual axial strains

Table A-2. (Continued)

LRES	Response
19	Cladding residual radial strains
20	Fuel residual hoop strains
21	Fuel residual axial strains
22	Fuel residual radial strains
23	Interface pressure (Pa)
24	Cladding effective plastic strain

Variable Name	Description and Restriction	Default Value
IFLAG	Flag for check runs =0, design and confounding arrays =1, add nominal FRAP run =2, add complete uncertainty analysis	0
ISTART	Flag for restarting from previous analysis =0, no =1, yes	0

2.2 EVALUATION MODEL OPTION

A set of ten EM flags are used to specify the EM options. One, flag IMSWCH in the FRPCON NAMELIST is used to set all options on or off, or to specify that some combination of the EM model options and best-estimate BE model options is to be used.

The input variables for the EMFPCN NAMELIST are given below. They correspond to the nine EM requirements. All variables are defaulted to zero.

The EM input cards follow a $EMFPCN card and end with a $END card. If IMSWCH = 0 or 1, these cards must be omitted.

NAMELIST EMFPCN

Variable	Description and restriction	Default Value
IMPOWR	EM power requirement index =0, not assumed to be required =1, assumed to be required and input appropriately	0
IMFUEL	EM fuel dimensional change index =0, BE dimensional changes =1, EM dimensional changes	0
IMFDNS	EM fuel densification index =0, BE densification used =1, EM densification used	0
IMRELO	EM fuel relocation index =0, BE relocation used =1, EM relocation used	0
IMCLAD	EM cladding deformation index =0, All deformation mechanisms included =1, No permanent deformation included	0
IMGAPC	EM gap conductance index =0, BE gap conductance used =1, EM gap conductance used	0

Variable Name	Description and Restriction	Default Value
IM93WC	EM fuel thermal conductivity index =0, Thermal conductivity based on 97 w/cm =1, Thermal conductivity based on 93 w/cm and uncracked fuel	0
IMENRG	EM stored energy index =0, Stored energy based on 298 K =1, Stored energy based on 273 K	0
IMFGAS	EM fission gas release =0, BE fission gas release used =1, EM fission gas release used	0

2.3 PLOT INPUT

The following is the input data required for plotting. If no plots are desired, follow the "$END" card of the preceding input with card 1 below. If plots are desired, a full set of plot data is required and the following plots versus time, power, or burnup (see NPLTAB) will be created for each axial node specified.

1. Cladding Surface Temperature
2. Fuel Centerline Temperature
3. Gas Pressure
4. Cladding Hoop Strain
5. Fuel Axial Elongation
6. Cladding Axial Elongation
7. Local Rod Power

8. Surface Temperature of Fuel

9. Gap Heat Transfer Coefficient

10. Cladding Surface Heat Transfer Coefficient

11. Average Temperature of Cladding

12. Zircaloy Oxide Thickness

13. Mole Fraction of Helium

14. Plenum Temperature

15. Increase in Gas Moles

16. Coolant Mass Flux

17. Stored Energy

18. Coolant Pressure

19. Unrelocated Gap Thickness

20. Bulk Coolant Temperature

Card No. 1 - Specification of the number of axial nodes for which plots are desired

Columns	Format*	Name	Quantity
1-5	I	NPLTNO	Number of axial nodes for which plots are desired. If no plots wanted, input the number 0.

Card No. 2 - Specification of axial nodes at which plots are wanted

Columns	Format	Name	Quantity
1-5	I	IAPLT(1)	The first axial node at which plots are wanted
6-10	I	IAPLT(2)	The second axial node at which plots are wanted

Repeat as necessary for IAPLT (K), K being an axial node number

Card No. 3 - Time, local rod power, or burnup axis

Columns	Format	Name	Quantity
1-10	F	TSTART	Minimum time, power, or burnup on time axis (hr, sec)

*I = integer value, F = floating point value, A = alpha numeric value.

11-10	F	TEND	Maximum time, power, or burnup on time axis (hr, sec)
21-30	F	AXLT	Length of time axis (in.)
31-70	A	LABLT	Label to be given time axis

Card No. 4 - Cladding surface temperature axis

Columns	Format	Name	Quantity
1-10	F	TSMIN	Minimum cladding surface temperature on axis (°F,K)
11-20	F	TSMAX	Maximum cladding surface temperature on axis (°F,K)
21-30	F	AXLTS	Length of surface temperature axis (in.)
31-70	A	LABLTS	Label to be given surface temperature axis

Card No. 5 - Fuel centerline temperature axis

Columns	Format	Name	Quantity
1-10	F	TCLMIN	Minimum fuel centerline temperature on axis (°F,K)

11-20	F	TCLMAX	Maximum fuel centerline temperature on axis (°F,K)
21-30	F	AXLTMP	Length of centerline temperature axis (in.)
31-70	A	LABLTM	Label to be given centerline temperature axis

Card No. 6 - Gas pressure axis

Column	Format	Name	Quantity
1-10	F	PMIN	Minimum gas pressure on axis (psia, N/m^2)
11-20	F	PMAX	Maximum gas pressure on axis (psia, N/m^2)
21-30	F	AXLP	Length of gas pressure axis (in.)
31-70	A	LABLP	Label to be given gas pressure axis

Card No. 7 - Cladding hoop strain axis

1-10	F	EPSMIN	Minimum cladding hoop strain on axis (dimensionless)
11-20	F	EPSMAX	Maximum cladding hoop strain on axis

(dimensionless)

21-30	F	AXLEPS	Length of cladding hoop strain axis (in.)
31-70	A	LABLE	Label to be given cladding hoop strain axis

Card No. 8 - Fuel axial displacement axis

Columns	Format	Name	Quantity
1-10	F	UZFMIN	Minimum fuel axial displacement on axis (ft,m)
11-20	F	UZFMAX	Maximum fuel axial displacement on axis (ft,m)
21-30	F	AXLUZF	Length of fuel axial displacement axis (in).
31-70	A	LABLUF	Label to be given fuel axial displacement axis

Card No. 9 - Cladding axial displacement axis

Columns	Format	Name	Quantity
1-10	F	UZCMIN	Minimum cladding axial

			displacement on the axis (ft,m)
11-20	F	UZCMAX	Maximum cladding axial displacement on axis (ft,m)
21-30	F	AXLUZC	Length of cladding axial displacement axis (in.)
31-70	A	LABLUC	Label to be given cladding axial displacement axis

Card No. 10 - Fuel rod power axis

Columns	Format	Name	Quantity
1-10	F	PMIN	Minimum linear fuel rod power on axis (kW/ft, kW/m)
11-20	F	PMAX	Maximum linear fuel rod power on axis (kW/ft, kW/m)
21-30	F	PLEN	Length of linear fuel rod power axis (in.)
31-70	A	PLABL	Label to be given linear fuel rod power axis

Card No. 11 - Fuel surface temperature axis

Columns	Format	Name	Quantity
1-10	F	TFSMIN	Minimum fuel surface tmperature on axis (°F,K)
11-20	F	TFSMAX	Maximum fuel surface temperature on axis (°F,K)
21-30	F	TFSLEN	Length of surface temperature axis axis
31-70	A	TFSLAB	Label to be given fuel surface temperature axis

Card No. 12 - Gap heat transfer coefficient axis

Columns	Format	Name	Quantity
1-10	F	HGMIN	Minimum gap heat transfer coefficient on axis (Btu/hr-°F-ft^2, W/m^2-K)
11-20	F	HGMAX	Maximum gap heat transfer coefficient on axis (Btu/hr-°F-ft^2, W/m^2-K)
21-30	F	HGLEN	Length of gap heat transfer coefficient axis (in.)
31-70	A	HGLABL	Label to be given gap heat transfer coefficient axis

Card No. 13 - Cladding Surface heat transfer coefficient axis

Columns	Format	Name	Quantity
1-10	F	HSMIN	Minimum surface heat transfer coefficient on axis (Btu/hr.°F.ft^2, w/m^2.K)
11-20	F	HSMAX	Maximum surface heat transfer coefficient on axis (Btu/hr.°F.ft^2, w/m^2.K)
21-30	F	HSLEN	Length of surface heat transfer coefficient axis (in.)
31-70	A	HSLAB	Label to be given surface heat transfer coefficient axis

Card No. 14 - Average cladding temperature axis

Columns	Format	Name	Quantity
1-10	F	TAMIN	Minimum average cladding temperature on axis (°F,K)
11-20	F	TAMAX	Maximum average cladding temperature on axis (°F,K)
21-30	F	TALEN	Length of average cladding temperature axis (in)

31-70	A	TALABL	Label to be given average cladding temperature axis

Card No. 15 - Zircaloy-Oxide thickness axis

Columns	Format	Name	Quantity
1-10	F	ZOMIN	Minimum ZrO_2 thickness on axis (in.,mm)
11-20	F	ZOMAX	Maximum ZrO_2 thickness on axis (in.,mm)
21-30	F	ZOLEN	Length of ZrO_2 thickness axis (in.)
31-70	A	ZOLABL	Label to be given ZrO_2 thickness axis

Card No. 16 - Helium mole fraction axis

Columns	Format	Name	Quantity
1-10	F	MFMIN	Minimum helium mole fraction on axis
11-20	F	MFMAX	Maximum helium mole fraction on axis
21-30	F	MFLEN	Length of helium mole fraction axis (in.)
31-70	A	MFLABL	Label to be given helium mole fraction axis

Card No. 17 - Plenum temperature axis

Columns	Format	Name	Quantity
1-10	F	TPMIN	Minimum plenum temperature on axis (°F,K)
11-20	F	TPMAX	Maximum plenum temperature on axis (°F,K)
21-30	F	TPLEN	Length of plenum temperature axis (in.)
31-70	A	TPLABL	Label to be given plenum temperature axis

Card No. 18 - Rod gas increase axis

Columns	Format	Name	Quantity
1-10	F	RGMIN	Minimum gas increase on axis (percent of initial)
11-20	F	RGMAX	Maximum gas increase on axis (percent of initial)
21-30	F	RGLEN	Length of gas increase axis (in.)
31-70	A	RGLABL	Label to be given gas increase axis

Card No. 19 - Coolant Mass flux axis (plot of average mass flux in coolant channels surrounding fuel rod)

Columns	Format	Name	Quantity
1-10	F	GMIN	Minimum mass flux on axis (lbm/ft^2.hr, kg/m^2.s)
11-20	F	GMAX	Maximum mass flux on axis (lbm/ft^2.hr, kg/m^2.s)
21-30	F	GLEN	Length of mass flux axis (in.)
31-70	A	GLABL	Label to be given mass flux axis

Card No. 20 - Fuel stored energy axis

Columns	Format	Name	Quantity
1-10	F	SEMIN	Minimum stored energy on axis (btu/lbm, cal/kg)
11-20	F	SEMAX	Maximum stored energy on axis (btu-bm, cal/kg)
21-30	F	SELEN	Length of average stored energy axis (in.)
31-70	A	SELABL	Label to be given average stored energy

axis

Card No. 21 - Coolant pressure axis (plot of average pressure in coolant channel surrounding fuel rod)

Card	Format	Name	Quantity
1-10	F	PCMIN	Minimum coolant pressure on axis (psia, N/m^2)
11-20	F	PCMAX	Maximum coolant pressur on axis (psia, N/m^2)
21-30	F	PCLEN	Length of coolant pressure axis (in.)
31-70	A	PCLABL	Label to be given coolant pressure axis

Card No. 22 - Unrelocated gap thickness axis

Columns	Format	Name	Quantity
1-10	F	THKMIN	Minimum gap thickness on axis (mil,m)
11-20	F	THKMAX	Maximum gap thickness on axis (mil,m)
21-30	F	THKLEN	Length of gap thickness axis (in.)
31-70	A	THKLAB	Label to be given gap thickness axis

Card No 23 - Bulk Coolant temperature axis

Columns	Format	Name	Quantity
1-10	F	TEMIN	Minimum bulk temperature on axis (°F,K)
11-20	F	TBMAX	Maximum bulk temperature on axis (°F,K)
21-30	F	TBLEN	Length of bulk temperature axis (in.)
31-70	A	TBLAB	Label to be given bulk temperature axis

3. OUTPUT DESCRIPTION

The output from FRAPCON-2 consists of several discrete sections. Each section will be described below in the order the user would encounter it.

The first page is an exact listing of the cards the program reads as data (Figure A-1). The WRITE statements which create this output are in SUBROUTINE ECHO1.

If the uncertainty option flag is set to "1", the next section of output will present uncertainty analysis output (Figure A-2).

The next output section to appear in the printout is the NAMELIST FRPCN with the values for those variables (Figure A-3). This information is created by the WRITE statements in subroutine SETUP.

```
        1         2         3         4         5         6         7         8
12345678901234567890123456789012345678901234567890123456789012345678901234567890

IFA=432, ROD 1
 $FRPCN
 IM=35,NA=4,NR=11,NF=4,NC=3,MECHAN=1,NGASR=2,
 IM = 60,
 IM = 12,
 $END
 $FRPCON
 RSNTR =104.0, TSINT = 3092.0,  FLUX = 2.1E17,
 CPL=0.984,DCI=0.4295,DCO=0.5035,DE=0.6,DEN=95.,DISHSD=.0,DP=0.4205,
 DSPG=0.3,DSPGH=0.03,ENRCH=10.,FA=1.15,FGPAV=15,        GO(1)=0.0,
 HDISH=0.0,HPLT=0.5,ICM=2,IDXGAS=1,IQ=0,JDLPR=0,JN=8,JST=0,
 NOPT=0,NSP=0,NUNITS=1,P2(1)=500,RC=0.035,           TOTL=1.87,TW(1)=464,
 IPLANT = -1,
 RAPOW(1)= 1.183,1.1375,1.095,1.055,1.018,.985,.959,.927,.902,.88,.851,
 QF(1)=0.580,0.67,0.781,0.862,0.917,0.968,0.996,1.0,
 QMPY(14) = 8*13.7,6*12.8,3*13.7,12.4,3*11.,2*12.2,3*11.4,2*10.2,11.2,
 QMPY(43) = 3*12.2,11.2,10.2,9.2,2*8.4,9.4,10.4,8*11.4,
 TIME(22) = 125.2,147.,168.,189.,210.,230.,230.2,250.,270.,270.2,270.4,
 TIME(33) = 285.,300.,300.2,310.,310.2,324.,347.,347.2,359.,359.2,359.4,
 TIME(44) = 375.,406.,406.2,406.4,406.6,421.,436.,436.2,436.4,436.6,
 TIME(54) = 455.,475.,495.,515.,535.,555.,570.,
 QMPY(1)=1.,2.,3.,4.,5.,6.,7.,8.,9.,10.,11.,12.,13.,
 QMPY(14) = 8*13.7,8*12.8,5*13.7,12.4,4*11.,2*12.2,5*11.4,2*10.2,11.2,
 QMPY(50) = 6*12.2,11.2,10.2,9.2,4*8.4,9.4,10.4,14*11.4,
 TIME(1)=.075,.150,0.225,0.300,0.375,0.450,0.525,0.600,0.675,
 TIME(10) = 0.750,0.825,0.900,0.975,1.050,10.,20.,40.,60.,80.,102.,125.,
 TIME(22) = 125.2,140.,155.,170.,185.,200.,215.,230.,230.2,240.,250.,
 TIME(33) = 260.,270.,270.2,270.4,280.,290.,300.,300.2,310.,310.2,320.,
 TIME(44) = 330.,340.,347.,347.2,359.,359.2,359.4,370.,380.,390.,400.,
 TIME(55) = 406.,406.2,406.4,406.6,406.8,416.,426.,436.,436.2,436.4,
 TIME(65) = 436.6,447.,458.,469.,480.,490.,500.,510.,520.,530.,540.,
 TIME(76) = 550.,560.,570.,
 X(1)=0.0,0.25,0.541,0.933,1.241,1.550,1.858,1.87,
 JDLPR = 1,
 $END


        1         2         3         4         5         6         7         8
12345678901234567890123456789012345678901234567890123456789012345678901234567890
36 INPUT CARDS
```

Fig. A-1. Card list generated by ECHO1.

DESIGN MATRIX FOR A 2**(7- 3) FRACTIONAL FACTORIAL
INCLUDING FOLDOVER RUNS

RUNS	FACTORS 1	2	3	4	5	6	7
1	1.	1.	1.	1.	1.	1.	1.
2	-1.	1.	1.	-1.	-1.	1.	-1.
3	1.	-1.	1.	-1.	1.	-1.	-1.
4	-1.	-1.	1.	1.	-1.	-1.	1.
5	1.	1.	-1.	1.	-1.	-1.	-1.
6	-1.	1.	-1.	-1.	1.	-1.	1.
7	1.	-1.	-1.	-1.	-1.	1.	1.
8	-1.	-1.	-1.	1.	1.	1.	-1.
9	-1.	-1.	-1.	-1.	-1.	-1.	-1.
10	1.	-1.	-1.	1.	1.	-1.	1.
11	-1.	1.	-1.	1.	-1.	1.	1.
12	1.	1.	-1.	-1.	1.	1.	-1.
13	-1.	-1.	1.	-1.	1.	1.	1.
14	1.	-1.	1.	1.	-1.	1.	-1.
15	-1.	1.	1.	1.	1.	-1.	-1.
16	1.	1.	1.	-1.	-1.	-1.	1.

CONFOUNDING ARRAY

*	1	2	3	4	5	6	7
1	0	6	4	5	7	3	1
2	0	0	1	2	3	7	4
3	0	0	0	3	2	5	6
4	0	0	0	0	1	4	7
5	0	0	0	0	0	6	5
6	0	0	0	0	0	0	2
7	0	0	0	0	0	0	0

Figure A-2 Uncertainty printout.

```
$FRPCN
IAXSYM  = 0,
IM      = 12,
MECHAN  = 1,
NA      = 4,
NC      = 3,
NF      = 4,
NGASR   = 2,
NR      = 11,
$END
```

Figure A-3. Namelist FRPCN.

```
*IFIRST* 3017 *ILAST* 16822

 THE NUMBER OF ARRAYS IS    275

 THE LENGTH OF THE A-ARRAY IS      16822

   1     13     2      5
   3     11     4    301
   5    301     6    306
   7    311     8    316
   9    321    10    326
  11    331    12    336
  13    341    14    346
  15    351    16    356
  17    361    18    366
  19    371    20    376
  21    381    22    386
  23    391    24    396
  25    401    26    406
  27    411    28    416
  29    421    30    426
  31    431    32    436
  33    441    34    446
  35    451    36    456
  37    461    38    466
  39    471    40    476
```

Figure A-4. Dynamic dimensioning output.

SUBROUTINE POINTR prints a column of numbers that follow the $END from NAMELIST FRPCN. These numbers designate array locations as calculated by the dynamic dimensioning capability of the code (Figure A-4).

The NAMELIST FRPCON is the next section of output (Figure A-5). This will be followed by any diagnostic messages generated by the data checking routine in the code, SUBROUTINE CHECK.

SUBROUTINE PRINT1 generates the table of physical dimensions which appear after the diagnostics messages, or the $END of NAMELIST FRPCON (Figure A-6). The heading at the top of the page is generated by SUBROUTINE PGHEAD. It contains the FRAPCON code version number, the MATPRO version number, the run date, an option indicator (see Table A-3) and the page number for future reference. The title also appears in this page heading.

The time dependent variables which may be input by the user are generated by the PRINT1 subroutine and are listed on page 2 of the output (Figure A-7). Plot information will also be output here.

Page 3 which is generated by SUBROUTINE AXHEF, gives information on how the code interpreted the user's input with respect to axial and radial power profiles. Initial fill gas composition is also output. The zero power cladding axial expansion is provided for data comparison purposes (Figure A-8).

```
$FRPCON
COMP    = 0.0,
CPL     = .984E+00,
DCI     = .4295E+00, 0.0, 0.0, 0.0, 0.0, 0.0, 0.0, 0.0, 0.0, 0.0, 0.0, 0.0,    0.0, 0.0, 0.0, 0.0, 0.0,
          0.0, 0.0, 0.0,
DCO     = .5035E+00, 0.0, 0.0, 0.0, 0.0, 0.0, 0.0, 0.0, 0.0, 0.0, 0.0, 0.0,    0.0, 0.0, 0.0, 0.0, 0.0,
          0.0, 0.0, 0.0,
DE      = .6E+00, 0.0, 0.0, 0.0, 0.0, 0.0, 0.0, 0.0, 0.0, 0.0, 0.0, 0.0, 0.0,   0.0, 0.0, 0.0, 0.0, 0.0,
          0.0, 0.0,
DELTAZ  = 0.0, 0.0, 0.0, 0.0, 0.0, 0.0, 0.0, 0.0, 0.0, 0.0, 0.0, 0.0, 0.0, 0.0, 0.0, 0.0, 0.0, 0.0, 0.0,
          0.0,
DEN     = .95E+02,
DISHSD  = 0.0,
DP      = .4205E+00, 0.0, 0.0, 0.0, 0.0, 0.0, 0.0, 0.0, 0.0, 0.0, 0.0, 0.0,    0.0, 0.0, 0.0, 0.0, 0.0,
          0.0, 0.0, 0.0,
DSPG    = .3E+00,
DSPGW   = .3E-01,
ENRCH   = .1E+02,
FA      = .115E+01,
FGPAV   = .15E+02,
FLUX    = .21E+18,
LINKT   = 5,
GO      = 0.0, 0.0, 0.0, 0.0, 0.0, 0.0, 0.0, 0.0, 0.0, 0.0, 0.0, 0.0, 0.0, 0.0, 0.0, 0.0, 0.0, 0.0, 0.0,
          0.0, 0.0, 0.0, 0.0, 0.0, 0.0, 0.0, 0.0, 0.0, 0.0, 0.0, 0.0, 0.0, 0.0, 0.0, 0.0, 0.0, 0.0, 0.0,
          0.0, 0.0, 0.0, 0.0, 0.0, 0.0, 0.0, 0.0, 0.0, 0.0, 0.0, 0.0, 0.0, 0.0, 0.0, 0.0, 0.0, 0.0, 0.0,
          0.0, 0.0, 0.0, 0.0, 0.0, 0.0, 0.0, 0.0, 0.0, 0.0, 0.0, 0.0, 0.0, 0.0, 0.0, 0.0, 0.0, 0.0, 0.0,
          0.0, 0.0, 0.0, 0.0, 0.0, 0.0, 0.0, 0.0, 0.0, 0.0, 0.0, 0.0, 0.0, 0.0, 0.0, 0.0, 0.0,
HDISH   = 0.0,
HPLT    = .5E+03,
ICM     = 2,
IDXGAS  = 1,
IPLANT  = -1,
```

Figure A-5. Namelist FRPCON.

```
XXXXXXXXXXXXXXXXXXXXXXXXXXXXXXXXXXXXXXXXXXXXXXXXXXXX
X                **** FRAPCON ****                 X
X       STEADY-STATE FUEL ROD ANALYSIS CODE        X
X     MOD 002 VERS001     MAT PRO MOD 11  REV 1    X
X  RUN DATE =  27/10/80  OPTIONS 52100000 PAGE    1 X
X  IFA-432, ROD 1                                  X
XXXXXXXXXXXXXXXXXXXXXXXXXXXXXXXXXXXXXXXXXXXXXXXXXXXX
XXXXXXXXXXXXXXXXXXXXXXXXXXXXXXXXXXXXXXXXXXXXXXXXXXXXXXXXXXXXXXXXXXXXXXXXXXXXXXXXXXXXXXXXXXXXXXXXXXXXXXXXXXXXXXXXXXXXXXX
CLADDING MATERIAL IS ZIRCALOY-2
CLADDING OUTSIDE DIAMETER,         CM(IN.)        1.28E+00(5.04E-01)
CLADDING INSIDE DIAMETER,          CM(IN.)        1.09E+00(4.30E-01)
CLADDING THICKNESS,                MM(IN.)        9.40E-01(3.70E-02)
CLAD ARITHMETIC MEAN ROUGHNESS,    MM(MILS)       1.14E-03(4.50E-02)
DIAMETRAL GAP THICKNESS,           MM(MILS)       2.29E-01(9.00E+00)
FUEL PELLET DIAMETER,              CM(IN.)        1.07E+00(4.21E-01)
FUEL PELLET LENGTH,                CM(IN.)        1.27E+00(5.00E-01)
FUEL PELLET DISH DEPTH,            MM(IN.)        0.       (0.       )
FUEL PELLET DISH SHOULDER WIDTH,   MM(IN.)        0.       (0.       )
FUEL PELLET DISH SPERICAL RADIUS,  CM(IN.)        0.       (0.       )
FUEL PELLET CORE RADIUS,           MM(IN.)        8.89E-01(3.50E-02)
FUEL PELLET SINTERING TEMPERATURE,K(F)            1.97E+03(3.09E+03)
FUEL PELLET TRUE DENSITY,          PERCENT        9.50E+01
FUEL VOLUME,                       CU.M(CU.IN.)   4.97E-05(3.03E+00)
FUEL ARITHMETIC MEAN ROUGHNESS,    MM(MILS)       2.16E-03(8.50E-02)
FUEL STACK HEIGHT,                 M(FT.)         5.70E-01(1.87E+00)
FUEL DISH VOLUME FRACTION,                        2.77E-02
FUEL ENRICHMENT,                   WEIGHT PCT     1.00E+01
FUEL FISSION ATOMS/100 FISSIONS,                  3.00E+01
FUEL WATER CONCENTRATION,          PPM            0.
FUEL NITROGEN CONCENTRATION,       PPM            0.
PLENUM LENGTH,                     CM(IN.)        2.50E+00(9.84E-01)
PLENUM SPRING DIAMETER,            CM(IN.)        7.62E-01(3.00E-01)
PLENUM SPRING WIRE DIAMETER,       MM(IN.)        7.62E-01(3.00E-02)
PLENUM SPRING VOLUME,              CU.M(CU.IN.)   0.       (0.       )
PLENUM VOLUME,                     CU.M(CU.IN.)   2.34E-06(1.43E-01)
PLENUM SPRING TURNS,                              0.
ROD TOTAL VOID VOLUME,             CU.M(CU.IN.)   6.06E-06(3.70E-01)
ROD INTERNAL   HELIUM    PRESSURE,MPA(PSIA)       1.03E-01(1.50E+01)
ROD CRUD THICKNESS,                MM(MILS)       2.54E-02(1.00E+00)
CHANNEL EQUIVALENT DIAMETER,       CM(IN.)        1.52E+00(6.00E-01)
```

Figure A-6. Initial dimensions.

TABLE A-3 MODEL OPTION INDICATOR

example:

OPTIONS 7 2 1 0 0 0 0 0 0

number 1 2 3 4 5 6 7 8 9

Each number is designed to signify a model option.

The first number indicates the radial power profile option choice

=1, LASER generated: PWR uranium enriched
=2, LASER generated: BWR uranium enriched
=3, LASER generated: PWR plutonium enriched
=4, LASER generated: BWR plutonium enriched
=5, User supplied radial power profile
=6, FLUXD computed profile with zero enrichment
=7, FLUXD computed profile with enrichment greater than zero

The second number indicates the gas release option choice:

=1, Beyer-Hann with NRC high burnup correction
=2, Beyer-Hann without NRC high burnup correction
=3, ANS 5.4
=4, Booth diffusion
=5, GRASS or FAST-GRASS

The third number indicates the mechanics option choice.

=1, PELET/RADIAL
=2, FRACAS-I
=3, FRACAS-II

The remainder of the numbers are not presently used.

```
XXXXXXXXXXXXXXXXXXXXXXXXXXXXXXXXXXXXXXXXXXXXXXXXXXX
X                 **** FRAPCON ****                X
X         STEADY-STATE FUEL ROD ANALYSIS CODE      X
X      MOD 002 VERS001     MAT PRO MOD 11  REV 1   X
X  RUN DATE =  27/10/80  OPTIONS 52100000 PAGE   2 X
X  IFA-432, ROD 1                                  X
XXXXXXXXXXXXXXXXXXXXXXXXXXXXXXXXXXXXXXXXXXXXXXXXXXXX
```

POWER-TIME STEP	TIME (HRS)	TIME (DAYS)	POWER (KW/M)	POWER (KW/FT)	COOLANT PRESSURE (MPA)	COOLANT PRESSURE (PSIA)	COOLANT INLET TEMP. (K)	COOLANT INLET TEMP. (F)	COOLANT MASS FLUX (KG/S-M**2)	COOLANT MASS FLUX (LBM/HR-FT2)
1	1.8	.08	3.28	1.00	3.45	500.	513.	464.	0.	0.
2	3.6	.15	6.56	2.00	3.45	500.	513.	464.	0.	0.
3	5.4	.23	9.84	3.00	3.45	500.	513.	464.	0.	0.
4	7.2	.30	13.12	4.00	3.45	500.	513.	464.	0.	0.
5	9.0	.38	16.40	5.00	3.45	500.	513.	464.	0.	0.
6	10.8	.45	19.69	6.00	3.45	500.	513.	464.	0.	0.
7	12.6	.53	22.97	7.00	3.45	500.	513.	464.	0.	0.
8	14.4	.60	26.25	8.00	3.45	500.	513.	464.	0.	0.
9	16.2	.68	29.53	9.00	3.45	500.	513.	464.	0.	0.
10	18.0	.75	32.81	10.00	3.45	500.	513.	464.	0.	0.
11	19.8	.83	36.09	11.00	3.45	500.	513.	464.	0.	0.
12	21.6	.90	39.37	12.00	3.45	500.	513.	464.	0.	0.

THE STORED ENERGY IS NORMALIZED TO 77.00 DEGREES F

PLOTS NOT REQUESTED

Figure A-7. Power history.

```
                          XXXXXXXXXXXXXXXXXXXXXXXXXXXXXXXXXXXXXXXXXXXXXXXX
                          X                **** FRAPCON ****              X
                          X        STEADY-STATE FUEL ROD ANALYSIS CODE    X
                          X     MOD 002 VERS001    MAT PRO MOD 11  REV 1  X
                          X  RUN DATE = 27/10/80  OPTIONS 52100000 PAGE  3 X
                          X  IFA-432, ROD 1                               X
                          XXXXXXXXXXXXXXXXXXXXXXXXXXXXXXXXXXXXXXXXXXXXXXXX
                     XXXXXXXXXXXXX  AXIAL POWER SHAPE INFORMATION  XXXXXXXXXXXXX

   AXIAL DISTRIBUTION IS INPUT        ROD AVERAGE POWER IS INPUT         NUMBER OF AXIAL NODES=  4
                                                       X'S  IN FEET

                    XXXXXXXXXXXXXXXXXX  INPUT AXIAL SHAPE NUMBER    1  XXXXXXXXXXXXXXXXXX

  X(  1)=  0.0000   X(  2)=   .2500   X(  3)=   .5410   X(  4)=   .9330   X(  5)=  1.2410   X(  6)=  1.5500   X(  7)=  1.8580
  X(  8)=  1.8700   X(
 QF(  1)=   .5800  QF(  2)=   .6700  QF(  3)=   .7810  QF(  4)=   .8620  QF(  5)=   .9170  QF(  6)=   .9680  QF(  7)=   .9960
 QF(  8)=  1.0000  QF(

  INCREMENT     AXIAL STATION          UNNORMALIZED
               FEET      METERS          HEAT FLUX
     1         .2338     .07125             .6652
     2         .7013     .21374             .8131
     3        1.1688     .35624             .9037
     4        1.6363     .49873             .9742

                                 AVGQI =   .839053

   NORMALIZED HEAT FLUX AT TOP OF STACK =  .3000
      THE RADIAL POWER PROFILE FROM THE SURFACE TO THE CENTER IS
      RAPOW(1 TO 11) =    1.1830   1.1375   1.0950   1.0550   1.0180    .9850    .9590    .9270    .9020    .8800    .8530
   R(I),I=1,11      =     .2103    .1998    .1887    .1769    .1644    .1507    .1357    .1188    .0991    .0743    .0350


                          XXXXXXXXXX  INITIAL PLENUM GASES (MOLES)  XXXXXXXXXX

  AIR =  0.            NITROGEN =  0.           ARGON =  0.           FISSION GAS =  0.           HELIUM =   .25554E-03


                    ROD AVE BURNUP AT END OF LIFE (AMWDT) =      21.0
                    ROD TIME AVE HEAT FLUX (QBAR) =  146347.


 GAS LOOP  ITER =  4          PRESSURE LAST TWO LOOPS     24.05     26.77
                         TIME EXPIRED IN PELET  =    .953

       ZERO POWER CLADDING AXIAL EXPANSION (ROOM TEMPERATURE REFERENCE), MM(IN)       .61   ( .0240)
```

Figure A-8. Power profiles.

Starting with Page 4 the output is generated by the code as it runs the simulation. For each time step, there will be a page describing the state of the fuel rod for each axial region (Figure A-9), a summary page (Figure A-10). The output for each axial node contains such things as fuel rod linear heat rating, burnup, time in reactor, temperatures and dimensions, gas conductivity, gap size and conductance, stresses and strains in the cladding, and pellet-cladding interfacial pressure. If the PELET option is used, the effective fuel elastic moduli and the calculated fuel thermal conductivity degradation factor are also output.

The summary page includes information on the volumes and temperatures used in the gas pressure calculation, fission gas release and a complete summary for all the axial nodes. This summary for each axial node includes cladding stresses, total strains and permanent strains, fuel centerline temperature, fuel average temperature, cladding temperature, coolant temperature and the stored energy in the fuel. Finally, the cladding axial expansion is provided.

If the ANS-5.4 fission gas release model is used, a table and plot of fission gas release fraction versus half-life is output for the shorter half-life "radioactive" gases (Figure A-11). This page precedes the other output pages for that time step.

For the final time step, final summary pages are provided (Figures A-12, A-13). This summary contains information of interest with respect to peak power segment values for each time step.

4. JOB CONTROL LANGUAGE FOR CDC CYBER

The job control cards necessary to run FRAPCON-2 on CDC CYBER computers are listed below:

```
XXXXXXXXXXXXXXXXXXXXXXXXXXXXXXXXXXXXXXXXXXXXXXXXXXXXX
X                    **** FRAPCON ****                 X
X         STEADY-STATE FUEL ROD ANALYSIS CODE          X
X      MOD 002 VERS001     MAT PRO MOD 11  REV 1       X
X  RUN DATE = 28/10/80  OPTIONS 53100000 PAGE     61 X
X  IFA-432, ROD 1                                      X
XXXXXXXXXXXXXXXXXXXXXXXXXXXXXXXXXXXXXXXXXXXXXXXXXXXXX

 AXIAL REGION NUMBER  4          POWER-TIME STEP 29

AVG.  LINEAR HEAT RATING, KW/M(KW/FT)    36.52( 11.13)
LOCAL LINEAR HEAT RATING, KW/M(KW/FT)    40.92( 12.47)        ROD SURFACE HEAT FLUX, W/M**2(BTU/HR-FT**2)  1.02E+06(3.23E+05)
PEAK  LINEAR HEAT RATING, KW/M(KW/FT)    40.91( 12.47)

STEP STARTS AT TIME, DAYS(SEC)   215.00( 1.86E+07)            STARTING BURNUP,  MWS/KGU(MWD/MTU)     .9940E+06( 11505.)
TIME INCREMENT,      DAYS(SEC)    15.00( 1.30E+06)            BURNUP INCREMENT, MWS/KGU(MWD/MTU)     .6678E+05(   773.)
END STEP,            DAYS(SEC)   230.00( 1.99E+07)            END STEP BURNUP,  MWS/KGU(MWD/MTU)     .1061E+07( 12278.)

                                          RADIAL TEMPERATURE DISTRIBUTION

                                              RADIUS, CM(IN)                 TEMP, K(F)

                        FUEL--CENTER              .0889(  .0350)               2723.(4441.)
                        FUEL--.2*RADIUS           .1093(  .0430)               2719.(4435.)
                        FUEL--.4*RADIUS           .2185(  .0860)               2537.(4107.)
                        FUEL--.6*RADIUS           .3278(  .1291)               2077.(3278.)
                        FUEL--.8*RADIUS           .4371(  .1721)               1447.(2144.)
                        FUEL--OUTER SURFACE       .5463(  .2151)                824.(1023.)

                        CLADDING INNER SURFACE    .5486(  .2160)                579.( 583.)
                        CLADDING OUTER SURFACE    .6424(  .2529)                514.( 465.)

                        OXIDE SURFACE             .6425(  .2530)                513.( 464.)

                        COOLANT TEMPERATURE                                     513.( 464.)

    RADIAL GEOMETRY CHANGES              INTERFACE CONDITIONS                STRESSES, MPA(KSI)        STRAINS, PCT

PERCENT CHANGE IN                 GAS CONDUCTIVITY, W/M-K         1.59E-02    RADIAL    -33.8( -4.91)          -.25
FUEL RADIUS DUE TO                            (BTU/HR-FT-F)     ( 9.17E-03)   AXIAL     145.4( 21.08)           .27
                                                                              HOOP      248.0( 35.97)           .49
      DENSIFICATION        -.240  GAP CONDUCTANCE, W/M2-K         4.87E+03
      SWELLING              .713                (BTU/HR-FT2-F)  ( 8.57E+02)
      THERMAL EXPANSION    1.703
                        --------  INTERFACE RESISTANCE, M2-K/W    2.06E-04
        TOTAL              2.176                (HR-FT2-F/BTU) ( 1.17E-03)   CLAD-COOLANT FILM COEFFICIENT, W/M2-K    2.84E+05
                                                                                                     (BTU/HR-FT2-F) ( 5.00E+04)

PCT CHANGE IN CLADDING            FRACTION CONDUCTANCE DUE TO                 EFFECTIVE FUEL ELASTIC MODULI, PA(PSI)
   RADIUS DUE TO
                                        GAS CONDUCTANCE           .146                              RADIAL  3.35E+09( 4.86E+05)
      PERMANENT             .011        CONTACT                   .847                              AXIAL   7.20E+09( 1.04E+06)
      RECOVERABLE           .481        RADIATION                 .007
                        --------
        TOTAL               .492  INTERFACE PRESSURE, MPA         22.0        FUEL THERMAL CONDUCTIVITY
                                                   (PSI)      (3185.5)            DEGRADATION FACTOR   .483
```

Figure A-9. Output page for one axial node.

```
XXXXXXXXXXXXXXXXXXXXXXXXXXXXXXXXXXXXXXXXXXXXXXXXXXXXXXXX
X                    **** FRAPCON ****                    X
X          STEADY-STATE FUEL ROD ANALYSIS CODE            X
X       MOD 002 VERS001     MAT PRO MOD 11  REV 1         X
X  RUN DATE =  28/10/80  OPTIONS 53100000 PAGE   62 X
X  IFA-432, ROD 1                                         X
XXXXXXXXXXXXXXXXXXXXXXXXXXXXXXXXXXXXXXXXXXXXXXXXXXXXXXXX
```

POWER-TIME STEP 29

BURNUP TO END OF TIME STEP,MWD/KGU(MWD/MTU) 946897.(10959.)

COMPONENTS OF INTERNAL VOID AND TEMPERATURES

ITEM	ASSOCIATED TEMPERATURE, K(F)	FRACTION TOTAL VOLUME
PLENUM	555.(539.)	.450
GAP	682.(767.)	.099
ROUGHNESS	793.(968.)	.000
DISHES	1530.(2295.)	.269
POROSITY	1530.(2295.)	.000
CRACK	1530.(2295.)	.181

TOTAL VOID VOLUME, CU.CM(CU.IN.) 5.26(.321)
ROD INTERNAL GAS PRESSURE, MPA(PSIA) 8.420(1221.)

GAS COMPOSITION

GAS COMPONENT	CUMULATIVE FRACTION RELEASED,	CURRENT MOLE FRACTION
HE	.061	.038
H	0.000	0.000
N	0.000	0.000
AR	0.000	0.000
KR	.150	.144
XE	.850	.817
H2O	0.000	0.000

CUMULATIVE QUANTITY OF FREE GAS IN THE ROD, MOLES 6.7E-03
CUMULATIVE FISSION GAS RELEASE, PERCENT *****

MECHANICAL PARAMETERS AND RESULTS USING THE PELET SUBCODE

AXIAL REGION	CLADDING STRESSES, MPA(PSI) RADIAL ID	HOOP ID	HOOP OD	AXIAL	CLADDING STRAINS,PERCENT RADIAL ID	HOOP ID	HOOP OD	AXIAL
1	-17.8(-2584.)	107.7(15622.)	114.7(16630.)	70.3(10194.)	.01	.31	.29	.16
2	-25.3(-3669.)	166.6(24170.)	175.7(25482.)	107.4(15583.)	-.09	.41	.37	.22
3	-33.1(-4803.)	223.9(32469.)	241.3(35000.)	146.9(21301.)	-.22	.52	.47	.27
4	-33.8(-4905.)	225.4(32688.)	248.0(35973.)	145.4(21083.)	-.25	.55	.49	.27
PLENUM	-6.4(-922.)	18.1(2626.)	20.7(2999.)	11.3(1633.)	.18	.16	.16	.16

AXIAL REGION	CENTERLINE TEMPERATURE K(F)	FUEL AVERAGE TEMPERATURE K(F)	CLADDING AVERAGE TEMPERATURE K(F)	COOLANT TEMPERATURE K(F)	STORED ENERGY J/KG	CLADDING PERMANENT STRAINS,PERCENT RADIAL ID	HOOP ID	HOOP OD	AXIAL
1	1812.(2803.)	1238.(1768.)	536.(505.)	513.(464.)	2.85E+05	-.00	.00	.00	.00
2	2284.(3651.)	1490.(2222.)	541.(514.)	513.(464.)	3.71E+05	-.01	.01	.01	.00
3	2690.(4382.)	1682.(2567.)	544.(520.)	513.(464.)	4.47E+05	-.02	.01	.01	.00
4	2725.(4441.)	1712.(2623.)	546.(524.)	513.(464.)	4.59E+05	-.02	.01	.01	.00
PLENUM						-.00	.00	.00	.00

CLADDING AXIAL EXPANSION (ROOM TEMPERATURE REFERENCE), MM(IN) 1.36 (.0537)

TIME EXPIRED IN PELET = .967

Figure A-10. Output page for one time step.

FRACTION RADIOACTIVE GASES RELEASED

TIME STEP = 33
TIME AT END OF STEP = 260.0 DAYS

RELEASE FRACTION = FRACTION OF NON-DECAYED INVENTORY THAT RESIDES IN THE GAP

HALF-LIFE(SEC)	1.0E+01	3.2E+01	1.0E+02	3.2E+02	1.0E+03	3.2E+03	1.0E+04	3.2E+04	1.0E+05	3.2E+05	1.0E+0
FRACTION RELEASED	3.00E-03	5.32E-03	9.41E-03	1.66E-02	2.89E-02	4.97E-02	8.30E-02	1.31E-01	1.90E-01	2.53E-01	3.14E-0

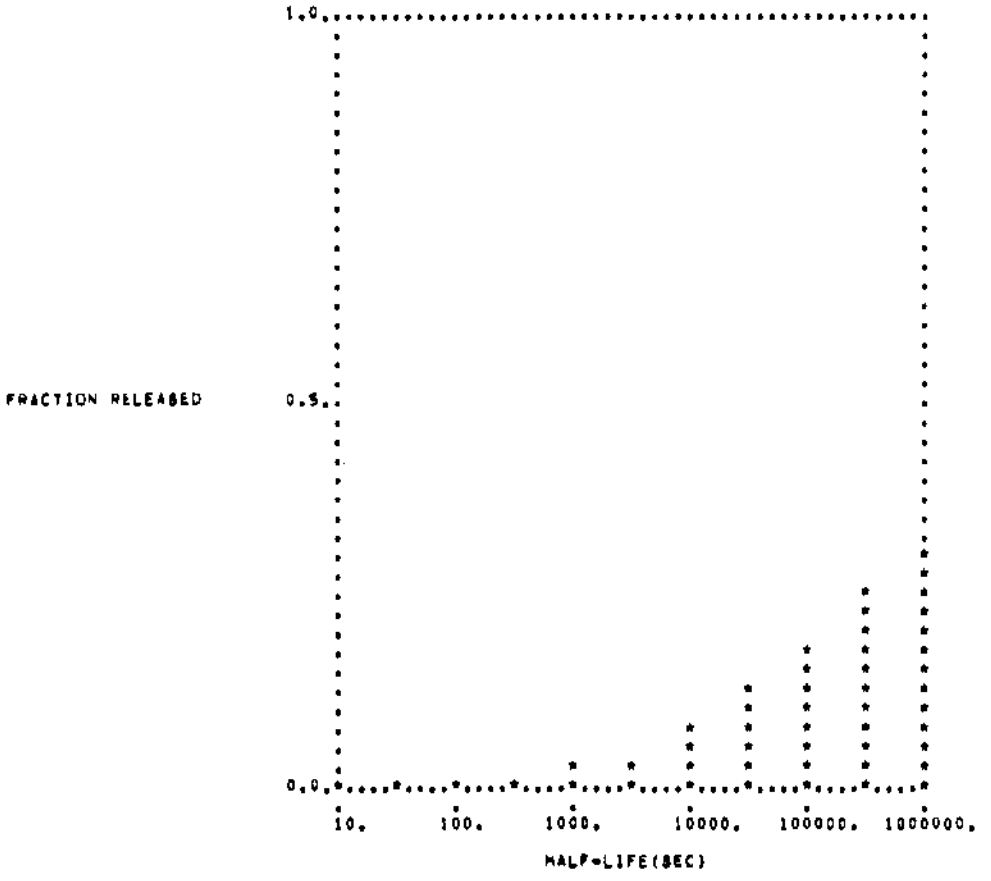

Figure A-11. ANS-5.4 radioactive (short-lived) fission gas release.

```
XXXXXXXXXXXXXXXXXXXXXXXXXXXXXXXXXXXXXXXXXXXXXXXXX
X                **** FRAPCON ****              X
X         STEADY-STATE FUEL ROD ANALYSIS CODE   X
X     MOD 002 VERS001    MAT PRO MOD 11  REV 1  X
X  RUN DATE = 28/10/80  OPTIONS 53100000 PAGE 44 X
X  IFA-432, ROD 1                               X
XXXXXXXXXXXXXXXXXXXXXXXXXXXXXXXXXXXXXXXXXXXXXXXXX
```

********** PEAK POWER AXIAL NODE OUTPUT **********

	TIME HOURS	BURNUP MWD/TU	POWER KW/FT	CLAD TEMP (F) OD.	AVG	ID.	GAP MILS	GAP (F)	FUEL TEMP (F) OD.	AVG	CENT	CONT. PSI	CLAD STRESS HOOP	AXIAL	STRAIN PCT	FUEL OD INCH	GAP CONDCT	FGAS PSI	ZRO2 MIL	H2 PPM
1	2.	0.	.97	464.	469.	473.	1.53	488.	502.	531.	610.	330.	-1463.	-918.	.1296	.42166	1041.	28.	.00	10.4
2	4.	1.	1.95	464.	473.	483.	1.50	510.	538.	625.	761.	379.	-812.	-723.	.1355	.42194	1080.	29.	.00	10.5
3	5.	2.	2.92	464.	478.	492.	1.47	532.	571.	719.	918.	442.	-142.	-508.	.1415	.42223	1124.	30.	.00	10.6
4	7.	3.	3.90	464.	483.	501.	1.44	552.	603.	812.	1077.	517.	546.	-276.	.1476	.42252	1171.	31.	.01	10.6
5	9.	5.	4.87	464.	487.	511.	1.41	571.	632.	905.	1239.	604.	1252.	-25.	.1539	.42282	1222.	32.	.01	10.7
6	11.	6.	5.85	464.	492.	520.	1.38	589.	659.	996.	1403.	708.	1977.	247.	.1603	.42312	1277.	33.	.01	10.7
7	13.	8.	6.82	464.	497.	529.	1.35	607.	684.	1086.	1567.	828.	2720.	541.	.1668	.42343	1337.	34.	.01	10.8
8	14.	11.	7.80	464.	501.	538.	1.32	623.	707.	1175.	1730.	969.	3482.	862.	.1734	.42375	1401.	35.	.01	10.8
9	16.	14.	8.77	464.	506.	547.	1.29	638.	728.	1261.	1893.	1131.	4247.	1224.	.1799	.42407	1471.	36.	.01	10.9
10	18.	17.	9.74	464.	510.	556.	1.25	652.	748.	1346.	2054.	1315.	5050.	1707.	.1860	.42439	1547.	37.	.01	10.9
11	20.	20.	10.72	464.	515.	566.	1.22	666.	766.	1429.	2215.	1522.	6028.	2372.	.1938	.42471	1628.	38.	.01	10.9
12	22.	24.	11.69	464.	519.	575.	1.19	678.	781.	1506.	2365.	1776.	7127.	3218.	.2018	.42495	1718.	39.	.01	11.0
13	23.	27.	12.67	464.	524.	584.	1.16	690.	796.	1583.	2518.	2048.	8364.	4175.	.2107	.42526	1811.	39.	.01	11.0
14	25.	32.	13.35	464.	527.	590.	1.14	697.	805.	1634.	2622.	2274.	9253.	4893.	.2170	.42546	1887.	40.	.01	11.1
15	240.	525.	13.35	464.	527.	590.	1.14	694.	797.	1586.	2530.	2668.	8331.	4965.	.2227	.42449	1955.	39.	.02	12.0
16	480.	1077.	13.35	465.	527.	590.	1.17	694.	798.	1570.	2495.	2919.	8019.	5138.	.2256	.42421	1952.	39.	.02	12.6
17	960.	2180.	13.35	465.	527.	590.	1.18	697.	803.	1574.	2498.	2982.	8018.	5239.	.2279	.42415	1904.	40.	.03	13.2
18	1440.	3283.	13.35	465.	528.	590.	1.18	702.	814.	1592.	2524.	3022.	8227.	5427.	.2309	.42421	1809.	42.	.03	13.7
19	1920.	4386.	13.35	465.	528.	590.	1.16	711.	831.	1636.	2601.	3151.	8843.	5946.	.2364	.42438	1686.	45.	.03	14.1
20	2448.	5599.	13.35	465.	528.	591.	1.14	722.	854.	1720.	2759.	3481.	10258.	7135.	.2455	.42472	1535.	52.	.04	14.5

Figure A-12. Final summary page.

```
XXXXXXXXXXXXXXXXXXXXXXXXXXXXXXXXXXXXXXXXXXXXXXXXXXXX
X               **** FRAPCON ****                  X
X        STEADY-STATE FUEL ROD ANALYSIS CODE       X
X     MOD 002 VERS001     MAT PRO MOD 11  REV 1    X
X  RUN DATE =  27/10/80  OPTIONS 52100000 PAGE  29 X
X  IFA-432, ROD 1                                  X
XXXXXXXXXXXXXXXXXXXXXXXXXXXXXXXXXXXXXXXXXXXXXXXXXXXX

END OF LIFE STRAIN RANGE (PERCENT) =      .0008

FISSION GAS CUMULATIVE FRACTION RELEASE =  .000744

ZRO2 WEIGHT GAIN ,(GM/M**2) =      .29
```

Figure A-13. EOL fission gas release fraction.

```
JOBNAME,...
ACCOUNT,...
ATTACH(FRPCON2,TAPE,ID=...)
COPYBF(FRPCON2,FRAPCON)
COPYBF(FRPCON2,FRACAS)
COPYBF(FRPCON2,PELET)
COPYBF(FRPCON2,AXISYM)
COPYBF(FRPCON2,MATPRO)
COPYBF(FRPCON2,GRASS)
COPYBF(FRPCON2,FGRASS)
COPYBF(FRPCON2,PLOT)
COPYBF(FRPCON2,SEGDIR)
RETURN(FRPCON2)
UPDATE(P=FRAPCON,C=CFRAP,F)
FTN(I=CFRAP,B=BFRAP,R=2,T)
UPDATE(P=PELET,C=CPEL,F)
FTN(I=CFRAC,B=BFRAC,R=2,T)
UPDATE(P=PELET,C=CPEL,F)
FTN(I=CPEL,B=BPEL,R=2,T)
UPDATE(P=AXISYM,C=CAXIS,F)
FTN(I=CAXIS,B=BAXIS,R=2,T)
UPDATE(P=MATPRO,C=CMAT,F)
FTN(I=CMAT,B=BMAT,R=2,T)
UPDATE(P=GRASS,C=CGRAS,R=2,T)
FTN(I=CGRAS,B=BGRAS,R=2,T)
UPDATE(P=FGRASS,C=CFGRAS,F)
FTN(I=CFGRAS,B=BFGRAS,R=2,T)
UPDATE(P=PLOT,C=CPLOT,F)
FTN(I=CPLOT,B=BPLOT,R=2,T)
REWIND,BFRAP,BFRAC,BPEL,BAXIS,BMAT,BGRAS,BFGRAS,BPLOT.
COMMENT. THESE BINARY FILES MAY NOW BE
COMMENT. COPIED OUT TO PERMANENT STORAGE
REWIND,SEGDIR.
MAP(PART)
RFL,320000.
```

```
COMMENT. THE RFL CARD WILL VARY FROM MACHINE
COMMENT. TO MACHINE AND DEPENDING ON THE INPUT
COMMENT. PARAMETERS SPECIFIED
SEGLOAD(1=SEGDIR,8=FRAPGO)
LOAD,BFRAP,BMAT,....
COMMENT. BFRAP AND BMAT ARE ALWAYS REQUIRED
COMMENT. BFRAC IS REQUIRED FOR FRACAS-II
COMMENT. BPEL IS REQUIRED FOR PELET.
COMMENT. BGRAS IS REQUIRED FOR GRASS.
COMMENT. BFGRAS IS REQUIRED FOR FAST/GRASS
COMMENT. BAXIS IS REQUIRED FOR AXISYM
COMMENT. BPLOT IS REQUIRED FOR PLOTS
NOGO.
COMMENT. FRAPGO MAY BE COPIED OUT TO PERMANENT
COMMENT. STORAGE TO SAVE RELOADING EACH TIME.
FRAPGO,PL=100000.
*EOR
*EOR
*EOR
*EOR
*EOR
*EOR
*EOR
*EOR
*EOR
DATA STREAM
*EOF
```

If the different files are copied out to permanent storage as suggested by the comment cards, the sequence of job control cards can be begun with the FRAPGO card in succeeding runs. An RFL card will always be needed, however.

APPENDIX B

MATERIAL PROPERTIES CORRELATIONS EMPLOYED BY FRAPCON-2

APPENDIX B

MATERIALS PROPERTIES CORRELATIONS EMPLOYED BY FRAPCON-2

A materials properties subcode is used to provide the computational subcodes of FRAPCON-2 with gas, fuel, and cladding materials properties. Those properties used by FRAPCON from Reference 3 are presented in Table B-1.

Table B-1. MATERIALS PROPERTIES IN MATPRO USED BY FRAPCON-2

Property	Subroutine
Fuel Material Properties	
1. Specific Heat Capacity	FCP
2. Thermal Conductivity	FTHCON
3. Emissivity	FEMISS
4. Elastic Modulus	FELMOD
5. Thermal Expansion	FTHEXP
6. Poisson's Ratio	FPOIR
7. Fuel Swelling	FSWELL
8. Densification	FUDENS
9. Cesium Release	CESIOD
10. Iodine Release	CESIOD

Table B-1 (continued).

Cladding Material Properties

1. Axial Growth.....CAGROW
2. Thermal Conductivity.....CTHCON
3. Zr-Oxide Thermal Conductivity.....ZCTCON
4. Surface Emissivity.....ZOEMIS
5. Thermal Expansion (Axial and Hoop).....CTHEXP
6. Plastic Deformation.....CSTRES
   .....CSTRAN
   .....CSTRNI
   .....CANISO
7. Elastic Modulus.....CELMOD
8. Annealing.....CANEAL
9. Poisson's Ratio.....CPOIR
10. Hydrogen Uptake.....CHUPTK
11. Meyer Hardness.....CMHARD

Gas and Fuel Rod Material Properties

1. Gas Thermal Conductivity.....GTHCON
2. Gas Viscosity.....GVISCO
3. Physical Properties.....PHYPRP

APPENDIX C
SUBROUTINE RELATIONS TO MODELS

APPENDIX C

SUBROUTINE RELATIONS TO MODELS

The information contained in Appendix C provides the user with assistance in relating subroutine names with the function performed. Figure C-1 presents the FRAPCON-2 subroutine relations and heirarchy.

1. Interaction of Subroutine RADIAL With Other Subroutines

As noted in Section 2.4.2, subroutine RADIAL takes fuel temperatures and fuel/cladding dimensions as input and produces values at each axial node for the fuel thermal conductivity degradation, effective gap size, and effective fuel elastic moduli. Figure C-2 lists these items and the FORTRAN variable name, and shows to which subroutine they go.

As shown, the fuel-cladding gap size (DG) and the fuel-cladding interfacial pressure (PRG) to the gap conductance calculation in subroutine GAPRS. The interfacial pressure additionally goes to the mechanical interaction calculation in the PELET subcode to subroutine ASOLVE. The fuel radial and axial effective elastic moduli come into PELET to the subroutines STIFF and STAFXL.

The degrading factor on the fuel thermal conductivity (CFAC) goes directly to the fuel pellet radial temperature calculator (DDLF) where it modifies both the MATPRO conductivity and its derivative with respect to temperature.

2. Interrelationship of Subroutines in the PELET Subcode

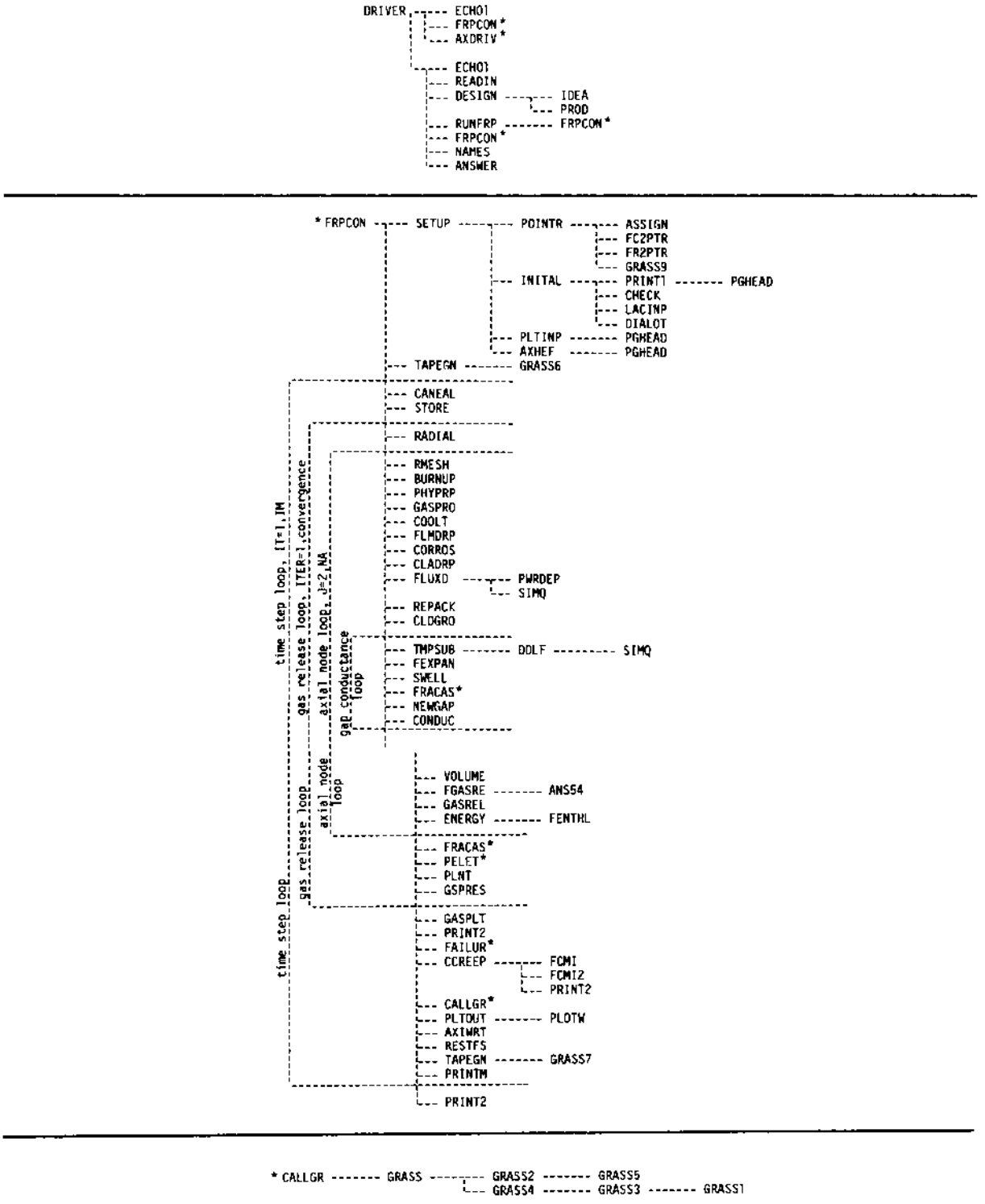

Fig. C-1 FRAPCON-2 subroutine relation and heirarchy.

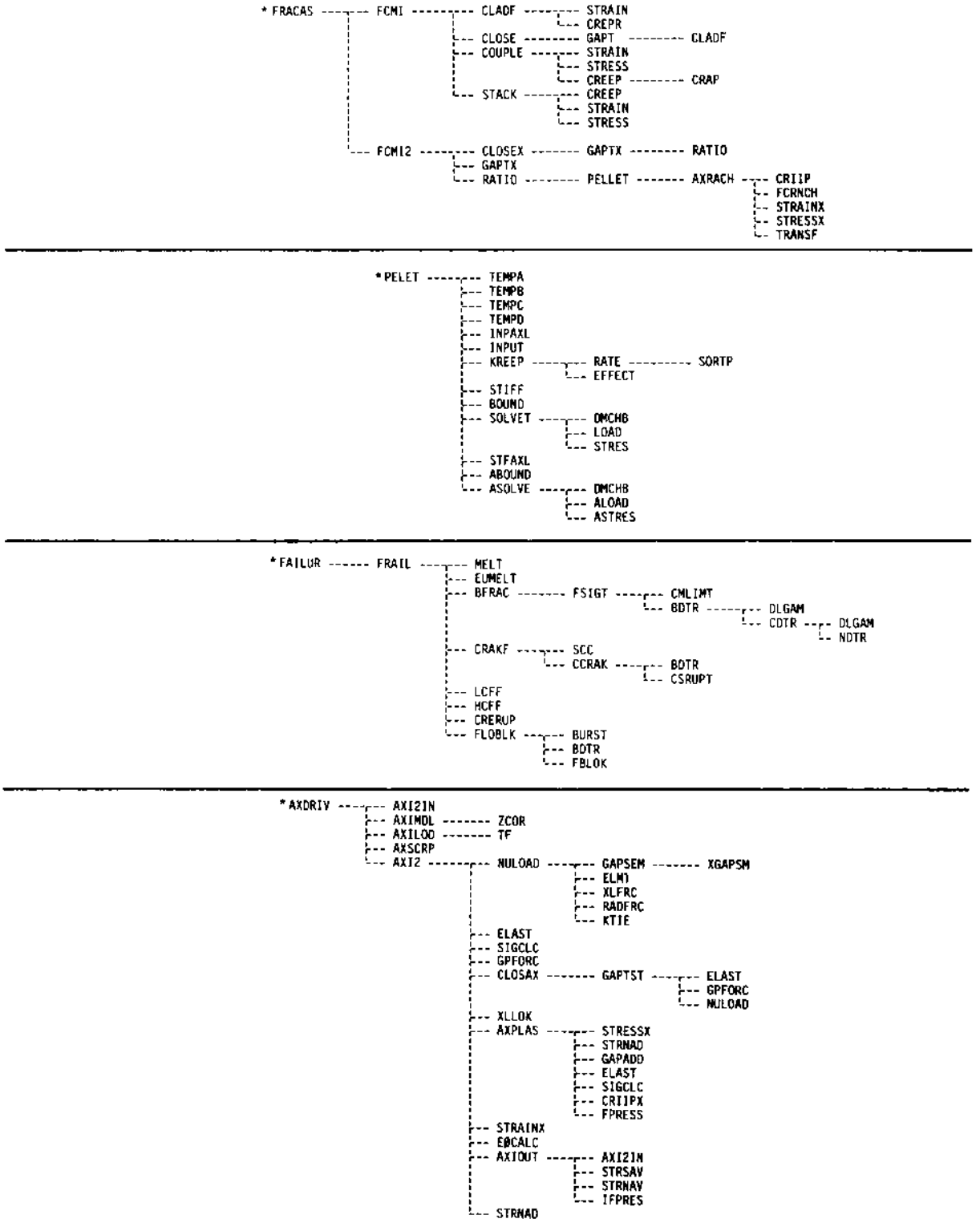

Figure C-1 (Cont.) FRAPCON-2 subroutine relation and heirarchy.

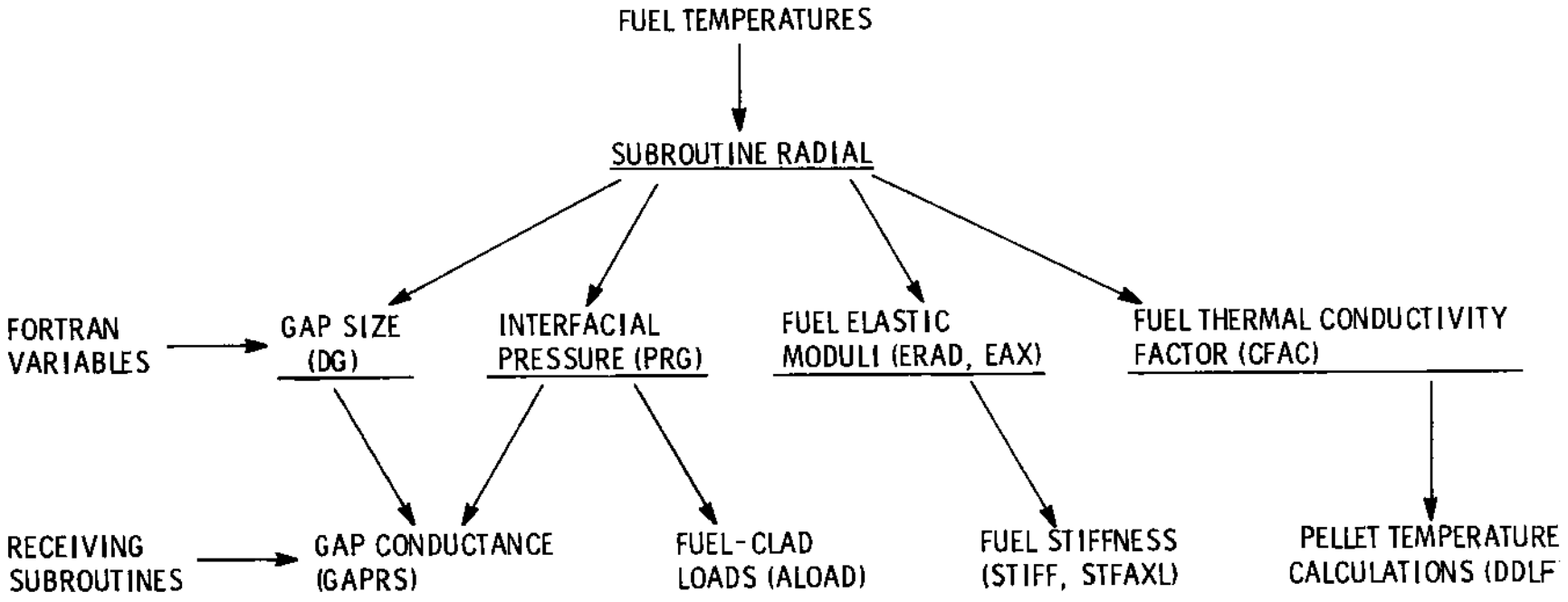

Figure C-2. Relation of subroutine RADIAL to other subroutines.

Function	Radial Model Subroutine	Axial Model Subroutine
Set up element and global stiffness matrix	STIFF	STFAXL
Apply boundary conditions and constraints	BOUND	ABOUND
Calculate nodal point loads	LOAD	ALOAD
Coordinate solution	SOLVET	ASOLVE
Perform solution of load-displacement equations	DMCHB	DMCHB
Calculate incremental and total stresses	STRES	ASTRES

Note that the entire KKA loop is repeated for each creep substep, the difference being that the CREEP-EFFECT-RATE subroutine series is called first to provide creep displacements and a translation of these to initial strains, which are treated within ALOAD/LOAD just like thermal strains.

The PNL fuel cladding mechanical interaction finite element calculation is performed in the PELET subcode, which is a collection of over 20 subroutines. PELET calculates incremental stresses and strains in fuel and cladding each time step, and accrues these in total stress/strain arrays. In this section we will show how the PELET subroutines relate to one another. A flow chart showing the basis logic of PELET and the heirarchy of subroutines is given in Figure C-3.

PELET first calls INPUT and INPAXL (once per case) to set up the node and degree of freedom numbering sequences for the radial and axial models, respectively. PELET then calls TEMPA, TEMPB, TGEMPC and TEMPD to calculate current temperatures to be assigned to each of the finite elements.

Then the elastic/plastic NKN loop begins. For NKN=1, elastic incremental calculations are performed; for NKN=2, creep and, if necessary, plastic deformations and corresponding stress corrections are calculated. A subloop (the ITI loop) is executed for NKN=2 only if the creep time step must be subdivided to accomplish the calculation.

Within the NKN loop resides the axial/radial loop (the KKA loop) which coordinates the radial/axial chained calculation. For KKA=1, the axial model calculation is performed; for KKA=2, the radial models representing each axial node are executed.

Within the KKA loop resides the axial region loop (KA loop) which runs through all the axial regions of the rod. Within this loop reside the calls to radial-model subroutines. The function of the various subroutines within the axial and radial models are listed below.

PELET FLOWCHART

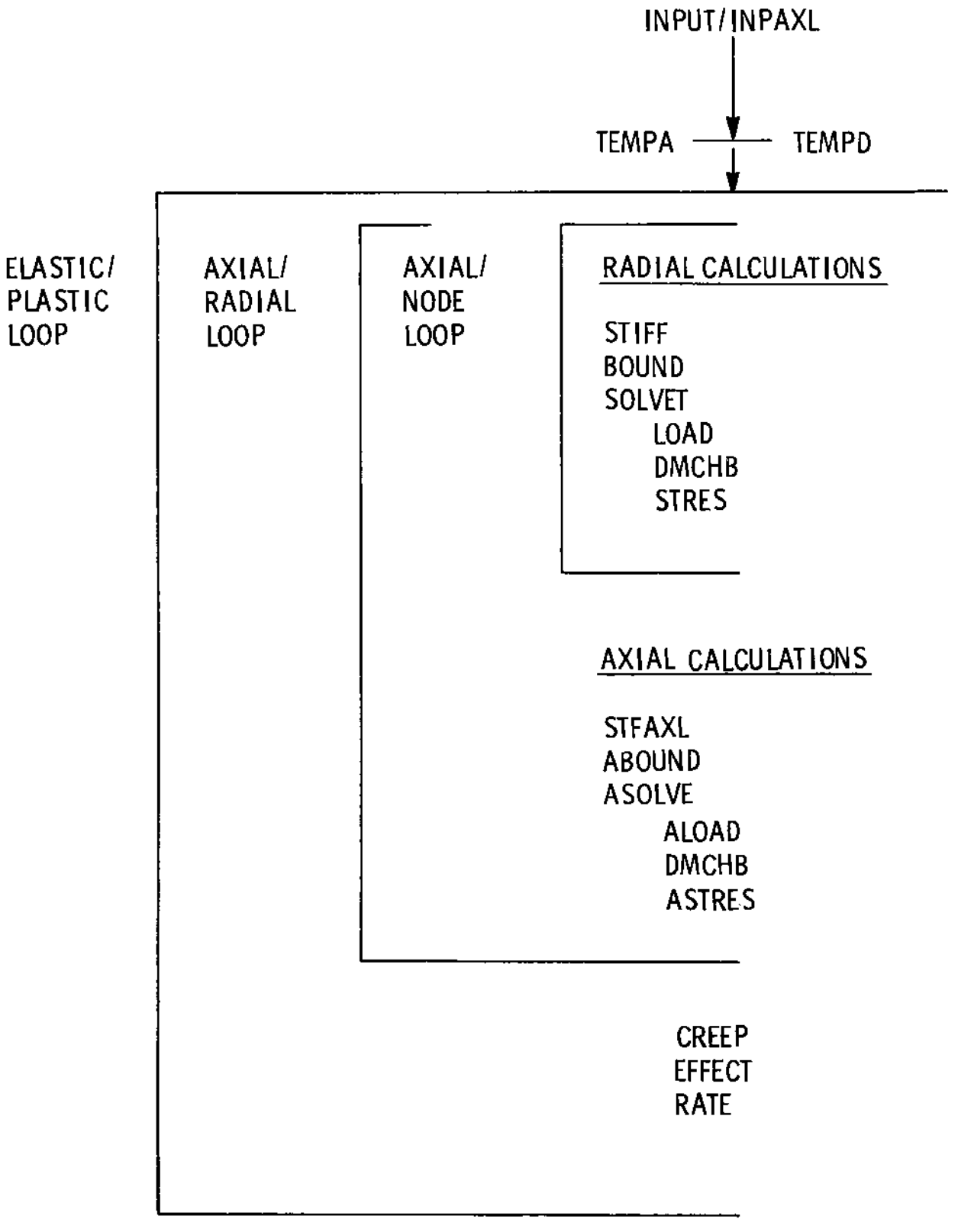

Figure C-3. Heirarchy and sequence of subroutines within the PELET subcode.

NRC FORM 335 (7-77) U.S. NUCLEAR REGULATORY COMMISSION

BIBLIOGRAPHIC DATA SHEET

1. REPORT NUMBER (Assigned by DDC): NUREG/CR-1845

4. TITLE AND SUBTITLE (Add Volume No., if appropriate): FRAPCON-2: A Computer Code for the Calculation of Steady State Thermal-Mechanical Behavior of Oxide Fuel Rods

2. (Leave blank)

3. RECIPIENT'S ACCESSION NO.

7. AUTHOR(S): G.A. Berna, M.P. Bohn, W.N. Rausch, R.E. Williford, D.D. Lanning

5. DATE REPORT COMPLETED: MONTH December, YEAR 1980

9. PERFORMING ORGANIZATION NAME AND MAILING ADDRESS (Include Zip Code):
EG&G Idaho, Inc.
P.O. Box 1625
Idaho Falls, ID 83401

Pacific Northwest Laboratory
P.O. Box 999
Richland, WA 99352

DATE REPORT ISSUED: MONTH January, YEAR 1981

6. (Leave blank)

8. (Leave blank)

12. SPONSORING ORGANIZATION NAME AND MAILING ADDRESS (Include Zip Code):
Division of Reactor Safety Research
Office of Nuclear Regulatory Research
U.S. Nuclear Regulatory Commission
Washington, DC 20555

10. PROJECT/TASK/WORK UNIT NO.

11. CONTRACT NO.: FIN A6050, B2043

13. TYPE OF REPORT: Technical/Interim Report

PERIOD COVERED (Inclusive dates):

15. SUPPLEMENTARY NOTES

14. (Leave blank)

16. ABSTRACT (200 words or less)

FRAPCON-2 is a FORTRAN IV computer code that calculates the steady state response of light water reactor fuel rods during long-term burnup. The code calculates the temperature, pressure, deformation, and failure histories of a fuel rod as functions of time-dependent fuel rod power and coolant boundary conditions. The phenomena modeled by the code include: (a) heat conduction through the fuel and cladding, (b) cladding elastic and plastic deformation, (c) fuel-cladding mechanical interaction, (d) fission gas release, (e) fuel rod internal gas pressure, (f) heat transfer between fuel and cladding, (g) cladding oxidation, and (h) heat transfer from cladding to coolant. The code contains necessary material properties, water properties, and heat transfer correlations. FRAPCON-2 is programmed for use on the CDC Cyber 175 and 176 computers.

The FRAPCON-2 code is designed to generate initial conditions for transient fuel rod analysis by either the FRAP-T6 computer code or the thermal-hydraulic code, RELAP4/MOD7 Version 2.

17. KEY WORDS AND DOCUMENT ANALYSIS

17a. DESCRIPTORS

17b. IDENTIFIERS/OPEN-ENDED TERMS

18. AVAILABILITY STATEMENT: Unlimited

19. SECURITY CLASS (This report): Unclassified

21. NO. OF PAGES

20. SECURITY CLASS (This page): Unclassified

22. PRICE: $

NRC FORM 335 (7-77)

UNITED STATES
NUCLEAR REGULATORY COMMISSION
WASHINGTON, D. C. 20555

OFFICIAL BUSINESS
PENALTY FOR PRIVATE USE, $300

POSTAGE AND FEES PAID
U.S. NUCLEAR REGULATORY
COMMISSION